From signal to shape: investigating how signaling pathways generate a newly evolved morphology

by

Sarah Jacquelyn Smith

Bachelor of Science, University of Texas at Arlington, 2013

Submitted to the Graduate Faculty of

The Dietrich School of Arts and Sciences in partial fulfillment

of the requirements for the degree of

Doctor of Philosophy

University of Pittsburgh

2019

UNIVERSITY OF PITTSBURGH

DIETRICH SCHOOL OF ARTS AND SCIENCES

This dissertation was presented

by

Sarah Jacquelyn Smith

It was defended on

August 8, 2019

and approved by

Dr. Gerard Campbell, Associate Professor, Department of Biological Sciences

Dr. Deborah Chapman, Associate Professor, Department of Biological Sciences

Dr. Lance Davidson, Professor, Department of Bioengineering

Dr. Jeffrey Hildebrand, Associate Professor, Department of Biological Sciences

Dissertation Advisor: Dr. Mark Rebeiz, Associate Professor, Department of Biological Sciences

From signal to shape: investigating how a signaling pathway generates a newly evolved morphology

Sarah Jacquelyn Smith, PhD

University of Pittsburgh, 2019

The development of anatomical form is multifaceted, involving both the patterning of gene expression and the morphogenesis of tissues at the cellular level. However, our understanding of how these two processes are integrated remains unclear. Studies of rapidly evolving anatomical structures address this question by identifying genetic alterations that affect morphogenesis. I examined the posterior lobe, a recently evolved appendage-like structure on the genitalia of members of the *Drosophila melanogaster* clade. During posterior lobe development, expansion of *unpaired* (*upd*), a ligand of the JAK/STAT pathway, is observed in species that develop this structure. I characterized the regulatory region of *upd* and uncovered a posterior lobe enhancer. Through CRISPR/Cas9 deletion of this enhancer, I found that it is vital for expression of *upd* in the posterior lobe and is required for proper lobe development. To investigate how expansion of JAK/STAT signaling contributed to posterior lobe development, I measured its cellular morphology and found that the posterior lobe forms through elongation of cells along their apico-basal axis. I identified the differential expression and deposition of the apical extracellular matrix (aECM) protein Dumpy and demonstrated a requirement for dumpy during posterior lobe development and evolution. In addition, I have identified a required role for the cellular effector, short stop (shot), which may act cooperatively with or in in parallel to Dumpy. I have determined that *shot* is regulated by the JAK/STAT pathway in the cells of the posterior lobe. This work highlights the complexity of development by linking the expanded expression of a signaling

pathway ligand with a novel morphogenetic process through the activation of a cellular effector. In addition this research uncovered a yet unseen role for the aECM in evolution of novel morphologies, emphasizing its novel role in regulating extreme changes in cell height.

Table of contents

List of tables

List of figures

List of videos

Preface

First I would like to thank the many scientists who have played an influential role in my journey. I would like to thank my advisor, Mark Rebeiz, who has been vital to the success of this project and cultivated a scientific environment that is welcoming to all and allowed exploration of novel ideas. In addition, I would like to thank the members of my committee, Gerard Campbell, Debbie Chapman, Lance Davidson, and Jeff Hildebrand, who have all provided fruitful discussion and insights on my dissertation project. I would like to particularly thank Lance Davidson for his tremendous insights on the morphogenesis side of the posterior lobe. This side of my dissertation project would not be where it is today without his help. In addition, his influence was vital in steering the direction of research I will pursue in the future. I would also like to thank Dr. Andre Pires da Silva and Dr. Manish Parihar, who fostered my love for research during my undergraduate career. I would also like to thank everyone at the University Pittsburgh Biological Sciences Department, especially my fellow graduate students, who have helped encourage me through difficult time. Finally, I would like to thank the members of the Rebeiz lab for their endless support, spirited insights, and for dressing up as *drosophila* genes with me.

I would also like to thank my family for their support throughout the years. Particularly for always supporting me in my numerous career changes, which allowed me to finally find what I am passionate about. In particular I would like to thank my mom, Carroll Smith, who I dearly wish could read this, but I know she would be proud. “Because I knew you… I have been changed for good.” – from *Wicked* (Schwartz, S., 2003).

1.0 Introduction

The information presented in this chapter was published in the journal *Current Opinion in Genetics & Development* (S. J. Smith, Rebeiz, & Davidson, 2018).

A major goal of developmental biology is to elucidate how the diverse anatomical structures throughout the organism take on their unique shapes from undefined embryonic tissues. The formation of even the simplest three-dimensional structure requires the deployment of tissue-specific gene regulatory networks (GRNs) that operate through transcriptional regulation to ultimately activate cellular effectors (Table 1.1). Once activated through transcriptional, post-transcriptional, or post-translational mechanisms, these effector molecules function to directly alter ubiquitously expressed proteins, such as the actin cytoskeleton (Table 1.1). Cumulatively, this results in a context-specific alteration to the mechanical properties of the cell, contributing to formation of the anatomical structure(Bernadskaya & Christiaen, 2016; Gilmour, Rembold, & Leptin, 2017; Heller & Fuchs, 2015; Peter & Davidson, 2015) (Figure 1.1). However, it has been difficult to understand the interface of GRN-effector connections to understand how combinations of cellular effectors are precisely patterned to shape anatomy, and how these GRN-effector connections diversify to modify anatomical form during evolution. The goal of understanding how to connect GRNs to anatomy is complicated by mechanical or signaling influences from neighboring tissues, that are regulated by different GRNs, painting a complex and interconnected picture of multiple GRNs activated in separate tissues affecting the morphogenesis of a single structure (Bernadskaya & Christiaen, 2016; Gilmour et al., 2017). While development can be studied at the level of GRNs, cellular effectors, or biophysical mechanics, it is critical that we comprehend how these distinct systems are connected and influence each other in an integrated

way. Here, I will review this developmental phenomenon in epithelial tissues, highlighting several recent studies that illuminate each facet of this problem while emphasizing the novel insights they provide. Further, I propose that the study of evolutionary modifications can provide insights into how these systems interface by examining how GRN-effector connections are modified during evolution, and review up-and-coming evolutionary developmental biology (evo-devo) model systems in which these questions can be explored.

1.1 The specification of developmental programs by gene regulatory networks

GRNs control the regulation of gene transcription in time, space, and intensity (Peter & Davidson, 2015) to generate precise expression outputs that affect tissue morphology (Figure 1.1A & Table 1.1) (Levine, 2010; Peter & Davidson, 2011). Recent work on the ventral furrow of *Drosophila melanogaster* illustrates how cell-to-cell variations in gene expression can be generated. A nuclear localized gradient of the transcription factor Dorsal establishes the dorsoventral axis of the embryo, and downstream genes Fog and T48 are expressed in a similar gradient along this axis (Figure 1.1)(Leptin, 1995). One might hypothesize cells with the highest levels of nuclear Dorsal would transcribe *fog* and *t48* mRNA at a higher rate. However, the gradients of *fog* and *t48* are instead established in a progressive manner, with cells receiving the strongest Dorsal signal activating transcription earlier than cells receiving lower levels of Dorsal (Lim, Levine, & Yamazaki, 2017). This causes higher levels of *fog* and *t48* transcripts to accumulate in cells with the highest amounts of Dorsal. These dynamic differences in *fog* and *t48* expression are vital for morphogenesis of the ventral furrow as both genes encode cellular effectors that help establish an activity gradient of non-muscle myosin II that drives apical constriction,

which is essential for proper invagination of the ventral tissue (Figure 1.1)(Heer et al., 2017). Such observations emphasize the important role transcriptional dynamics can play by producing variation in gene expression, which can have fundamental mechanical consequences on morphogenesis.

1.2 At the interface between GRNs and effector molecules

As *Drosophila* ventral furrow formation illustrates, GRNs spatially and temporally pattern the level of expression of specific regulatory factors that impart on each cell a unique *trans*-regulatory environment, capable of activating a particular number of cellular effector genes, which control aspects of cellular behavior (Figure 1.1B & Table 1.1) (Bernadskaya & Christiaen, 2016; Gilmour et al., 2017). However, it is important to note that there are few universal correlations between the expression of a specific cellular effector and a certain cell behavior, because cellular context is important. Diverse cellular contexts can result from a change in the milieu of co-expressed cellular effectors, but can also result from changes in the cell's mechanical microenvironment, (e.g. strain applied to the cell), which will be discussed in the next section. As the effector repertoire of a cell is greatly influenced by its GRN, disentangling how GRNs interface with collections of cellular effectors that encode the cell's physical responses represents a pressing need in this field.

The importance of understanding connections between GRNs and their target cellular effectors is particularly well demonstrated by the formation of morphologically diverse denticles on the larva of *Drosophila*. Denticles are actin rich epithelial projections that adorn the ventral surface of *Drosophila* larva(Price, Roberts, McCartney, Jezuit, & Peifer, 2006). Many signaling

pathways interact to regulate the position and development of these structures, and converge to activate the transcription factor, *shavenbaby* (*svb*) (Delon, Chanut-Delalande, & Payre, 2003), which is required for a cell to adopt the denticle fate. In the denticle, Svb regulates cellular effectors that promote various morphogenetic processes including actin reorganization, interaction with the extracellular matrix, and cuticle formation (Chanut-Delalande, Fernandes, Roch, Payre, & Plaza, 2006; Dickinson & Thatcher, 1997; Price et al., 2006). Interestingly*, svb* and several of its downstream cellular effector targets are also required for formation of other actin rich projections in *Drosophila*, such as the adult wing hairs, aristal laterals, and adult abdominal trichomes (Delon et al., 2003). Although these epithelial projections all require *svb,* they are morphologically quite distinct, raising the possibility that *svb* regulates the formation of rudimentary actin rich projections, but that the final phenotype depends on the cellular context. Rizzo and Besjovec found that the transcription factor SoxNeuro (SoxN) is required to generate distinctive denticle morphologies observed on the larva of *Drosophila* (Rizzo & Bejsovec, 2017). Both *svb* and *SoxN* are required to activate shared, but also distinct sets of downstream cellular effectors with *svb* controlling denticle height and SoxN regulating width. The authors hypothesized that these two transcription factors respond differently to upstream signaling gradients to generate the diverse phenotypes observed across the *Drosophila* larva.

As this case highlights, similar GRNs can be responsible for generating generic structures whose diverse morphologies are specified by local context. Understanding how this localized context is generated at the GRN level is important, but also vital is understanding how downstream cellular effectors are precisely patterned. Essential to understanding the importance of the outcome of the GRN-effector connection is elucidating how cellular effectors exert influences on cell behaviors.

1.3 Intrinsic and extrinsic physical responses to cellular effectors

Once a cellular effector is activated, it can produce intrinsic effects by altering the function of other effectors, for instance, modulating adhesion, remodeling the cytoskeleton, changing the cell's polarity, or targeting of cellular effectors to specific subcellular locations (Table1.1) (Nelson, 2003). Once positioned, multiple effectors operate together to dynamically regulate the cell's behavior, for instance, driving migration or initiating cell shape changes (Figure 1.1C)(Paluch & Heisenberg, 2009). Considering the interconnected nature of an epithelial tissue, these intrinsic changes can have extrinsic influences on neighboring cells and tissues. Extrinsic mechanics can influence or limit the range of shape changes the cells can adopt (Figure 1.1D). Within an epithelium, these intrinsic and extrinsic mechanical processes add up to create an integrated physical response leading to distinct cell behaviors, such as cell rearrangement and shape changes. Although far more comprehensive reviews of both intrinsic and extrinsic mechanisms of epithelial cell shape change exist (L. A. Davidson, 2012; Devenport, 2016; Heer & Martin, 2017; Lecuit & Lenne, 2007; Lecuit, Lenne, & Munro, 2011; Paluch & Heisenberg, 2009), I will examine recent examples that illustrate these interactions.

A case of oriented relaxation during dorsal closure in *Drosophila* highlights the importance of both intrinsic and extrinsic contributions to morphogenesis. Recent work has uncovered a mechanism whereby the cytohesin family member Steppke, an Arf-GEF, counteracts the assembly of actomyosin cables at the apical membrane of lateral epidermal cells (West et al., 2017). Steppke allows cell-cell junctions to relax and the tissue to stretch in response to tension from neighboring tissues during the process of dorsal closure in *Drosophila*. Thus, Steppke operates as an intrinsic factor in lateral epidermal cells by relaxing junctions but also plays a role within the mechanically

integrated dorsal closure movements as an extrinsic factor by reducing tension in the amnioserosa to aid in dorsal closure.

Intrinsic and extrinsic mechanisms also contribute to the formation of the ventral furrow during *Drosophila* gastrulation. As mentioned earlier, an intrinsically regulated gradient of non-muscle myosin II activity along the dorsal-ventral axis is important for invagination, however extrinsic mechanics are also vital for proper anterior-posterior orientation of actomyosin arrays within ventral furrow cells. Experimental treatments that changed the overall shape of the embryo or the dimension of the domain of gene expression in the surrounding tissue resulted in uniformly distributed actomyosin arrays in the ventral furrow (Chanet et al., 2017). This effect could be reversed through a variety of methods (e.g. laser ablations and knockdown of adhesion proteins), which restored directional tension to the ventral furrow cells and resulted in anterior-posterior actomyosin organization. This indicates that the overall shape of the embryo and the pattern of surrounding gene expression impose constraints that result in uneven tensions on the ventral furrow cells, which influences actomyosin organization in ventral furrow cells. This work highlights how intracellular force-generating and load-bearing structures might directly detect and respond to mechanical cues from the surrounding tissue to influence the final phenotype of the structure.

Finally, a striking example of the extrinsic mechanical influence of surrounding tissues on morphogenesis and gene regulation can be found in the patterning of periodic epithelial feather buds in chickens. A recent study reported that the dermal cells spontaneously aggregate below the epidermis due to their own contractility (Shyer et al., 2017). Dermal cell aggregates cause the overlying epithelial cells to bunch, resulting in the formation of a feather bud placode. Not only are epidermal cell mechanics affected by dermal cells movements, but gene regulation is also

altered when β-catenin in the epidermal cells sense the dermal cell aggregation and responds by turning on a follicle GRN (Shyer et al., 2017). Overall, this suggests that the physical and regulatory state of a cell can be influenced by the mechanical movements of neighboring tissues, similar to how a signaling pathway can alter the regulatory state of neighboring cells through secretion of ligands. This and other similar cases of differentiation in response to extrinsic mechanical influences are being identified (Chan, Heisenberg, & Hiiragi, 2017) and caution against focusing on intrinsic mechanical processes alone, highlighting the importance of examining the relative contributions of both intrinsic and extrinsic mechanical processes to morphogenesis.

1.4 Integrating an evolutionary perspective

So far, I have summarized recent work that is purely developmental, spanning a spectrum of morphogenetic processes that integrate GRNs, cellular effectors, and cellular mechanics. Such approaches can be complemented by evolutionary studies employing comparative methods. These studies can identify genetic variants that modify developmental processes, and have the potential to disentangle issues of cell autonomy raised by extrinsic mechanical influences and highlight which intrinsic processes were directly targeted during evolution. Below, I introduce comparative evo-devo model systems that have illuminated different aspects of morphogenesis and present new opportunities for deeper insights into the integration of GRNs, cellular effectors, mechanics, and morphogenesis.

1.4.1 Butterfly scales: connecting GRNs to the elaboration of single-cell appendages

Butterfly wings exhibit an enormous array of color patterns that has inspired numerous developmental, evolutionary, and ecological studies. The colors observed in butterfly wings can be formed by two mechanisms acting within the scale. The first way is through the use of different pigments, which selectively absorb certain wavelengths of light (Shawkey, Morehouse, & Vukusic, 2009). Many studies over the years have uncovered how some of these pigmentation patterns are genetically controlled. For example, Wnt signaling is responsible for regulating various pigmentation patterns across the wing (Gallant et al., 2014; A. Martin et al., 2012; A. Martin & Reed, 2014; Mazo-Vargas et al., 2017).

More relevant to morphogenesis, the other way to form color is through structural changes to the butterfly scale that alters the way light is scattered (Shawkey et al., 2009). The development of these complex scales begins with the projection of an epithelial cell that elongates and flattens to form the scale shape. Once scale morphogenesis is complete, the cell dies leaving both pigments and chitin, which forms the structural components of the scale (Dinwiddie et al., 2014). The three dimensional shape of each scale is quite intricate, consisting of many chitinous substructures such as the upper lamina, which is composed of ridges and microribs, and the smooth lower lamina, both of which can contribute to structural color (Stavenga, Leertouwer, & Wilts, 2014; Vukusic, Sambles, Lawrence, & Wootton, 1999; Wasik et al., 2014) (Figure 1.2A). Because chitin is secreted during the development of this epithelial appendage, there are likely multiple morphogenetic processes during scale development that can be affected to alter structural color.

In the genus *Bicyclus,* structural violet/blue color has independently evolved twice (Wasik et al., 2014). To determine how this structural color may have evolved, researchers used artificial selection to evolve violet/blue color in a subset of scales of *B. anynana*, a predominately brown-

pigmented species without structural color (Wasik et al., 2014). The authors detected an increase in thickness of the lower lamina of the scales that produce the structural color in both artificially selected and the naturally evolved species, suggesting that the lower lamina may be a common evolutionary target for violet/blue structural color evolution in *Bicyclus.*

How chitin is precisely secreted during butterfly scale development to form these architectural structures is unknown, however a previous study implicated F-actin (Dinwiddie et al., 2014). In this study, the authors observed single bundles of actin in developing pigmented scales, with rows of chitin secreted between each actin bundle. However, in structurally colored scales of *Agrulis vanillae,* double bundles of actin were observed between the chitin ridges in addition to an overall increase in the amount of F-actin present during scale formation. This suggests that F-actin organization may play a key role to direct chitin secretion to form the ridges that can impart structural color. In addition, recent research has implicated pigment biosynthesis genes as contributors to chitin structure in the butterfly scale (Matsuoka & Monteiro, 2018). Mutations in various pigment genes can alter both pigment production and the chitin structure of the scale, which may have possible implications in limiting the potential path of evolution.

The regulatory networks controlling structural color are understudied, but recent research has pinpointed the transcription factor Optix as a repressor of blue structural color in *Junonia coenia*. CRISPR/Cas9 induced knockout mutations of *optix* in *J. coenia* resulted in formation blue structural color in species that normally lack it (Figure 1.2A). Interestingly, this study identified two cellular effectors with known roles in F-actin filament organization that were downregulated in *optix* knockouts (Zhang, Mazo-Vargas, & Reed, 2017), correlating with the previous findings that F-actin may play an important role in determining where chitin is secreted.

Going forward, butterfly scales represent an excellent comparative model system to identify genes that regulate the morphogenesis of epidermal organs through their role in generating structural color. Of particular interest, artificially selected *B. anynana* strains could be used to genetically map loci that contribute variation in scale morphogenesis. Complementing this approach with descriptions of cellular effectors that are progressively activated during scale formation would illuminate the broader coupling of GRNs with effectors that operate during the formation of these complex structures.

1.4.2 The vertebrate tooth: elucidating evolutionarily important intrinsic and extrinsic mechanisms

Developmental and evolutionary biologists alike have long used teeth as a model system for many reasons, such as the ability to develop them *ex vivo* in culture and their abundant fossil record. Through the years, great progress has been made in understanding the gene network that patterns tooth development, including several signaling pathways expressed in a signaling center required to pattern tooth development (reviewed here (Biggs & Mikkola, 2014; Jernvall & Thesleff, 2012; Kim, Green, & Klein, 2017)). Within mammals, there is substantial diversity in tooth morphology, especially in number, shape, and orientation of cusps, which are elevations on the surface of the tooth that often form a point (Bergqvist, 2015). Much of our knowledge of tooth development comes from research in mammals, fueled by extensive knowledge and tools developed for mice (Kim et al., 2017), but one very useful approach to study the evolution of tooth morphology is to leverage the extensive fossil record of mammals to infer their ancestral and derived forms. For instance, reduction of Fibroblast Growth Factor 3 (Fgf3) levels in mice and mutations in Fgf3 in humans both lead to a more ancestral tooth morphology, suggesting its

involvement in more elaborate morphologies (Charles et al., 2009). Another study found that gradual decreases in ectodysplasin (Eda) and sonic hedgehog (SHH) signaling in the mouse were able to mimic a more ancestral phenotype including a reduction in cusp number and loss of cusps on lower molars, highlighting the importance of absolute levels of growth factor signaling for tooth morphology (Harjunmaa et al., 2014). Together these studies underscore important pathways that may be altered during tooth evolution, establishing promising systems where the connections between signaling events and specific cellular effectors that alter cell shape can be elucidated.

How cellular effectors control tooth shape is largely unexplored, but recent work has identified Rac1 and RhoA, regulators of F-actin, as important players that contribute to differences in tooth shape between gerbils and mice. Between their cusps, gerbils have ridges known as lophs that are missing in mouse (Figure 1.2B)(L. Li et al., 2016). Inhibition of Rac1 or increases in RhoA in gerbils induces cell shape changes that lead to tissue invagination, eliminating lophs between the cusps to mimic the mouse phenotype. Reciprocal experiments to reduce RhoA results in loph-like ridges in mice. This study illustrates how altering expression of cellular effector can elucidate their role in controlling cell behavior and their functional influence on gross morphological difference between species. Future work can begin to connect patterning events to these important cell shape changes.

In addition to changes in signaling pathway activity and intrinsic cellular effectors, surrounding tissues can also influence the shape of teeth. Cusps can form in either parallel or alternating arrays; variations in these patterns have repeatedly evolved (Figure 1.2C). Recent work has elucidated that the surrounding jaw influences the pattern of cusp formation through physical constraints (Renvoisé et al., 2017). Overall, given the great evolutionary diversity in tooth development, it will be interesting to determine the differences in GRNs regulating the diverse

shapes between different vertebrates, in addition to understanding how changes to GRNs in the jaw can extrinsically alter the overall shape of the tooth. More generally, comparative analyses of the co-evolution of signaling networks and morphogenesis operating during tooth formation may highlight ways that epidermal organs are malleable to processes primed to select new adaptive morphologies.

1.4.3 Drosophila dorsal appendage: how similar structures can form by different morphogenetic processes

The dorsal appendage is a tubular structure that forms on the eggshells of Drosophilid species and is utilized for respiration during embryonic development. Its formation is a well-studied developmental process that is accompanied by a striking diversity in number and morphology across species, making it an excellent model to examine the evolutionary origins of integrated GRNs, cell signaling, and cell mechanical systems (reviewed here (Miriam Osterfield, Berg, & Shvartsman, 2017; Pyrowolakis, Veikkolainen, Yakoby, & Shvartsman, 2017)). Early development of these structures begins with the projection of cells from the flat surface of the developing eggshell. Despite gross morphological similarities among species, distinct mechanisms have been found to drive the protrusion of these structures. In *D. melanogaster,* cell rearrangements drive protrusion of the nascent appendages, while in *Scaptodrosophila lebanonensis,* cell shape changes appear to be a major mechanical process in projecting the cells out (Figure 1.2D) (M. Osterfield, Schupbach, Wieschaus, & Shvartsman, 2015). Based on the observations of these two distinct cellular mechanisms, researchers recently examined patterning systems that might account for these differences in morphogenesis (O'Hanlon, Dam, Archambeault, & Berg, 2017). The intersection of the BMP and EGF pathways regulate the

formation of several eggshell structures including the dorsal appendage. The BMP signaling pathway displays similar patterning in both *D. melanogaster* and *S. lebanonesis,* but, major difference in the patterning of EGF signaling pathway is observed between the species. These changes result in one domain of expression of the transcription factor *broad* from which several dorsal appendages originate, as opposed to the two domains observed in *D. melanogaster* which each produce one dorsal appendage. This detailed knowledge of changes in patterning combined with the drastic difference in morphogenetic processes between *D. melanogaster* and *S. lebanonensis* positions the dorsal appendage for comparative analyses that can connect genetic changes in signaling pathways to downstream differences that regulate cellular effectors, providing a system to examine the importance of cell context on cellular effector function.

1.5 Conclusion

The process of developing an anatomical structure is not a simple one. It may involve many different levels that feedback upon one another and is best viewed from multiple complementary perspectives of GRNs, morphogenetic processes, and biomechanics. Studies often focus on individual steps of this process, but in order to move forward, integrative approaches must bridge these perspectives. I propose that the examination of evolutionary differences, combined with comparative morphogenetic studies can provide unique perspectives to help integrate these fields that will complement existing and upcoming developmental models. In particular, evo-devo model systems in which the contribution of individual genetic variants can be quantified (e.g. through genetic crosses) will be particularly powerful. Such systems will allow one to figure out which cells differ in cellular effector deployment and compare that information to quantitative measures

of cell behavior and cell mechanics, facilitating the discrimination of intrinsic from extrinsic physical responses. Identifying these processes and how they have been altered during evolution can be a source of inspiration for engineers seeking novel methods to engineer tissues and treat disease. Above and beyond identifying genetic variants, both developmental and evolutionary model systems will require a deeper understanding of the key cellular effectors, their mechanical consequences, and how their cell-type specific influences on morphogenesis are realized.

1.6 Figures and tables

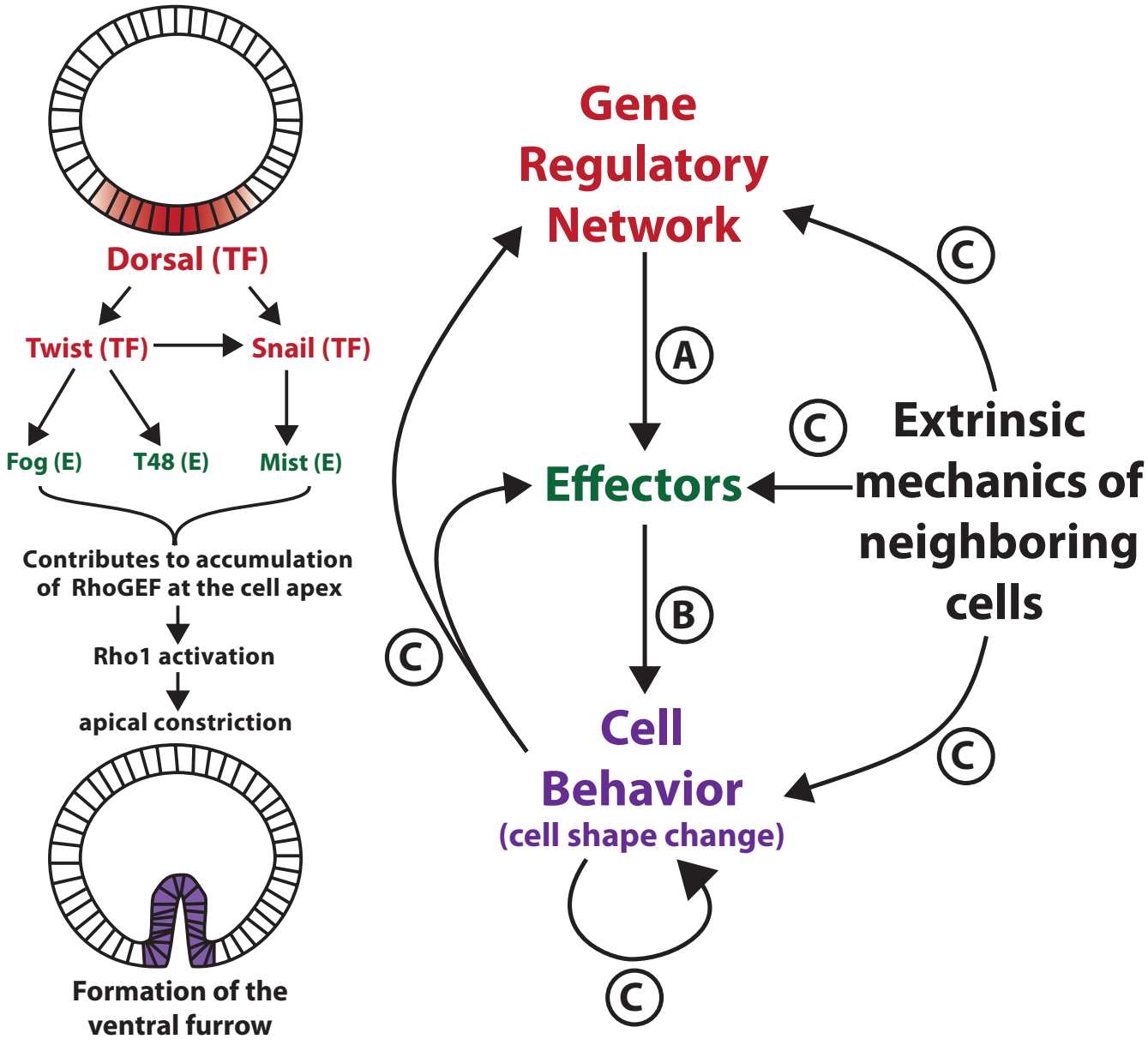

Figure 1.1 The influence of GRNs, cellular effectors, and neighboring mechanics on tissue morphogenesis.

Morphological structures are pre-patterned by GRNs (red) that turn on a precise set of effector molecules (green). These effectors control cell behaviors, here altering the shape of cells, together forming the final phenotype. (Left) An

invagination. (Right) Depiction of the interaction between gene regulatory networks, cellular effectors, and cell behaviors. While networks activate effectors (A), which drive changes in cell behaviors (B), development can also be influenced by signals and mechanical cues coming from neighboring cells in addition to feedback from different parts of the process (C).

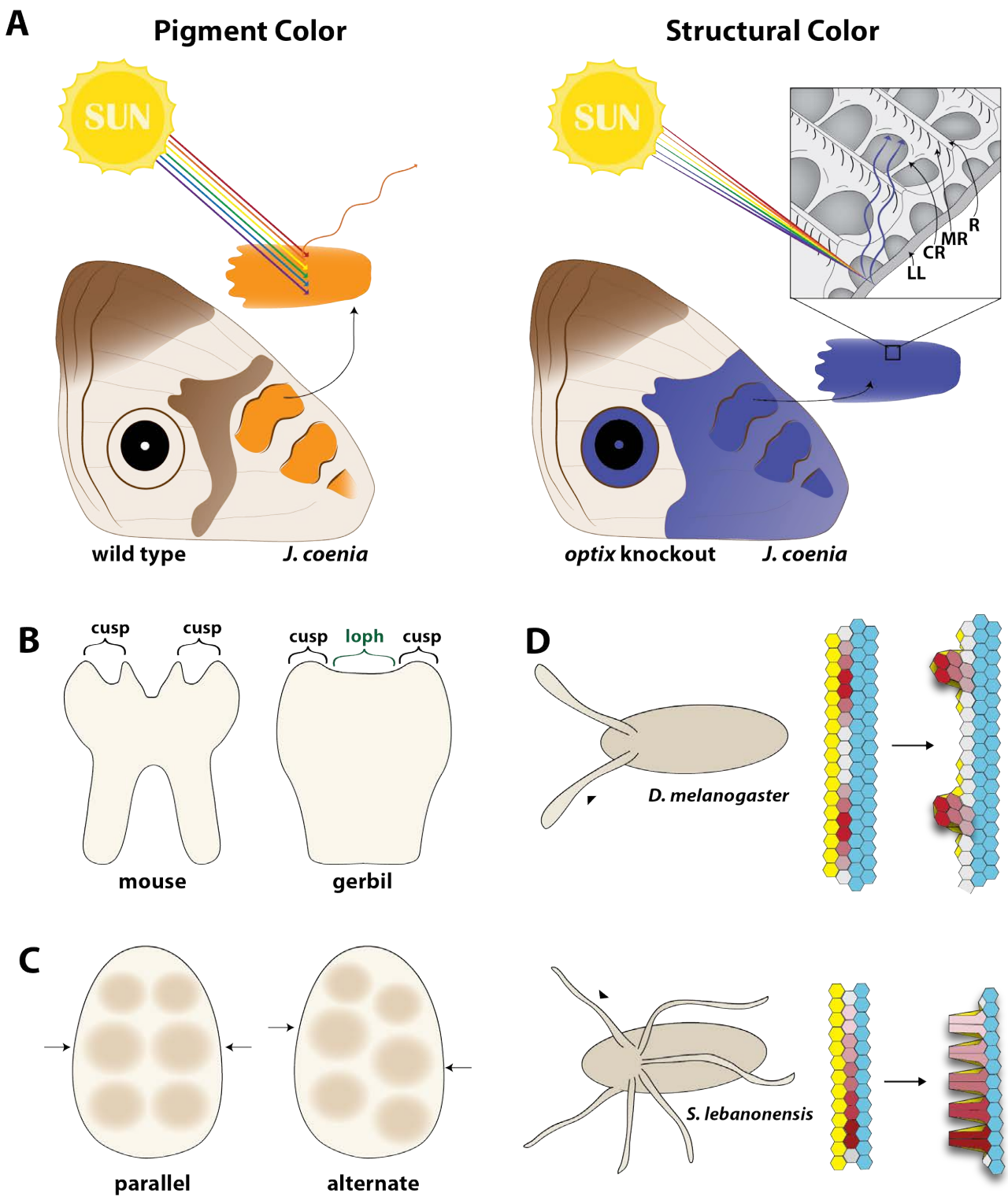
A
Pigment Color
Structural Color
SUN
SUN
R
MR
CR
LL
wild type
J. coenia
optix knockout
J. coenia
B
cusp
cusp
cusp
loph
cusp
mouse
gerbil
D
D. melanogaster
C
parallel
alternate
S. lebanonensis

Figure 1.2 Evo-devo models offer many routes to explore patterning and morhogenesis.

(A) In butterflies, colors can be formed using pigments, such as the ommochrome pigment (orange), which works by absorbing all wavelengths of light except orange. In contrast, structural colors are formed by reflection of light interacting with components of the scale to selectively reflect blue wavelengths in the *optix* knockout. The structure of the scale is quite complex consisting of a lower lamina (LL) connected to an upper lamina composed of ridges (R), microribs (MR), and crossribs (CR). (B-C) Differences in rodent molar morphology. (B) In a cross-sectional view of the mouse molar, cusps are separated, but in gerbils cusps are connected by a ridge called a loph. (C) Occlusal view of an adult tooth with cusps represented by circles. Cusps can either be parallel or alternate in their placement on the tooth. (D) Morphology of the dorsal appendage (arrowhead) of the *Drosophila* eggshell differs in placement and number between species. Early morphogenesis of these homologous structures also differ, with the dorsal appendage of *D. melanogaster* forming through neighbor exchange events (red cells) and the dorsal appendage of *S. lebanonensis* (also known as *S. pattersoni*) forming through cell shape changes (red cells).

Table 1.1 Glossary of Terms

Gene Regulatory Network (GRN)	GRNs are composed of signaling pathways, transcription factors, and cellular effectors. Signaling pathways pattern development through cell-cell communication, often resulting in the activation of a transcription factor. Transcription factors regulate gene expression by binding to individual enhancers of downstream genes (e.g. another transcription factor, cellular effector, etc). Each enhancer requires a different set of transcription factors to bind and gene activation will only occur in cells in which the correct sets of transcription factors are present. Overall this complex set of interactions patterns development and governs the final phenotype of the cell (Levine, 2010; Peter & Davidson, 2011).
Cellular Effector	Any gene that functions to non-transcriptionally activate, localize, or alter other core cellular proteins (e.g. actin, myosin, cadherin, etc.). Cellular effectors can be turned on via transcriptional regulation or can be proteins already present in the cell that are activated by other cellular effectors. Together cellular effectors function to alter the behavior of a cell by changing the mechanics within the cell or through altering mechanical connections to neighboring cells. Cellular effectors can allow a cell to express multiple phenotypes in response to different context without new transcription (Bernadskaya & Christiaen, 2016; Gilmour et al., 2017).

Intrinsic Mechanics	The combined effect of the cell effectors present within a cell that affects the cell's mechanics.
Extrinsic Mechanics	The combined influence of effectors operating in neighboring cells, transferred via direct cell-cell contacts, to alter a cell's intrinsic mechanics.

2.0 Expansion of apical extracellular matrix underlies the morphogenesis of a recently evolved structure

2.1 Introduction

Biologists have long been mesmerized by the appearance of morphological novelties, new structures that appear to lack homologs in other species groups (Moczek, 2008; Günter P. Wagner & Lynch, 2010). To understand the origins of these novel structures, significant effort has focused on determining how spatial and temporal patterning of genes are altered during evolution (Peter & Davidson, 2015; Rebeiz, Patel, & Hinman, 2015; Günter P. Wagner, 2014). This has indicated how developmental programs are often associated with morphological novelties, and they are frequently co-opted from other tissues. However, limited attention has been directed to how novel structures form at the cellular level. Understanding how a structure physically forms is important, as it can help explain which morphogenetic processes might be targeted during evolution. In addition, because most morphological novelties arose in the distant past, it is likely that the causative genetic changes will be obscured by additional changes scattered throughout relevant gene regulatory networks (Liu et al., 2019). Hence, understanding the morphogenetic basis of a novelty is critical to identifying the most important aspects of the gene regulatory networks that contributed to its origin.

Most studies of morphogenetic evolution have focused on structures subject to diversification, illuminating processes that contributed to their modification, as opposed to origination. For example, studies of tooth morphogenesis have elucidated how both internal mechanisms, such as cell shape changes (L. Li et al., 2016), and external forces, such as the

pressure from the surrounding jaw (Renvoisé et al., 2017) could be contributing factors in their diversification. An examination of the enlarged ovipositor of *Drosophila suzukii* revealed how a 60% increase in length was associated with increases in apical area and anisotropic cellular rearrangement (Green et al., 2019). In addition, differences in early morphogenetic mechanisms between distantly related species are observed in both the development of breathing tubes on the Drosophilid eggshell (M. Osterfield et al., 2015) and migration of sex comb precursors on *Drosophila* male forelegs (Atallah, Liu, Dennis, Hon, & Larsen, 2009; Tanaka, Barmina, & Kopp, 2009), together highlighting how rapid changes in morphogenetic mechanisms can evolve to form the same structure. Overall, these studies have illustrated how evolutionary comparative approaches can reveal morphogenetic processes critical to the sculpting of anatomical structures.

Morphogenesis is the product of both cell intrinsic processes, such as those conferred by the cytoskeleton or cell-cell junctions, and external forces from the environment in which the cell resides. Extracellular mechanics are relatively understudied compared to intracellular mechanics (Paluch & Heisenberg, 2009). An important component of the microenvironment of a cell is the extracellular matrix (ECM) which can be subdivided into two populations of ECM, the basal ECM and the apical ECM (aECM) (Brown, 2011; Daley & Yamada, 2013; Linde-Medina & Marcucio, 2018; Loganathan et al., 2016). While comparatively understudied, recent work has defined vital roles for aECM in the morphogenesis of structures, such as the *Drosophila* wing (Diaz-de-la-Loza et al., 2018; Etournay et al., 2015; Ray et al., 2015), denticles (Fernandes et al., 2010), and trachea (Dong, Hannezo, & Hayashi, 2014a), as well as in *C. elegans* neurons (Heiman & Shaham, 2009; Low et al., 2019). Despite recent interest in the aECM, its role in the evolution of morphogenetic processes is currently unknown.

Genital traits represent a particularly advantageous system in which to study the morphogenetic basis of novel structures. The study of morphological novelty is often difficult because most structures of interest evolved in the distant past, rendering it difficult to understand the ancestral ground state from which the novelty emerged. Genitalia are noted for their rapid evolution (Eberhard, 1985), and thus bear traits among closely-related species that have recently evolved in the context of a tissue that is otherwise minimally altered. For example, the posterior lobe, a recently evolved anatomical structure present on the genitalia of male flies of the *melanogaster* clade (Kopp & True, 2002)(Figure 2.1A), is a three-dimensional outgrowth that is required for genital coupling (Frazee & Masly, 2015; Jagadeeshan & Singh, 2006; LeVasseur-Viens, Polak, & Moehring, 2015). Besides the posterior lobe, the genitalia of lobed and non-lobed species are quite similar in composition, providing an excellent context in which to examine the morphogenesis of the ancestral structures from which the posterior lobe emerged.

Here, I find cell shape changes which increase cell height along the apico-basal axis drive morphogenesis of the posterior lobe. I investigated internal and external factors that might contribute to this height increase and find a correlation between the aECM protein Dumpy and the height of posterior lobe cells. Comparisons to non-lobed species uncovered the presence of a conserved aECM network on the genitalia that has expanded to cells that form the posterior lobe. This work shows how the formation of a morphological novelty depends upon novel aECM attachments, integrating cells into a larger pre-existing aECM network.

2.2 Results

2.2.1 The posterior lobe grows from the lateral plate epithelium

The male genitalia of *Drosophila* is a bilaterally symmetrical anatomical structure which forms from the genital disc during pupal development. In adults, the posterior lobe protrudes from a structure called the lateral plate (also known as the epandrial ventral lobe (Rice et al., 2019)) (Figure 2.1A,D; Video 2.1). In *D. melanogaster*, prior to posterior lobe formation, the lateral plate is fully fused to a neighboring structure called the clasper (also known as the surstylus (Rice et al., 2019))(Figure 2.1B)(Glassford et al., 2015).The lateral plate begins to separate from the clasper around 32 hours after pupal formation (APF) in *D. melanogaster* (Figure 2.2). Approximately 4 hours later, the posterior lobe begins to project from the plane of the lateral plate and achieves its final shape by 52 hours APF (Figure 2.1D; Figure 2.2). During posterior lobe development, cleavage of the lateral plate from the clasper continues, dropping the tip of the lateral plate behind the clasper and separating both tissues (Figure 2.1D; Figure 2.2). Full separation of the lateral plate and clasper stops slightly above (ventral to) the posterior lobe (Figure 2.2). By contrast, the lateral plate in the non-lobed species *D. biarmipes* remains flat throughout development, but all other morphogenetic events are very similar, forming on a schedule that is approximately 4 hours behind *D. melanogaster* (Figure 2.1C,E; Figure 2.2).

2.2.2 Posterior lobe cells increase in height to protrude from the lateral plate

To investigate which cellular behaviors are unique to lobed species, I examined how the posterior lobe grows from the lateral plate in both lobed and non-lobed species. First, I looked at

cell proliferation, which commonly contributes to morphogenesis through patterned and/or oriented cell division (Heisenberg & Bellaïche, 2013), such as observed during branching morphogenesis in the lung where oriented cell division expands the bud before it bifurcates into two branches (Schnatwinkel & Niswander, 2013). During stages prior to the development of the posterior lobe morphogenesis, I observed widespread cell proliferation throughout the entire genital epithelium (Figure 2.4). However, proliferation declines tissue-wide and all cell proliferation is essentially absent during posterior lobe development (Figure 2.4). Similar dynamics in proliferation are also observed in non-lobed species (Figure 2.4), suggesting that proliferation is not a major contributor to the morphogenesis of the posterior lobe.

Next I tested the possibility that cell intercalation could contribute to posterior lobe morphogenesis. Such processes may play a role in tissue elongation (Guirao & Bellaïche, 2017; Tada et al., 2012; Walck-Shannon & Hardin, 2014), such as in germ-band extension in *Drosophila* where directed cell intercalation results in a reduction in the number of cells on the anterior-posterior axis and an increase in the number of cells along the dorsal-ventral axis, elongating the tissue along the dorsal-ventral axis (Irvine & Wieschaus, 1994). To test this, I utilized live cell tracking during posterior lobe development. Initial observations of the outer face of the posterior lobe revealed few cell rearrangement events. When cell rearrangements did occur it was in response to a cell being removed from the apical surface (Video 2.2). Due to the limited number of cell rearrangement events observed during posterior lobe morphogenesis, cell intercalation does not appear to be a major driver of posterior lobe morphogenesis, causing us to instead examine changes in cell shape.

Changes to cell shape are quite common during tissue morphogenesis, as classically illustrated by the process of apical constriction that deforms tissues during many developmental

processes (Lecuit & Lenne, 2007; A. C. Martin & Goldstein, 2014). To examine cell shape, I utilized the Raeppli system to label individual cells with a fluorescent marker (mTFP1) (Kanca, Caussinus, Denes, Percival-Smith, & Affolter, 2014). I observed that cells within the posterior lobe are tall and thin, spanning from the basal to the apical surface of the epithelium (Figure 2.3A). Because cells span the full thickness of this tissue, I can approximate the height of the tallest cells in the posterior lobe by measuring tissue thickness. For these measurements, I used the lateral plate as an in-sample comparison, since it represents the tissue from which the posterior lobe protrudes and should differ from the lobe in morphogenetic processes. I observed a pronounced increase in thickness of the posterior lobe compared to the lateral plate (Figure 2.3B-C,F; Figure 2.5). The posterior lobe more than doubles in thickness with an average increase of 145.3% (+ 47.5µm), while the lateral plate only increases by 22.6% (+ 7.9µm) overall. In contrast, when non-lobed species are examined, no thickness changes are observed in the location where a posterior lobe would form, indicating that this increase in tissue thickness is unique to the posterior lobe (Figure 2.3B-E,G; Figure 2.5). Interestingly, this increase in thickness is a dynamic process during development. During the first 12 hours of posterior lobe development the lateral plate thickness decreases by 5.1µm, but the posterior lobe increases in thickness by 16.5µm on average (Figure 2.3F). By contrast, during the last 4 hours of development, rapid increases in thickness occur in both the posterior lobe and lateral plate, which increase on average by 31.0µm and 14.6µm respectively (Figure 2.3F). These observations reveal a slow phase of cell height increase during the first 12 hours of posterior lobe development, and fast phase during the last four hours of posterior lobe development. Together this data suggests that the cells of the posterior lobe undergo an extreme cell shape change to increase in length along their apico-basal axis, driving the posterior lobe cells to project out of the plane of the lateral plate.

2.2.3 Cytoskeletal components increase in concentration in posterior lobe cells

Elongation of cells along their apico-basal axes appears to be a major contributor to posterior lobe formation. To understand potential internal forces contributing to this cell shape change, I examined the organization of cytoskeletal components. As expected for a polarized epithelium, I found F-actin strongly localized to the apical cortex overlapping with E-cadherin throughout the entire genitalia (Figure 2.6A). In contrast with the adjacent tissues, F-actin is also concentrated along the apico-basal axis of posterior lobe cells (Figure 2.6A). This F-actin localization was unique to the posterior lobe, as it is less intense in neighboring structures, such as the lateral plate, clasper, and sheath, as well as in non-lobed species (Figure 2.6A; Figure 2.7). Next I evaluated microtubules by examining two post-translational modifications that appear on tubulin, acetylation of α-tubulin on lysine40, a stabilizing modification (Roll-Mecak, 2019; Xu et al., 2017), and tyrosinated tubulin, which has been associated with rapid microtubule turnover (Roll-Mecak, 2019; Webster, Gundersen, Bulinski, & Borisy, 1987). In the posterior lobe, acetylated tubulin levels are highest at the apex of the posterior lobe and weaken towards the basal side of the lobe (Figure 2.6B-C). Compared to other structures in the genitalia, acetylated tubulin is greatly increased specifically in the posterior lobe (Figure 2.6B-C). In contrast, the levels of acetylated tubulin in non-lobed species are similar throughout the genitalia (Figure 2.7). I found tyrosinated tubulin has a more consistent signal along the entire apico-basal axis in the posterior lobe (Figure 2.6B&D). The amount of tyrosinated tubulin in posterior lobe cells is increased compared to neighboring structures, but is weaker relative to the observed differences in acetylated tubulin. In non-lobed species the levels of tyrosinated tubulin are consistent across the entire genitalia (Figure 2.7). Collectively, these results suggest that changes in assembly and/or dynamics

of both F-actin and microtubule cytoskeletal networks could be contributing factors in changing the shape of posterior lobe cells to increase its height along the apico-basal axis.

2.2.4 An apical extracellular matrix associates with posterior lobe cells

In addition to investigating cell autonomous mechanisms leading to increases in tissue thickness, I also sought to identify sources of external forces which could play a role in posterior lobe morphogenesis. Extrinsic roles for the basal and apical extracellular matrix have been established in the pupal wing of *D. melanogaster* (Diaz-de-la-Loza et al., 2018; Etournay et al., 2015; Ray et al., 2015). I first attempted to characterize the basal ECM by analyzing a GFP-tagged version of Collagen IV (Viking:GFP). I observed that Viking:GFP, while present at very early stages of genital morphogenesis, is weakly present during posterior lobe formation across the entire genitalia (Figure 2.9), suggesting that minimal basal ECM is present at this time point. To further test for the presence of basal ECM, I examined another basal ECM component, Perlecan (Perlecan:GFP), and also observed weak signal (Figure 2.9). Together, this data suggests that the basal ECM is globally decreased in the genitalia during early pupal development, such that it is very weak during posterior lobe morphogenesis.

I next sought to determine if an aECM is present, and if so, whether it could potentially influence posterior lobe morphogenesis. A major component of the aECM is Dumpy, which is a gigantic (2.5 MDa) zona pellucida domain-containing glycoprotein (Wilkin et al., 2000). I examined a line in which Dumpy is endogenously tagged with a Yellow Fluorescent Protein (Dumpy:YFP). Dumpy:YFP forms a complex three-dimensional network over the pupal genitalia and is closely associated with cells of the posterior lobe (Figure 2.8; Video 2.3). At certain points in the genitalia, this aECM network of Dumpy can extend up to 39.4 μm on average above the

cells, which is taller than the thickness of posterior lobe cells at the beginning of development (Figure 2.10). The intricate complex morphology of this aECM network is hard to fully appreciate in flattened images due to its three-dimensional shape and spatially varying levels of Dumpy:YFP, making it difficult to see weaker populations of Dumpy without over-saturating more concentrated deposits.

In late pupal wing development, Dumpy anchors the wing to the surrounding cuticle, preventing the tissue from retracting away from the cuticle, which is important to properly shape the wing (Etournay et al., 2015; Ray et al., 2015). This same mechanism has been hypothesized to also occur in the leg and antennae (Ray et al., 2015), however, in the posterior lobe I do not find discrete anchorage points to the cuticle. Instead, I observed a large tether of Dumpy emanating from the anal plate and connecting with the pupal cuticle membrane that encases the entire pupa (Figure 2.11, Video 2.4)(Bainbridge & Bownes, 1981). This tether does not come in direct contact with posterior lobe associated Dumpy or other nearby structures such as the lateral plate, clasper, sheath, or phallus, suggesting that if Dumpy is contributing to posterior lobe evolution and morphogenesis, it is likely through a mechanism which does not depend on a direct mechanical linkage with the overlying pupal cuticle.

To investigate the role that Dumpy may play in posterior lobe morphogenesis, I examined its localization throughout development. Prior to posterior lobe development, future cells of the lobe lack apical Dumpy, and yet an intricate network associated with the clasper is observed (Figure 2.8A). However, from the early stages of posterior lobe development, as it first protrudes from the lateral plate, I observe large deposits of Dumpy associated with future lobe cells (Figure 2.8B). These deposits persist throughout most of its development (Figure 2.8C), becoming more restricted to the apex of the posterior lobe towards the end of posterior lobe development (Figure

2.8D). Throughout development, the posterior lobe associated Dumpy population is connected to the complex network of Dumpy attached to more medial structures such as the phallus (Figure 2.8 A2-D2), indicating that the posterior lobe is interconnected via the aECM with nearby structures (Figure 2.8). In contrast to the posterior lobe, the lateral plate has minimal Dumpy associated with it (Fig. 2.8 A1-D1). Only when I oversaturate the Dumpy:YFP signal can I observe a weak population of Dumpy associated with the lateral plate (Figure 2.12). Together, this indicates that the cells of the posterior lobe and the lateral plate substantially differ in the levels of associated Dumpy, suggesting a potential role in the morphogenesis of the posterior lobe.

2.2.5 Expansion of Dumpy expression is correlated with the evolution of the posterior lobe

The association of the posterior lobe with Dumpy suggests that changes in the expression of *dumpy* may have been significant during the evolution of the posterior lobe. To test if posterior lobe-associated Dumpy is a unique feature of species which produce a posterior lobe, I compared the spatial distribution of its mRNA in *D. melanogaster* with *D. biarmipes,* a species which lacks this structure. Early in pupal genital development at 32 hours APF I observe very similar expression patterns of *dumpy* between *D. melanogaster* and *D. biarmipes*, with expression at the base of the presumptive lateral plate-clasper (Figure 2.13A, Figure 2.14). From 36 to 40 hours APF, when the posterior lobe begins to develop, this pattern becomes restricted to a small region at the base of the lateral plate and clasper, near the anal plate in *D. biarmipes*, but is expanded in lobed species (Figure 2.13B, Figure 2.14). By 44 hours APF, expression of *dumpy* is reduced in the posterior lobe, as well as in non-lobed species, with strongest expression associated with the clasper in *D. biarmipes* (Figure 2.13A-B, Figure 2.14). Overall, these results indicate that expression of *dumpy* is expanded in a lobed species and correlates with the timing of the posterior

lobe's formation. In addition, considering that the developmental timing of *D. biarmipes* lags behind *D. melanogaster* by approximately 4 hours (Figure 2.2), this suggests that *dumpy* expression becomes restricted during an earlier developmental period in the non-lobed species *D. biarmipes*.

Although, it appears that the expression of *dumpy* has expanded in *D. melanogaster*, Dumpy is an extracellular protein, and cells expressing its mRNA may not correlate with its ultimate protein abundance or localization. Since an antibody for Dumpy is not available, I adapted lectin staining protocols which can detect glycosylated proteins like Dumpy in order to compare the distribution of aECM in species which lack posterior lobes. I found that fluorescein conjugated *Vicia villosa* lectin (VVA), which labels *N*-acetylgalactosamine (Tian & Hagen, 2007), approximately recapitulated Dumpy:YFP in *D. melanogaster.* VVA strongly associates with the posterior lobe, shows trace association with the lateral plate, and roughly mirrors the complex three-dimensional shape of the Dumpy aECM network covering the center of the genitalia (Figure 2.13C). When I examined VVA in the non-lobed species *D. biarmipes*, I observed strong VVA signal over the center of the genitalia with weak connections to the tip of the lateral plate, similar to what I observe in *D. melanogaster* (Figure 2.13 C-D). In contrast, I only found a weak strand-like structure emanating from the clasper and connecting to the crevice between the lateral plate and clasper where the presumptive posterior lobe would form (Figure 2.13D). These results correlate with the *in situ* results, where I observe high expression at the center of the genitalia and weak expression of *dumpy* at the base between the clasper and lateral plate in *D. biarmipes*, which may be responsible for forming the weak aECM connection from the clasper to the crevice. Further, I observed similar staining patterns in an additional non-lobed species, *D. ananassae* (Figure 2.15). Collectively, these data suggest that an ancestral aECM network was associated with

the central genital structures, including the phallus, sheath, and clasper, and a weak association in the crevice next to prospective posterior lobe cells. During the course of evolution, expression of *dumpy* has expanded to integrate cells of the posterior lobe, creating a prominent connection to the aECM network.

2.2.6 Dumpy is required for proper posterior lobe formation

Thus far, I observed a strong association of the aECM with cells that form the posterior lobe, a trait which is much less pronounced in non-lobed species. To determine if Dumpy plays a role in posterior lobe formation, I next employed transgenic RNAi to knock down its expression. Previous studies of *dumpy* characterized a VDRC RNAi line that is effective at reducing its function (Ray et al., 2015). I used a driver from the *Pox neuro* gene (Boll & Noll, 2002) to reduce *dumpy* levels in the posterior lobe. This resulted in a drastic decrease in the size and alterations to the shape of the posterior lobe compared to a control RNAi (Figure 2.16). In *dumpy* knockdown individuals, I observe a variable phenotype, and even within single individuals, the severity of phenotype differs between left and right posterior lobes (Figure 2.16A; Figure 2.17). Knockdown was completed at both 25°C and 29°C, as higher temperatures increase the efficacy of the Gal4/UAS system (Duffy, 2002). At higher temperatures, the *dumpy* knockdown phenotype trended towards more severe defects (Figure 2.16B). Together, these results suggest that posterior lobe development is sensitive to levels of *dumpy*, and that *dumpy* plays a vital role in shaping the posterior lobe.

2.2.7 Correlation of Dumpy deposition and cell height in the posterior lobe

I next sought to determine when during development *dumpy* knockdown influences the morphogenetic progression of the posterior lobe. This was important because I observed both a slow and a fast phase of lobe development (Figure 2.1F), and also reasoned that posterior lobe cells secrete cuticle once they have adopted their final adult conformations, of which any of these phases could represent a critical Dumpy-dependent stage of development. I found that *dumpy* knockdown individuals manifest phenotypes very early on (Figure 2.18A) and continue to show abnormal lobe development through the end of its formation (Figure 2.18B). Interestingly, differences in the height of cells on the ventral side of the posterior lobe are not observed between control and *dumpy* knockdown treatments, instead defects in cell height are observed in the more dorsally-localized cells of the posterior lobe (Figure 2.18A-B). This correlates with the phenotypes of the adults in the *dumpy* knockdown in which the ventral tip is usually of normal height with defects observed towards the dorsal side (Figure 2.16A). However, this phenotype appears counterintuitive, as Dumpy protein normally associates along the entire posterior lobe, so why does the ventral side of the posterior lobe develop to normal height when Dumpy is absent? To better understand this phenotype, I examined Dumpy:YFP localization in the *dumpy* knockdown background. I observed weak association of Dumpy with the tallest cells on the ventral side of the posterior lobe both in early (Figure 2.18D n=5/5 samples) and late (Figure 2.18F n=4/5 samples) stages compared to control animals. In contrast, no Dumpy was observed in contact with the short cells on the dorsal side (Figure 2.18D & F). Together, this highlights a correlation between the height of posterior lobe cells and presence of dumpy. One of the late samples lacks a Dumpy connection to the ventral cells, correlating with the observation that not all adult samples are fully extended on the ventral side (Figure 2.19). This suggests that ventral cell connections to the Dumpy

aECM network may be lost late in development, ultimately causing a shortening of these cells. In addition, I observed more severe phenotypes of *dumpy* knockdown in the *dumpy-yfp* background (compared to the *dumpy*-WT background alone), suggesting that Dumpy:YFP is a mild hypomorph (not shown). I also observed at early time points highly variable strands of Dumpy in the middle of the lobe (between the ventral and dorsal sides) (Figure 2.20). These strands visually resembled the weak strands of VVA observed in *D. biarmipes* (Figure 2.13D), in that they emanate from the clasper and connect to the crevice between the posterior lobe and clasper. Overall, the most pronounced phenotypic defects manifest in regions with the strongest reduction in Dumpy aECM deposition, implying that Dumpy's presence is required for posterior lobe cells to elongate and project from the lateral plate.

2.3 Discussion

Here, I determined how a morphological novelty forms at the cellular level, and in doing so, revealed distinctive cell and aECM interactions underlying its development and evolution. I identified how an extreme change in the shape of cells in the developing posterior lobe accounts for its novel morphology. While intrinsic cytoskeletal components may contribute to this process, these results highlight the critical role played by a vast extrinsic network of ECM on the apical side of the epithelium. It was unexpected that such an elaborate supercellular matrix structure would participate in the evolution of a seemingly simple novelty. Below, I consider the potential roles played by the aECM in posterior lobe development and diversification, and discuss how studies of morphogenesis can illuminate the simple origins of structures that might otherwise seem impossibly complex to evolve.

2.3.1 Potential mechanisms for aECM-mediated control of cell height in the posterior lobe

This work demonstrates an important role for the aECM protein, Dumpy, in the growth of the posterior lobe, as exhibited by the dramatic phenotypes in the *dumpy* RNAi background and the strong association of Dumpy:YFP with only the tallest cells in these experiments. This data is consistent with three possible mechanisms. First, Dumpy could serve as a structural support while autonomous cell mechanical processes drive apico-basal elongation. Second, the cells of the posterior lobe could be pulled mechanically through their connection to the Dumpy aECM. This process could operate passively, deforming cells of the lobe, but could also drive changes in the cytoskeleton in response to external tensions. Finally, the aECM could play a direct role by altering cell signaling dynamics, as has been exhibited by the basal ECM (Kirkpatrick, Dimitroff, Rawson, & Selleck, 2004; Kreuger, Perez, Giraldez, & Cohen, 2004; X. Wang, Harris, Bayston, & Ashe, 2008). Previous research has shown that the JAK/STAT pathway is important for posterior lobe development (Glassford et al., 2015), and their ability to signal to the correct cells could be altered in the absence of Dumpy. Of course, these models are not mutually exclusive and some combination of these mechanisms may be integrated to shape the posterior lobe. The observation of increased cytoskeletal components in posterior lobe cells and the reduced height of cells that lack Dumpy in the knockdown experiments are consistent with all three mechanisms, which are difficult to differentiate experimentally. When I examine morphogenesis in non-lobed species, I observed that the lateral plate drops below the clasper (Figure 2.2). Assuming this ancestral process still occurs in lobed species, it is quite possible that the aECM 'holds' cells of the posterior lobe during the early stages of posterior lobe development while the lateral plate is pulled down, causing cells of the posterior lobe to elongate to relieve the stress. Future manipulative biomechanical studies will be required to explore these possibilities.

2.3.2 The role of aECM in the diversification of genital structures

Genitalia represent some of the most rapidly diversifying structures in the animal kingdom, and these results suggest the aECM may participate in the modification of *Drosophila* genital structures. The shape of the posterior lobe is extremely diverse among species of the *melanogaster* clade (Coyne, 1993). These results demonstrate that reducing the levels of Dumpy can affect the shape of the posterior lobe, with extreme knockdown phenotypes approximating the posterior lobe of *D. mauritiana*. Furthermore, the clasper and phallus show dense deposits of Dumpy, suggesting that the aECM could play important roles in diversifying these remarkably variable structures. During the course of evolution, one could imagine that by altering which cells are connected to the aECM, the strength of those connections, or the forces acting on those connections could lead to changes in morphological shape. Hence identifying causative genes that differentiate these structures could uncover novel mechanisms for genetically controlling the behavior of this aECM and behaviors of cells bound to this dynamic scaffold.

2.3.3 Integrating cells into a pre-existing aECM network to generate morphological novelty

In comparing the morphogenesis of a novel structure to close relatives which lack it (representing a proxy for the ancestral state), I identified a likely path by which the aECM became associated with the posterior lobe. The aECM, while understudied, has been implicated in the morphogenesis of many structures (Diaz-de-la-Loza et al., 2018; Dong et al., 2014a; Etournay et al., 2015; Fernandes et al., 2010; Heiman & Shaham, 2009; Low et al., 2019; Ray et al., 2015), and yet, its role during the evolution of novel structures is largely unexplored. I find a conserved

aECM network associated with central genital structures (clasper, sheath, and phallus) in both lobed and non-lobed species. In non-lobed species, *dumpy* is expressed weakly at the base between the lateral plate and clasper resulting in a thin connection of aECM from clasper to the crevice (Figure 2.21). By contrast, lobed species express high levels of *dumpy* between the presumptive posterior lobe and clasper, resulting in large amounts of aECM in the crevice. I hypothesize that this increase in aECM allows cells at the base of the lateral plate to be integrated into this ancestral aECM network (Figure 2.21), a step which was likely significant to the evolution of the posterior lobe. Overall, this suggests that the aECM could be an unexpected target for generating novel anatomical structures.

The expanded *dumpy* expression I observed caused us to consider how the posterior lobe gained this aECM attachment. Interestingly, previous work found a gene regulatory network (GRN) that regulates development of an ancestral embryonic structure, the posterior spiracles, which was co-opted during the evolution of the posterior lobe and regulates its development (Glassford et al., 2015). Previous work has shown that *dumpy* is expressed in the posterior spiracles (Wilkin et al., 2000), and I have observed a thin tether of Dumpy:YFP connecting the posterior spiracles to the surrounding embryonic cuticle (Figure 2.22Ff). This is consistent with previously identified roles for Dumpy in epithelia-cuticle attachment in the wing (Etournay et al., 2015; Ray et al., 2015) and hypothesized role in the muscle, leg, and antenna (Ray et al., 2015; Wilkin et al., 2000). Identification of regulatory elements which activate *dumpy* in the posterior lobe will be necessary to determine whether its role in the posterior spiracle was relevant to the evolution of expanded genital expression.

Evolution is thought to act through the path of least resistance. When confronted with the remarkable diversity of genital morphologies present in insects, one must wonder how the intricate

projections, bumps, and divots form in its underlying epithelia. Models of co-option have been appealing because they establish pre-existing mechanisms in place that can be rapidly ported to new locations to generate massive changes in a tissue. My examination of the cellular processes during posterior lobe morphogenesis highlights a different way that co-option may work. Here, the aECM mechanism I uncovered appears to be a path of least resistance because this tissue already uses a vast network of aECM to potentially pattern other structures, such as the phallus and its multiple elaborations (Kamimura, 2010; Peluffo et al., 2015; Rice et al., 2019). Because this network of aECM represents a pre-existing condition, it is easy to appreciate how cells of the posterior lobe could evolve novel extracellular connections to this network to generate a new protrusion. On the other hand, tissues which lack such an ancestral network may well be less likely to evolve projections through this mechanism. While the aECM is required for this morphogenetic process, I envision that additional networks and processes must be contributing to the full morphogenesis of the posterior lobe. Determining genetic changes which underlie such remarkable cellular responses represents a major looming challenge in evo-devo research (S. J. Smith, Rebeiz, & Davidson, 2018).

2.4 Figures and videos

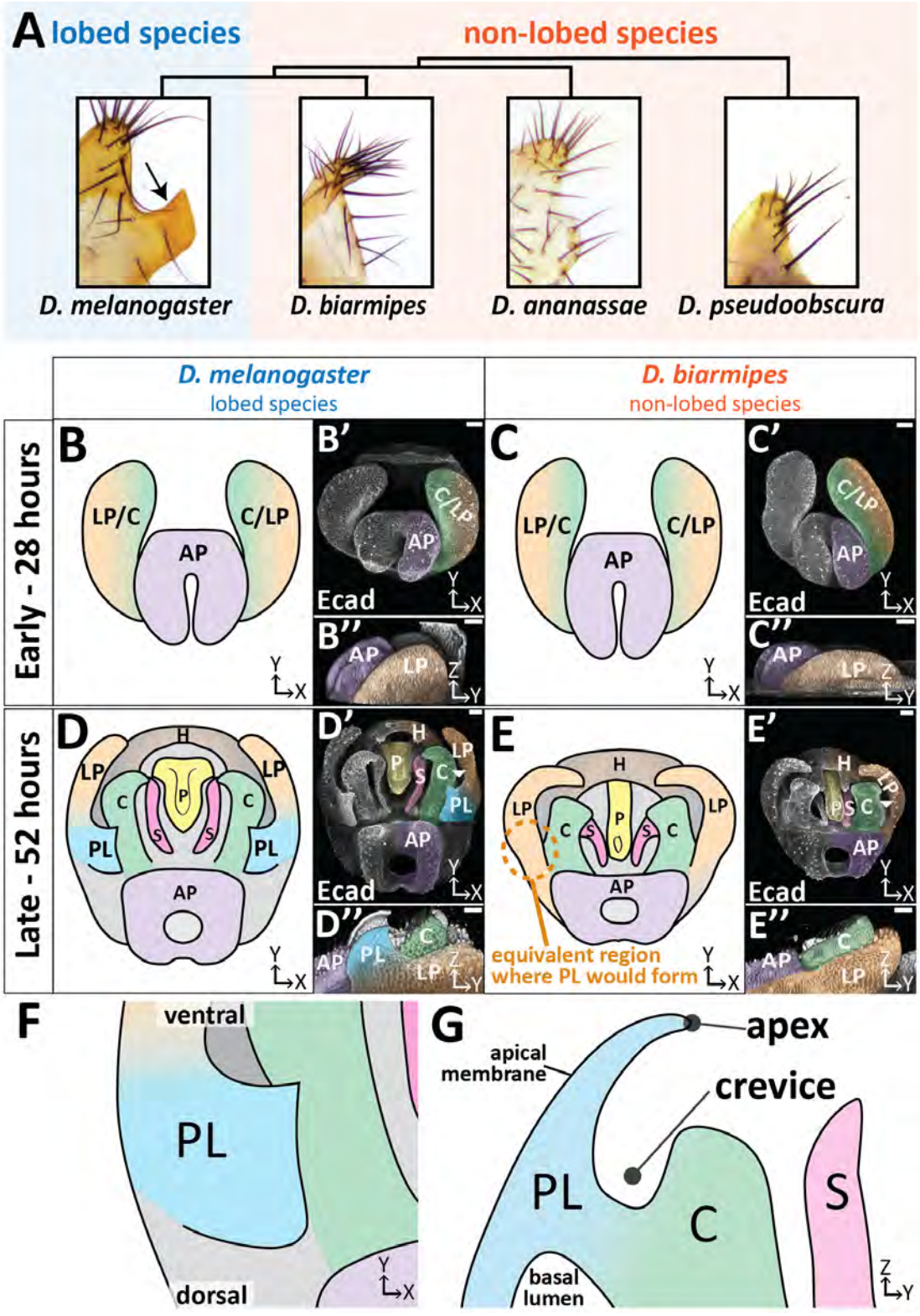

Figure 2.1 The posterior lobe a novel protrusion from the lateral plate of D. melanogaster.

(A) Phylogenetic tree with representative bright-field images of adult cuticle of the lateral plate and posterior lobe (arrow). (B-E) Illustration, (B'-E') maximum projection, and (B''-E'') three-dimensional projection of early (28 hours APF) and late (52 hours APF) developing genitalia showing the posterior lobe projecting form the lateral plate of *D. melanogaster* (D''), but absent in *D. biarmipes* (E''). Relevant structures are labeled: posterior lobe (PL), lateral plate (LP), clasper (C), sheath (S), phallus (P), anal plate (AP), and hypandrium (H). All max projections are oriented with ventral side towards to top and dorsal sides towards the bottom. (F) Zoomed in illustration of posterior lobe and (G) a cross-sectional/lateral view of the posterior lobe. The highest point of the lobe is the apex and the invagination between the lobe and the clasper is termed the crevice (G). Scale bar, 20μm.

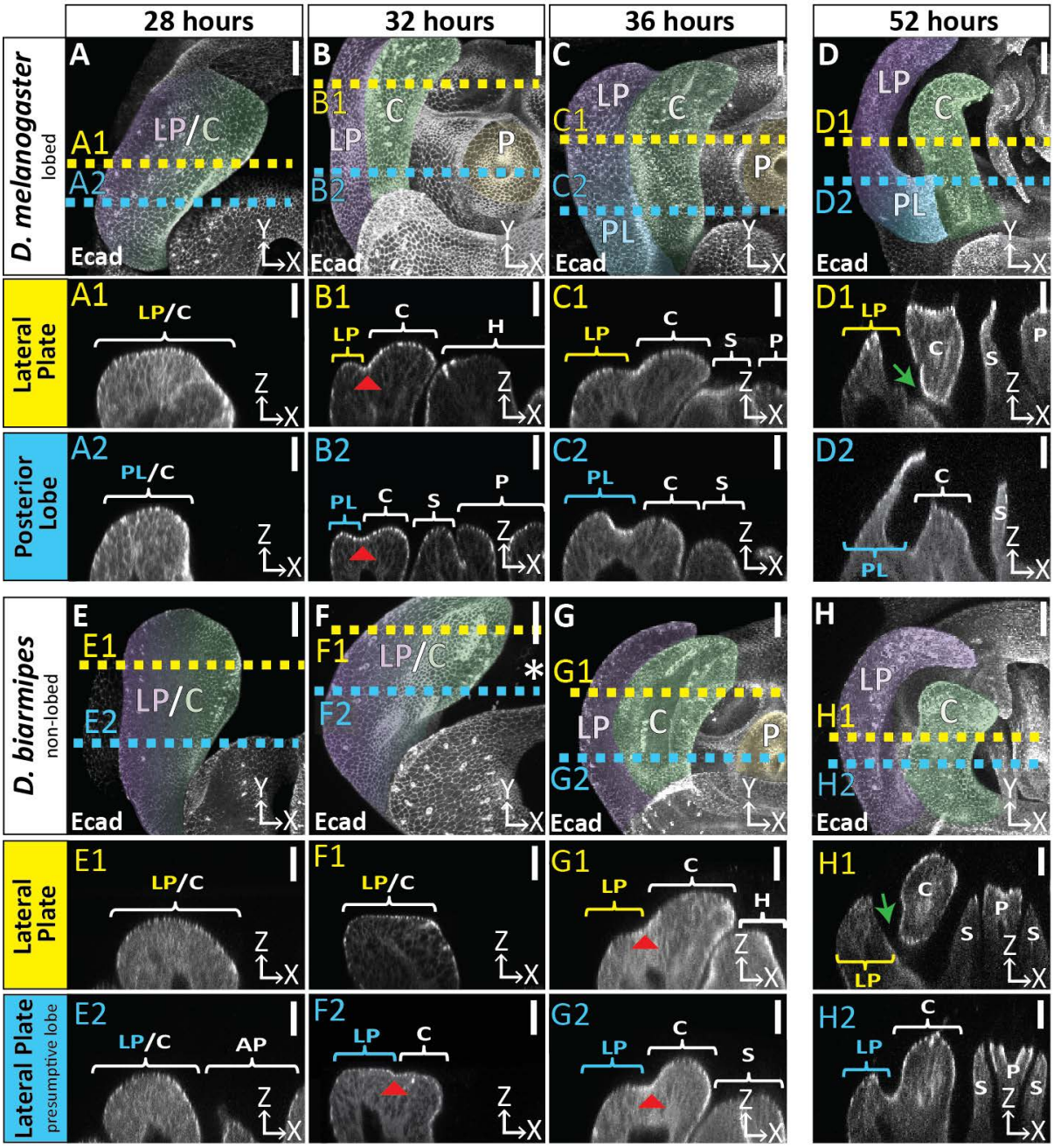

Figure 2.2 Developmental timing of lobed vs non-lobed genitalia.

Developmental time course of the lobed species *D. melanogaster* (A-D) and the non-lobed species *D. biarmipes* (E-H) with E-cadherin label. Location of respective cross sections indicated in yellow for lateral plate and blue for posterior lobe (*D. melanogaster)* or equivalent location in non-lobed species (*D. biarmipes*). Relevant structures are labeled: posterior lobe (PL), lateral plate (LP), clasper (C), sheath (S), and phallus (P). Scale bar, 20μm. At 28 hours

APF the genitalia looks relatively similar between *D. melanogaster* (A-A2) and *D. biarmipes* (E-E2). At 32 hours APF in *D. melanogaster* the clasper and lateral plate have fully begun to cleave (B1-2 red arrowhead=cleavage), the lateral plate is lower than the clasper (B1), and the hypandrium, sheath, and phallus have fully everted and are neighboring the clasper and lateral plate (B1-2). *D. biarmipes* lags behind approximately 4 hours. At 32 hours APF there is slight cleavage near the dorsal side of the lateral plate and clasper (F2 red arrowhead), but no cleavage has occurred at the ventral side (F1). In addition, the sheath, hypandrium, and phallus have not everted yet (F1-2). At 36 hours APF in *D. biarmipes,* cleavage has begun along the full length of the lateral plate and clasper (G1-2 red arrowhead), the lateral plate is lower than the clasper (G1-2), and the hypandrium, sheath, and phallus have everted and are next to the lateral plate and clasper (G1-2). As development proceeds later at 52 hours APF the lateral plate and clasper fully separate at the ventral side of the genitalia in both *D. melanogaster* (D1 green arrow) and *D. biarmipes* (H1 green arrow). Full cleavage does not span the length of the lateral plate and clasper (D2 and H2) and stops right before the posterior lobe forms (D2) and also stops before reaching the very dorsal side of the lateral plate and clasper in *D. biarmipes* (H2).

Video 2.1 The posterior lobe protrudes from the lateral plate.

Three-dimensional projections of *D. biarmipes* (left) and *D. melanogaster* (right) samples at 52 hours APF labeled with E-cadherin.

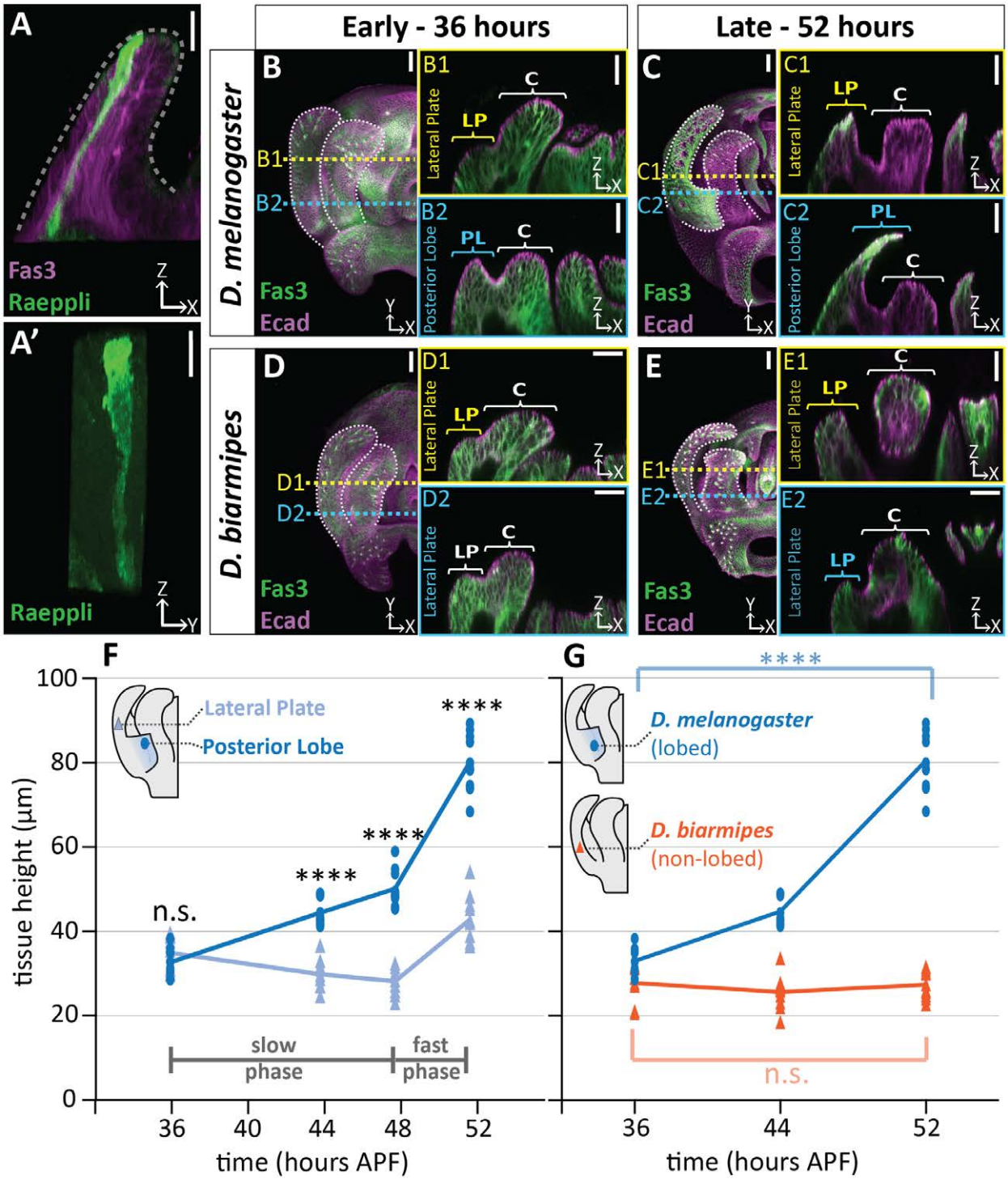

Figure 2.3 Posterior lobe cells increase in height to project out from the lateral plate.

(A) A single cell in the posterior lobe labeled with Raeppli-mTFP1 (green) spans the height of the tissue labeled with lateral membrane marker fasciclin III (Fas3, magenta). Apical side of posterior lobe identified with dotted line. Sample

is 44h after pupal formation (APF), but was heat shocked for 1 hour at 24h APF causing it to develop faster and more closely resembles a 48h APF sample. Scale bar, 10μm. n=4 (B-E) Maximum projections of early (36h APF) and late (52h APF) genital samples labeled with Fas3 (lateral membranes, green) and E-Cadherin (apical membranes, magenta). Location of respective cross sections indicated in yellow for lateral plate (B1-E1) and blue for posterior lobe (*D. melanogaster)* (B2-C2) or equivalent location in non-lobed species (*D. biarmipes*) (D2-E2). Scale bar, 20μm. (F) Quantification of tissue thickness of the lateral plate (light blue) and posterior lobe (dark blue). Illustration represents approximate location of cross-section that was used for tissue height measurement. Individual data points a presented; n=10 per each time point. (G) Quantification of tissue thickness of the posterior lobe in *D. melanogaster* (dark blue) and equivalent location in non-lobed species *D. biarmipes* (orange). Illustration represents approximate location of cross-section that was used for tissue thickness measurement. Individual data points presented with line representing the mean; n≥9 per each time point. Statistical significance is indicated (paired t-test for F and unpaired t-test for G; ****p≤0.0001; n.s.=not significant p≥0.05). *D. melanogaster* tissue height measures in (G) are replotted from (F) to facilitate direct comparisons with *D. biarmipes.*

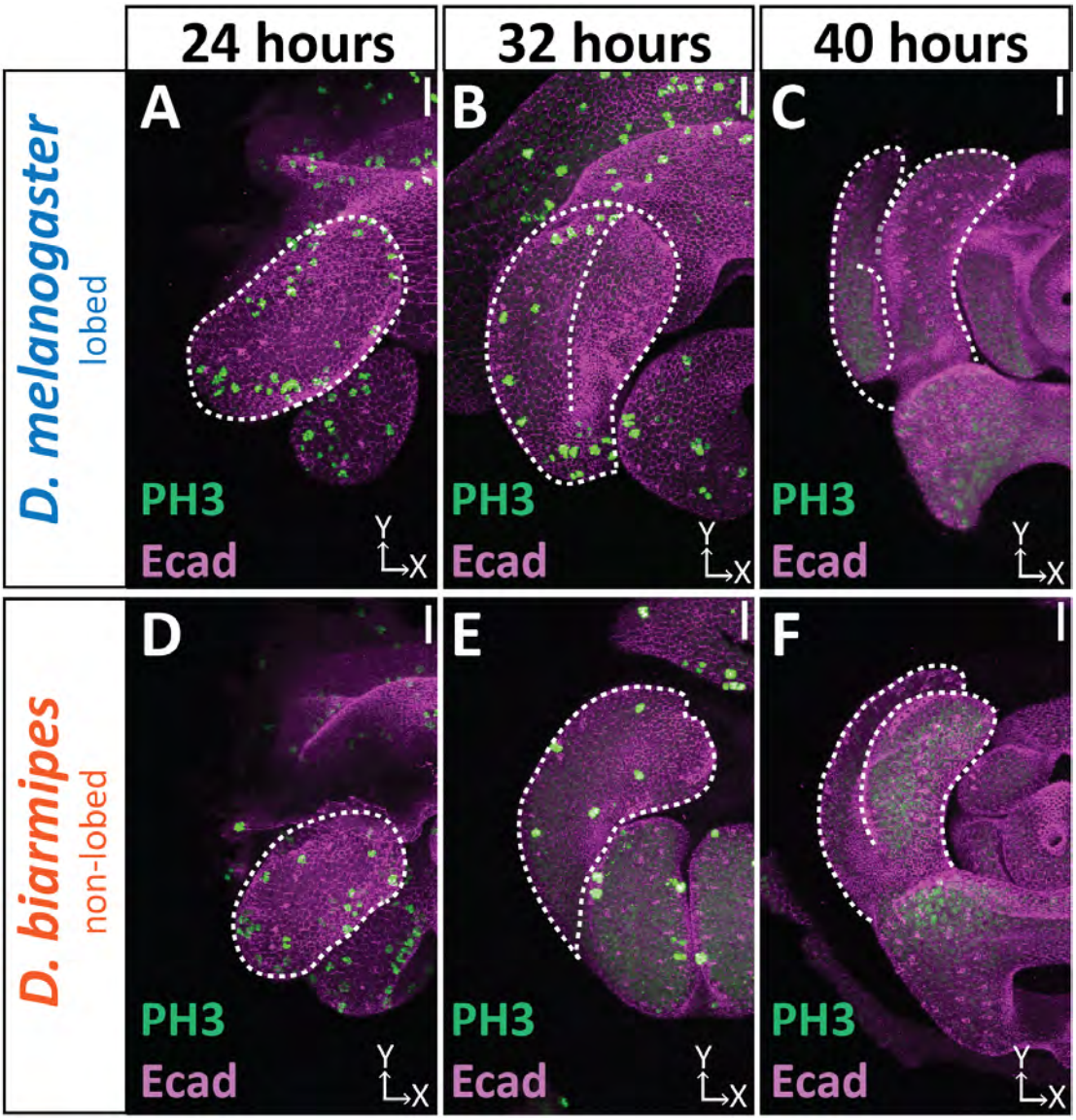

Figure 2.4 Cell division dynamics do not differ between lobed and non-lobed species.

Developmental time course with Phospho-Histone H3 (Ser 10) (PH3; green) labeling actively dividing cells and Ecad (magenta) labeling the apical membrane of the tissue. Only superficial slices are shown to avoid fat body signals beneath lateral plate and clasper. n ≥ 3 per each time point. Scale bar, 20μm. In both *D. melanogaster* and *D. biarmipes* cell division is widespread at 24 hours APF (A & D). Cell division is decreased by 32 hours APF (B & E). By 40 hours APF no cell division is occurring (C & F).

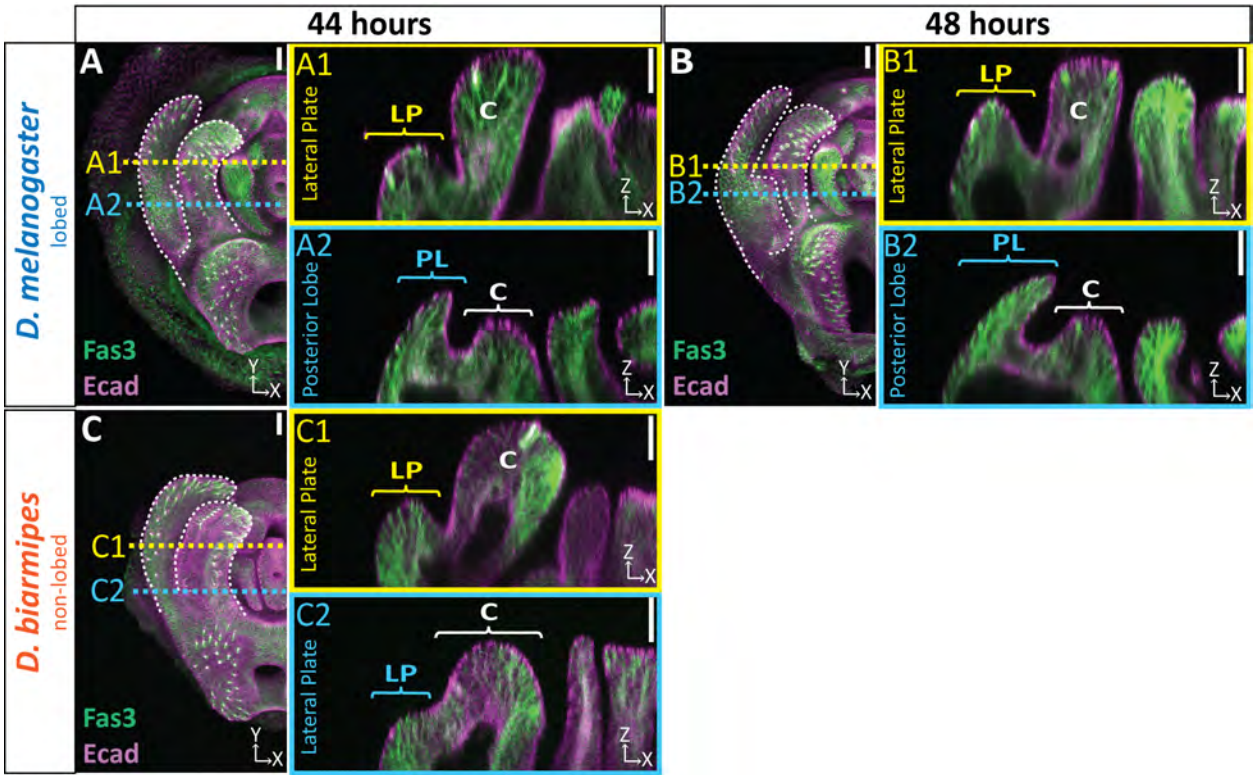

Figure 2.5 Extended time course of tissue thickness in lobed and non-lobed species.

Extended time course for samples quantified in Figure 2F-G. (A-C) Max and cross-section view of 44 hours APF (A & C) and 48 hours APF (B) genital samples with lateral membrane labeled with Fas3 (green) and apical membrane labeled with Ecad (magenta). Location of respective cross sections indicated in yellow for lateral plate (A1-C1) and blue for posterior lobe (*D. melanogaster*) or equivalent location in non-lobed species (*D. biarmipes*) (A2-C2). n≥ 9 per experiment. Scale bar, 20μm.

Video 2.2 Minor cell rearrangement during posterior lobe development.

Live imaging of posterior lobe development with GFP tagged armadillo (apical membrane marker) illustrating a cell dropping from the apical surface and a neighboring cell filling in the gap. Imaging starts at approximately 36 hours APF. Due to uncontrolled temperatures during imaging that were cooler than normal growing conditions, the posterior lobe develops slower and the time indicated is not comparable to other images in the manuscript which were all grown under controlled settings. Based on the thickness of the posterior lobe at the end of the movie the posterior lobe is between 48 to 52 hours APF. Cells were tracked manually and indicated with colored dots. Some dots disappear towards the end of the movie as they become difficult to track due to the signal from cells on the medial side of the posterior lobe.

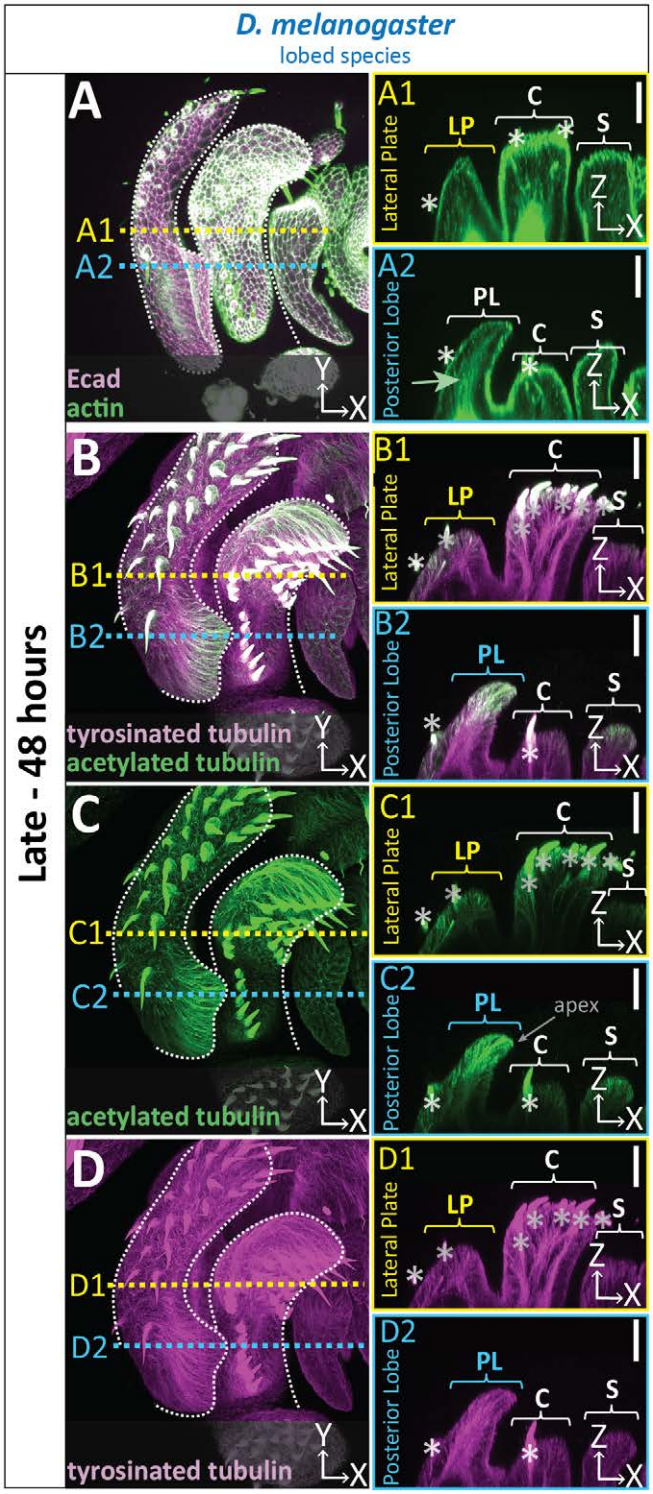

Figure 2.6 Cytoskeletal components are concentrated in posterior lobe cells.

(A-D) Maximum projection, and respective cross-sections of late (48h APF) genital samples of the lobed species *D. melanogaster* labeled with F-actin/phalloidin and Ecad (A), acetylated tubulin (B,C), and tyrosinated tubulin (B,D). Location of respective cross sections indicated in yellow for lateral plate (A1-D1) and blue for posterior lobe (A2-D2). Cross-sections are maximum projections of a restricted 5.434μm thick section to provide a complete view of cytoskeletal components along the apico-basal axis. All cross-sections are oriented with apical side at the top and basal side at the bottom. Asterisk identifies bristles which have high levels of F-actin and tubulin. Bright basal signal in A1 and A2 are fat bodies. Bottom layers were removed in panel A to remove fat body signal which overwhelmed other details. (B-D2) Panels C and D show separate channels of panel B. Relevant structures labeled: Posterior lobe (PL), lateral plate (LP), clasper (C), and sheath (S). Scale bar, 20μm. n≥ 3 per experiment.

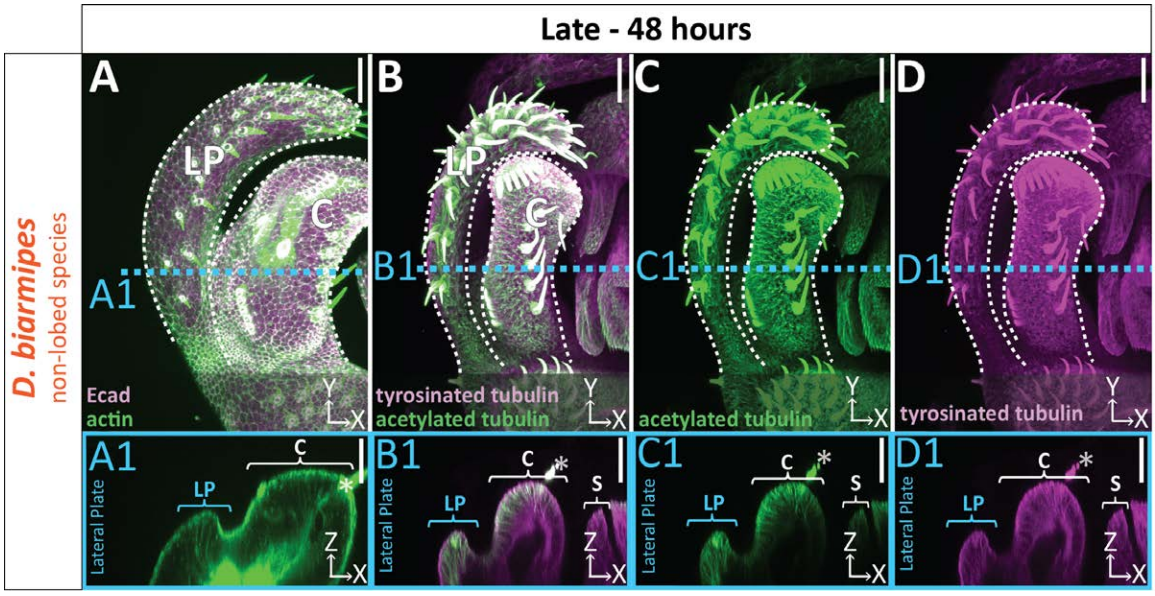

Figure 2.7 Uniform distribution of cytoskeletal components in non-lobed species.

(A-D) Max projections of late (48h APF) genital samples of non-lobed species *D. biarmipes* labeled with F-actin/phalloidin and Ecad (A), acetylated tubulin (B,C), and tyrosinated tubulin (B,D). Location of respective cross sections indicated in blue for presumptive posterior lobe cells (A1-D1). Cross-sections are maximum projection of a restricted 5.434µm thick section to display the full view of the cytoskeleton along the apico-basal axis. All cross-sections are oriented with apical side at the top and basal side at the bottom. Asterisk identifies bristles which have high levels of F-actin and tubulin. Bright basal signal in A1 are fat bodies. Bottom layers were removed in panel A to avoid fat body signal which masked other details. Panels C and D show separate channels of panel B. Relevant structures labeled: Lateral plate (LP), clasper (C), and sheath (S) labeled. Scale bar, 20µm. n≥ 3 per experiment.

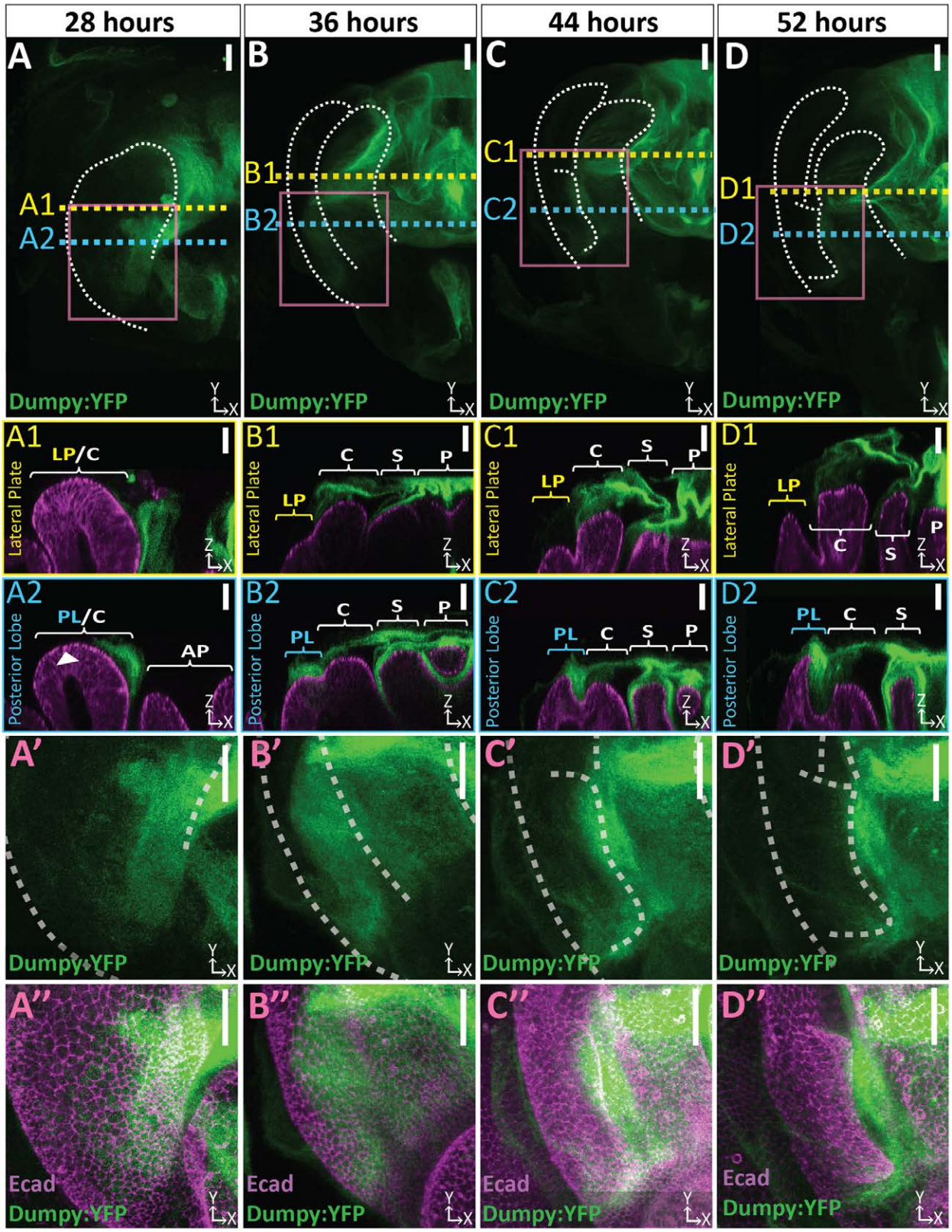
28 hours
36 hours
44 hours
52 hours
A
B
C
D
A1
A2
B1
B2
C1
C2
D1
D2
Dumpy:YFP
A1
LP/C
Lateral Plate
B1
C
S
P
LP
C1
D1
A2
PL/C
AP
Posterior Lobe
B2
PL
C2
D2
A'
B'
C'
D'
A''
B''
C''
D''
Ecad
Dumpy:YFP

Figure 2.8 Dumpy deposition is correlated with posterior lobe development.

(A-D) Maximum projection and (A'-B'') respective zoom, indicated with pink box, labeled with Dumpy:YFP (green) and Ecad (magenta) for each time point. Location of respective cross sections indicated in yellow for lateral plate (A1-D1) and blue for posterior lobe (A2-D2). Arrowhead in (A2) indicates future posterior lobe cells. Cross-sections are oriented with apical side at the top and basal side at the bottom. Relevant structures labeled: Posterior lobe (PL), lateral plate (LP), clasper (C), sheath (S), and phallus (P). Scale bar, 20μm. n≥ 4 per experiment. Images were independently brightened to show relevant structures.

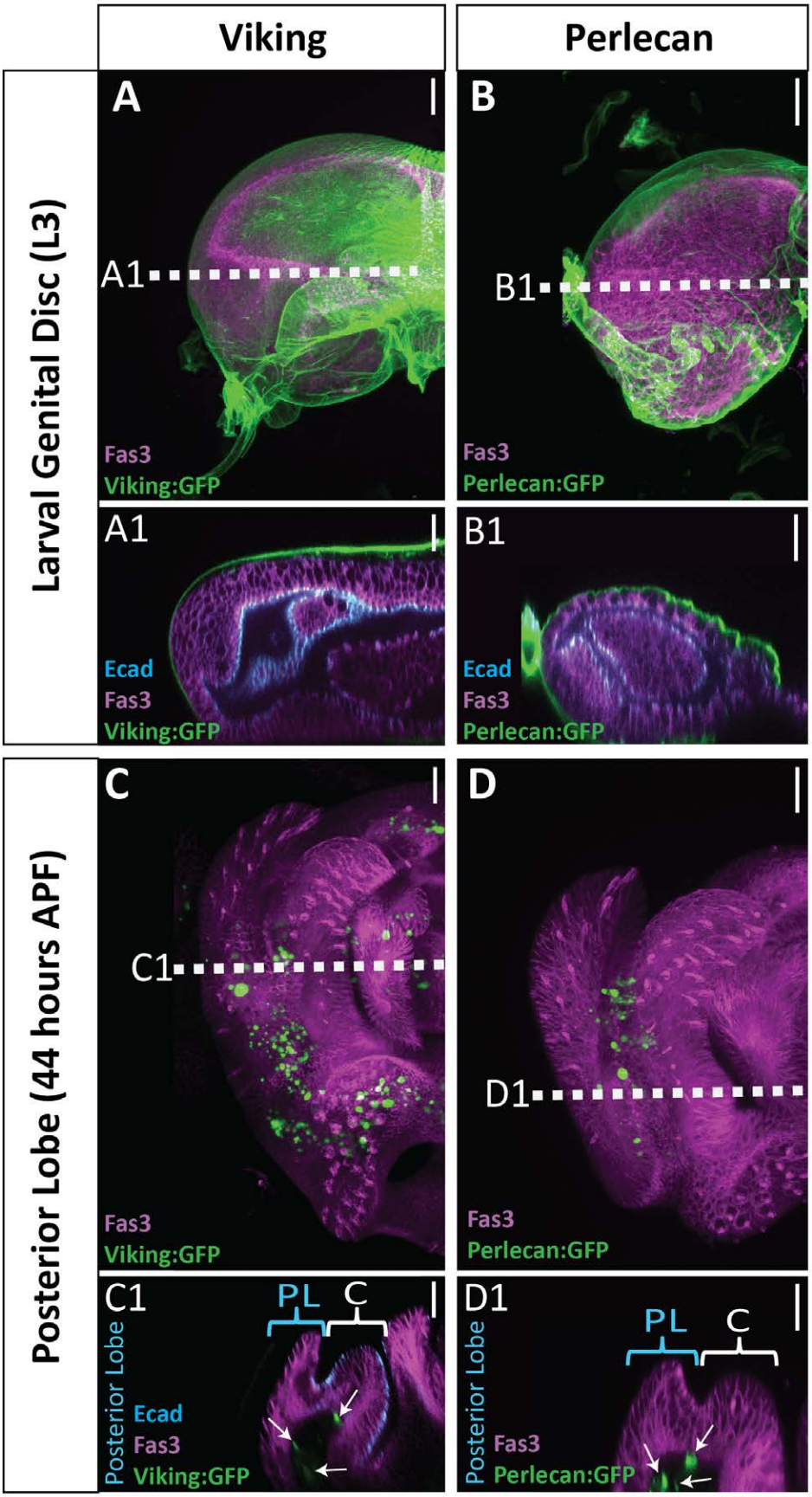
Viking
Perlecan
Larval Genital Disc (L3)
A
A1
Fas3
Viking:GFP
B
B1
Fas3
Perlecan:GFP
A1
Ecad
Fas3
Viking:GFP
B1
Ecad
Fas3
Perlecan:GFP
Posterior Lobe (44 hours APF)
C
C1
Fas3
Viking:GFP
D
D1
Fas3
Perlecan:GFP
C1
PL
C
Posterior Lobe
Ecad
Fas3
Viking:GFP
D1
PL
C
Posterior Lobe
Fas3
Perlecan:GFP

Figure 2.9 Limited basal ECM present during posterior lobe morphogenesis.

Basal ECM markers Collagen IV (Viking:GFP; green)(A & C) and Perlecan (Perlecan:GFP; green) (B & D) in L3 larval genital disc (A & B) and in 44 hours APF genitalia (C & D). Image settings were the same for each marker between larval and pupal samples. Sporadic dots observed are fat bodies (white arrows in cross section), which fill the basal lumen of the pupal genital epithelium. Location of respective cross sections indicated in white. Cross-sections for larval samples are oriented basal sides out, as the disc has not yet everted. Pupal samples are oriented with apical side at the top and basal side at the bottom. Higher amounts of basal ECM are observed in larvae compared to 44 hour APF genital samples. Relevant structures labeled: Posterior lobe (PL) and clasper (C). Scale bar, 20μm.

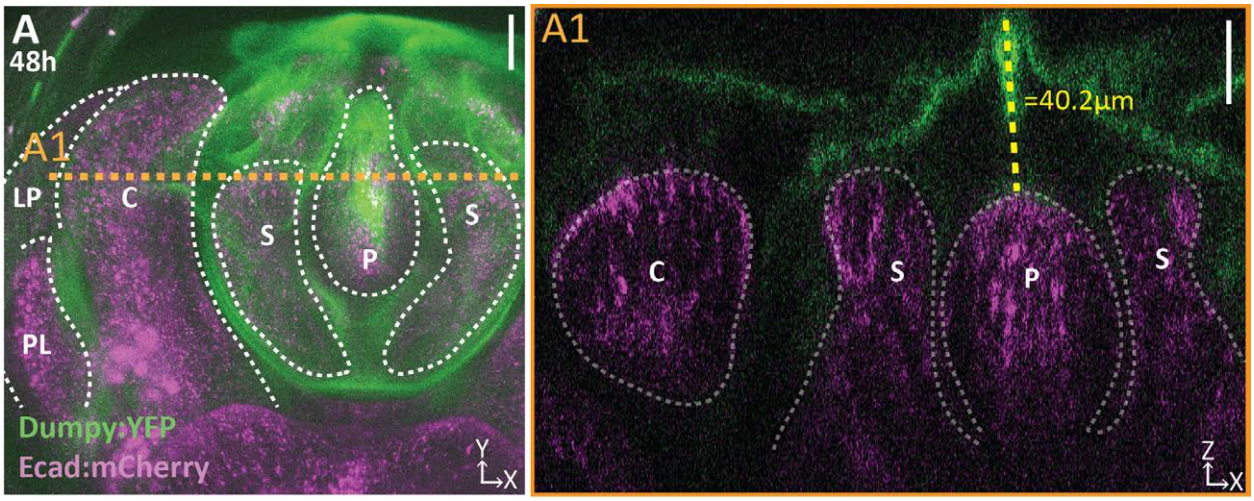

Figure 2.10 Dumpy extends above the apical surface of the phallus.

(A) Projection of Dumpy:YFP (green) and Ecad:mCherry (magenta) imaged live at 48 hours APF. Location of respective cross sections indicated in orange. (A1) Cross section showing extent of Dumpy:YFP observed above the surface of the genitalia. Relevant structures labeled: Posterior lobe (PL), lateral plate (LP), clasper (C), sheath (S), and phallus (P). Scale bar, 20µm. n=3.

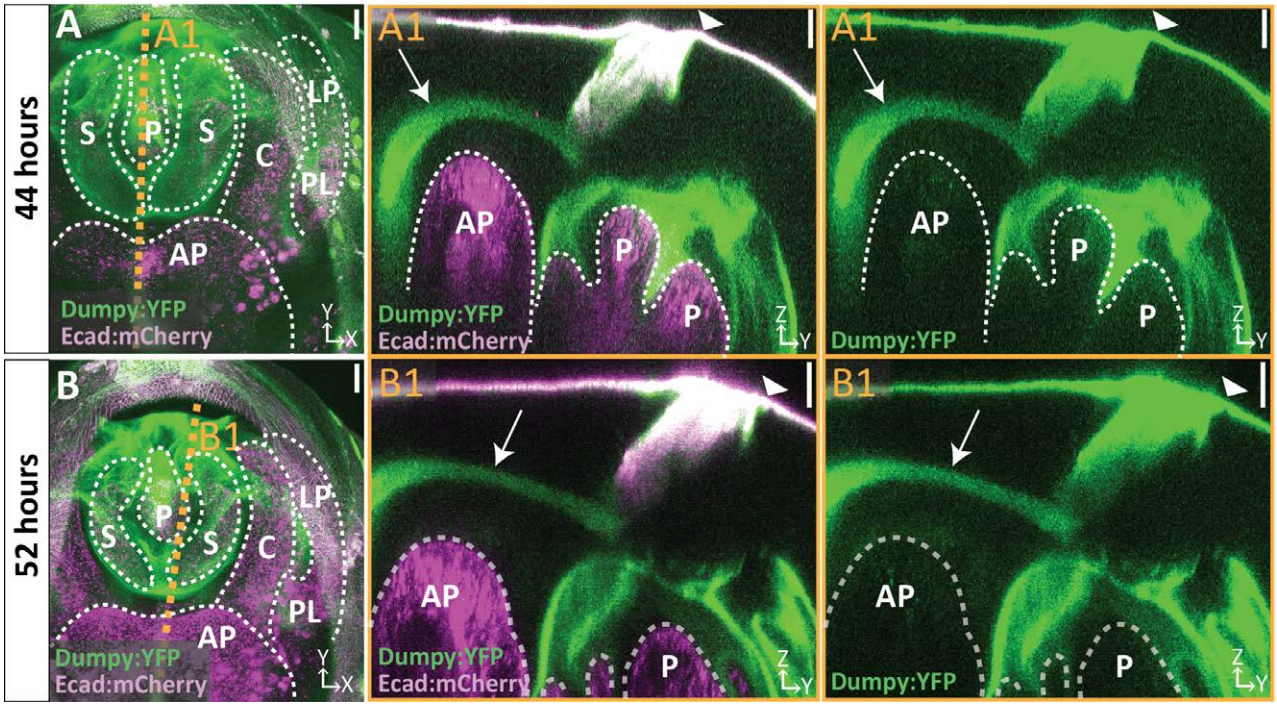

Figure 2.11 A tether of Dumpy connects the genitalia to the pupal cuticle membrane that encases the developing pupa.

(A-B) Live imaging of Dumpy:YFP (green) and Ecad:mCherry (magenta) at respective time points. Location of respective cross sections indicated in orange. (A1-B1) Cross-sections are max projection of a 4.94µm (A1) and 1.73µm (B1) thick section to show full tether (arrow) and its connection to the cuticle (arrowhead) and anal plate. All cross-sections are oriented with apical side at the top and basal side at the bottom. Relevant structures labeled: Posterior lobe (PL), lateral plate (LP), clasper (C), sheath (S), phallus (P), and anal plate (AP). Scale bar, 20µm. n=1 per each time point.

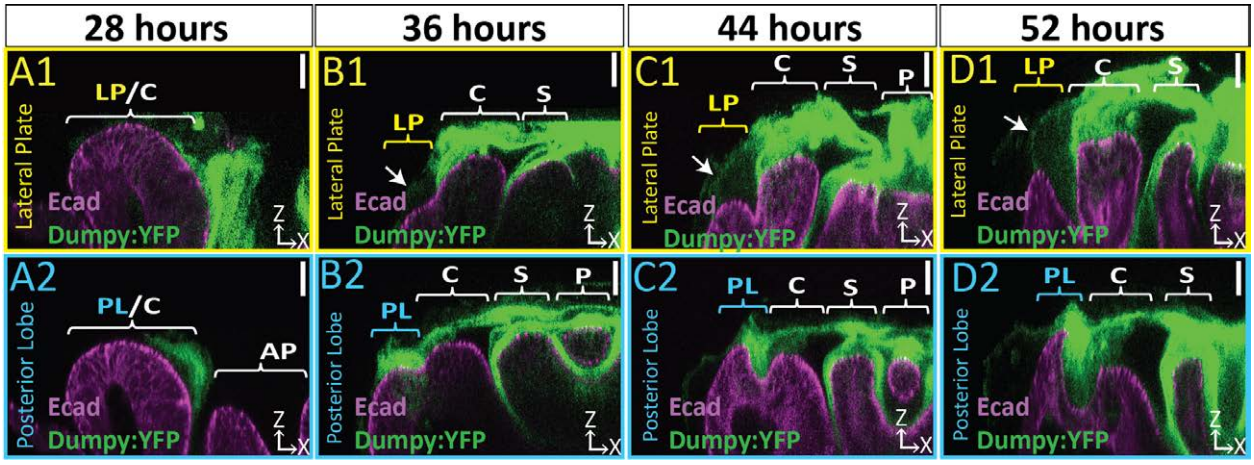

Figure 2.12 The Dumpy aECM network extends weak connection to lateral plate.

(A-D) Brightened images of respective cross sections from Figure 2.3 of lateral plate (A1-D1) in yellow and posterior lobe in blue (A2-D2). Cross-sections are oriented with apical side at the top and basal side at the bottom. Relevant structure labeled: Posterior lobe (PL), lateral plate (LP), clasper (C), sheath (S), and phallus (P). Scale bar, 20μm. n≥ 4 per experiment. Images were overexposed to show relevant structures.

Video 2.3 Three-dimensional structure of the genital Dumpy aECM network.

Part 1 of the movie shows 3D rotation of 52 hour APF genital sample with Dumpy:YFP (green) and E-cadherin (magenta) labels. Part 2 of the movie shows a cross-sectional view starting at the ventral side of the posterior lobe and moving towards the dorsal side of the posterior lobe and part 3 shows the same view but starting at the ventral tip of the lateral plate and moving towards the ventral side of the posterior lobe. In the upper-right corner there is a guide that roughly depicts the running location of the cross section. Cross-sections are oriented with apical side at the top and basal side at the bottom. Relevant structures labeled: Posterior lobe (PL), lateral plate (LP), clasper (C), sheath (S), and phallus (P).

Video 2.4 A tether of Dumpy connects the genitalia to the surrounding cuticle.

3D rotation of Dumpy:YFP (green) and Ecad:mCherry (magenta) imaged live at 44 hours APF. Relevant structures labeled: Posterior lobe (PL), lateral plate (LP), clasper (C), sheath (S), phallus (P), and anal plate (AP).

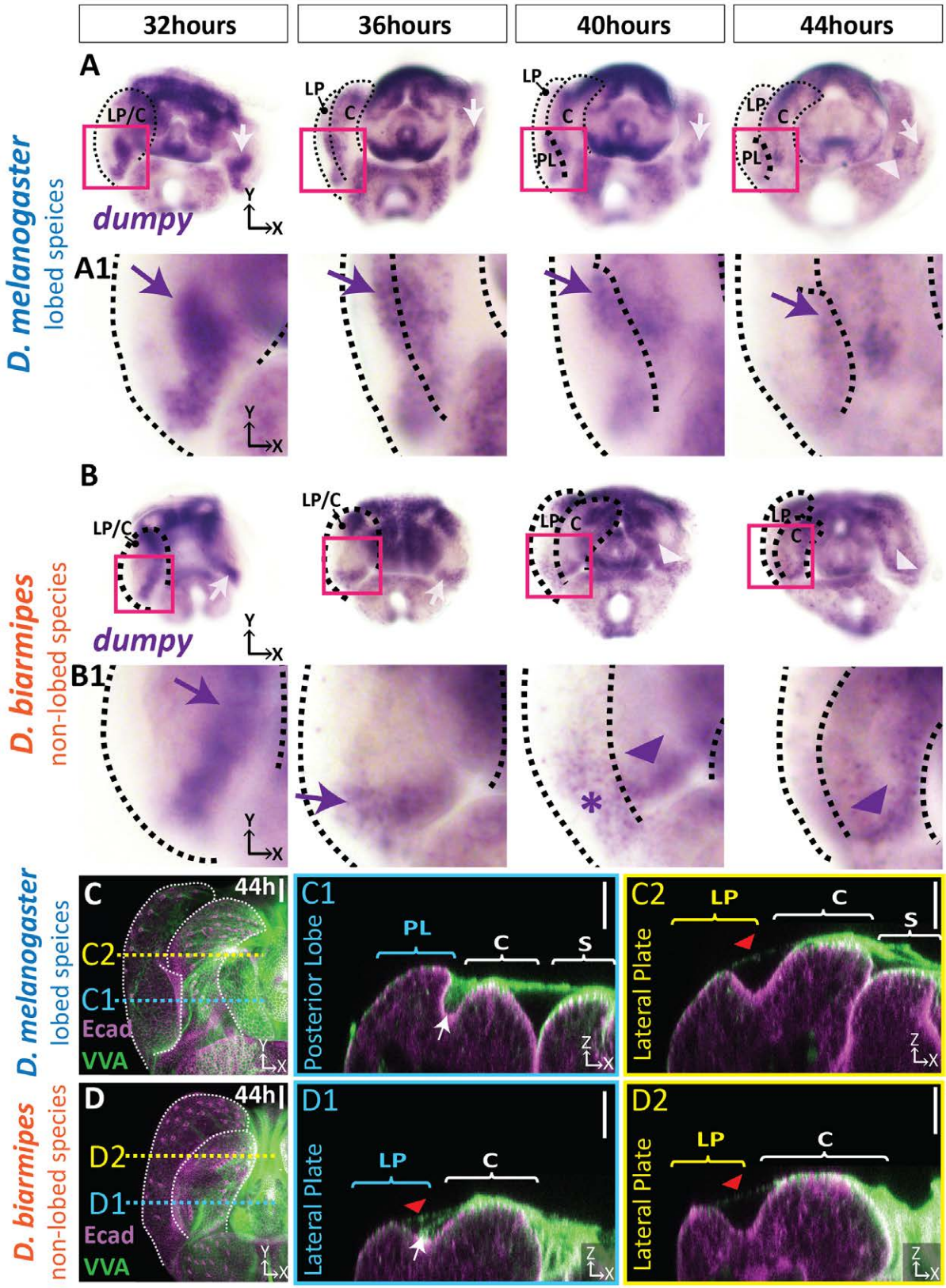
32hours
36hours
40hours
44hours
D. melanogaster
lobed speices
D. biarmipes
non-lobed species
A
A1
B
B1
LP/C
LP
C
PL
dumpy
Y
X
C
C1
C2
D
D1
D2
44h
Ecad
VVA
Z
PL
S
Posterior Lobe
Lateral Plate

Figure 2.13 aECM is spatially expanded in lobed species compared to non-lobed species.

(A-B) *in situ* hybridization for *dumpy* mRNA in the lobed species *D. melanogaster* (A) and the non-lobed species *D. biarmipes* (B). Pink box outlines location of zoom in for A1 and B1. Posterior lobe associated expression highlighted with arrow (purple/white) for strong expression, asterisk for weak expression, and arrowhead for clasper-specific expression. Expression observed in *D. melanogaster* at 44 hours APF is not present in all samples (see Figure 2.14). (C-D) aECM is labeled with *Vicia villosa* lectin (VVA; green) and apical membrane labeled with Ecad (magenta) at 44 hours APF in *D. melanogaster* (C) and *D. biarmipes* (D). Location of respective cross sections indicated in yellow for lateral plate (C2-D2) and blue for posterior lobe in *D. melanogaster* (C1) and corresponding position in *D. biarmipes* (D1). All cross-sections are oriented with apical side at the top and basal side at the bottom. White arrows highlight the crevice localization between the lateral plate and clasper, which the aECM fills in *D. melanogaster* (C1), but only a weakly stained strand-like structure of aECM appears in *D. biarmipes* (D1). Tendrils of aECM can also be observed connecting to the lateral plate in both species (red arrowheads). Relevant structures labeled: Posterior lobe (PL), lateral plate (LP), clasper (C), sheath (S), and phallus (P). Scale bar, 20μm. n=at least 5 per experiment.

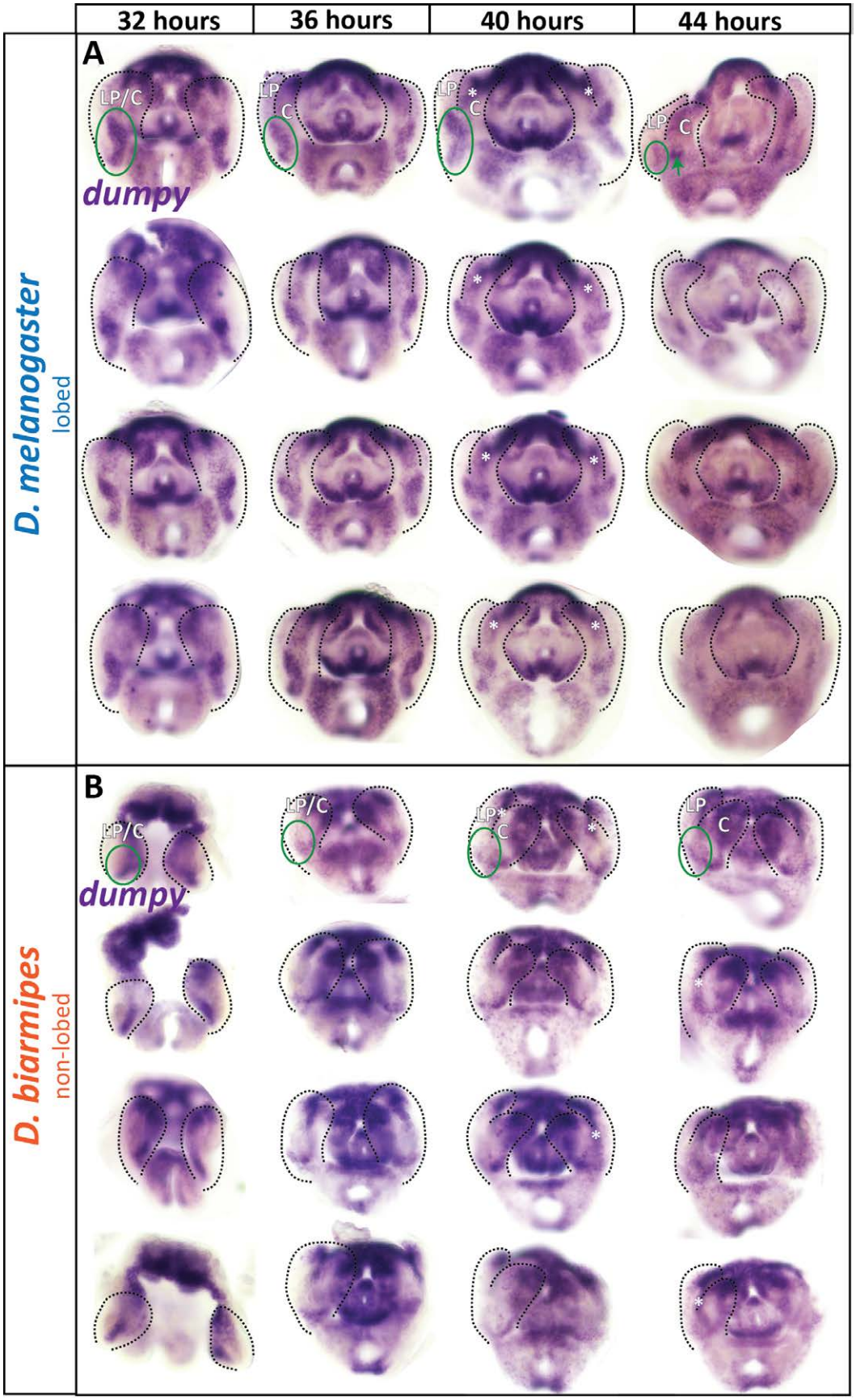
32 hours
36 hours
40 hours
44 hours
A
LP/C
LP
C
dumpy
D. melanogaster
lobed
B
LP/C
LP
C
dumpy
D. biarmipes
non-lobed

Figure 2.14 *dumpy* expression is spatially expanded in lobed species compared to non-lobed species.

(A-B) Additional *in situ* hybridization samples for *dumpy* mRNA in lobed species *D. melanogaster* (A) and non-lobed species *D. biarmipes* (B) to show full range of expression observed in experiment. Samples without outlines on one side are due to the tissue being damaged on that side. Green circle in first image highlights relevant location at the base of the lateral plate, but not included in the remaining images to leave images unobstructed. Asterisk indicates the expression is deep in the sample and not expressed in lateral plate or clasper cells. n= 4 per experiment.

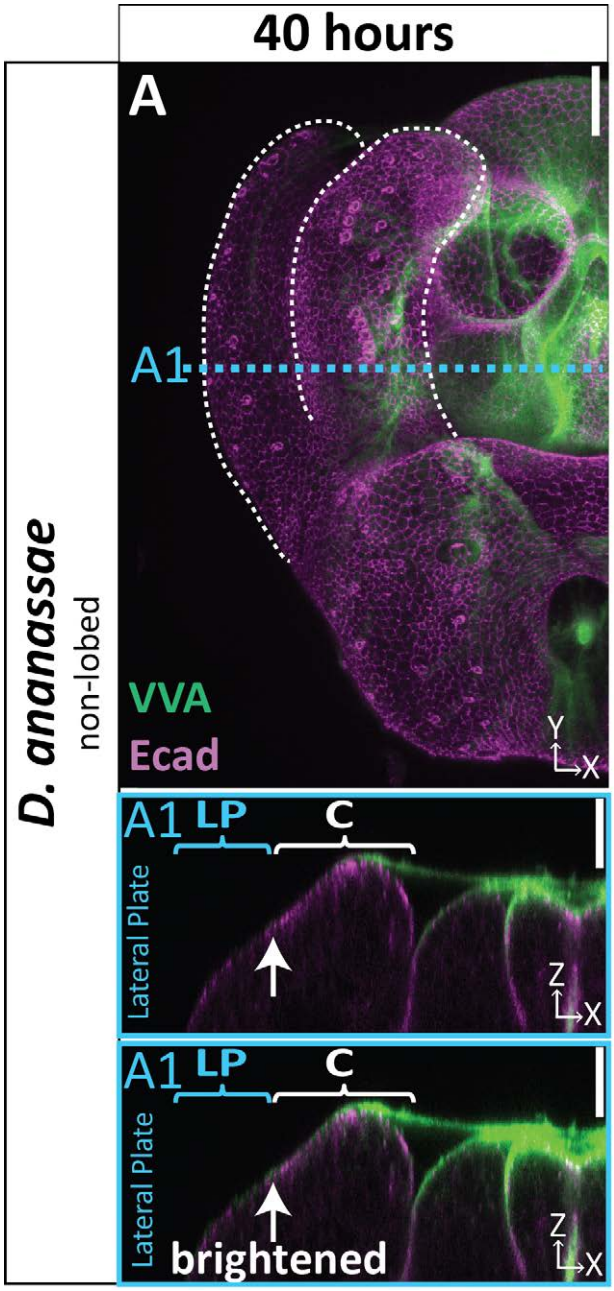

Figure 2.15 aECM not expanded in non-lobed species *D. ananassae*

(A-C) aECM labeled with VVA (green) and apical membrane labeled with Ecad (magenta) at 40 hours APF in non-lobed species *D. ananassae*. Location of respective cross-sections indicated in blue. Top cross-section displayed with normal brightness to show details and bottom cross-section has been brightened to show where all populations of aECM are located. All cross-sections are oriented with apical side at the top and basal side at the bottom. White arrow highlights the 'crevice' between the lateral plate and clasper, which is not pronounced at 40 hours APF in *D.*

ananassae. Relevant structures labeled: lateral plate (LP) and clasper (C) labeled. Scale bar, 20μm. n=at least 2 per experiment.

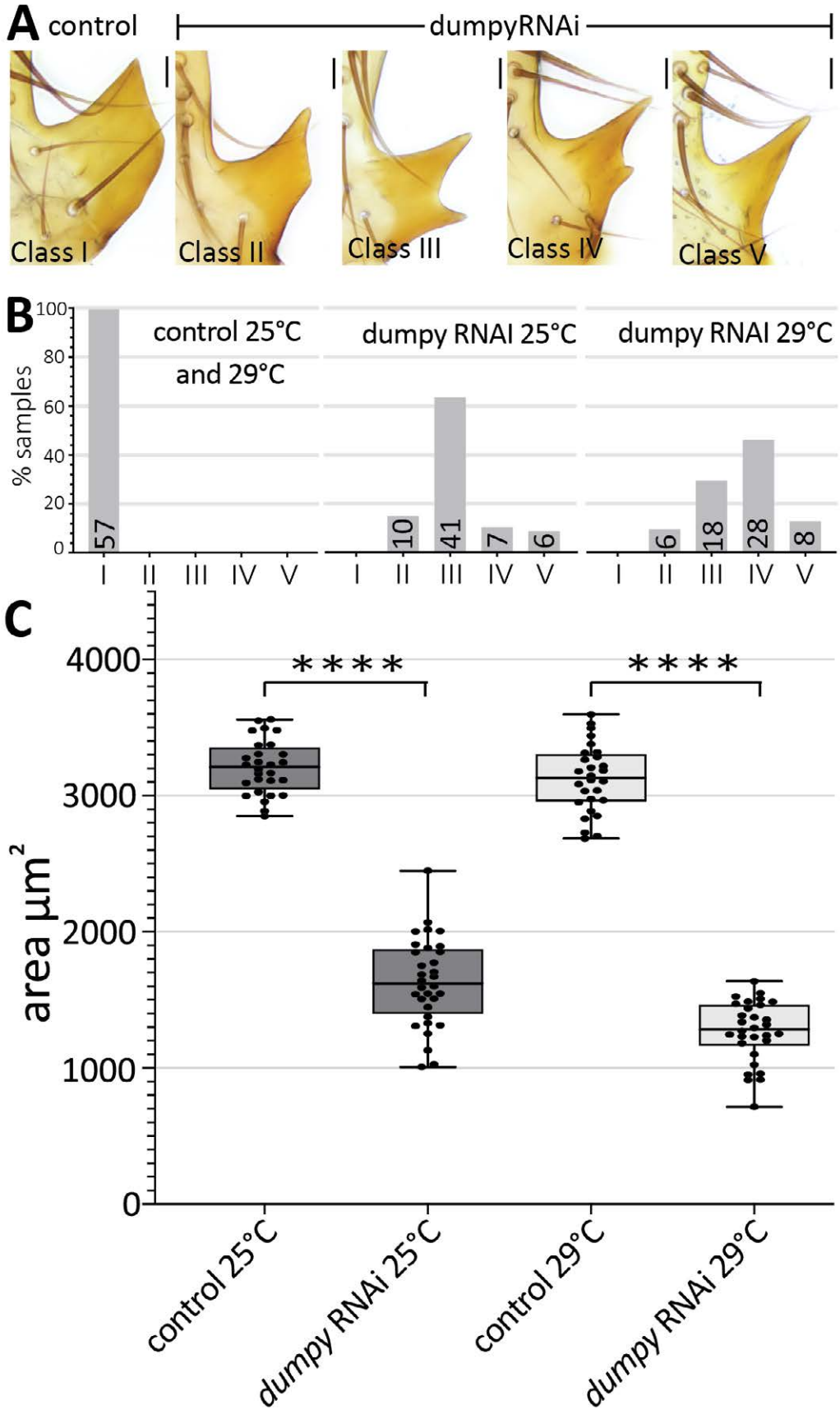
A
control
dumpyRNAi
Class I
Class II
Class III
Class IV
Class V
B
% samples
control 25°C
and 29°C
dumpy RNAI 25°C
dumpy RNAI 29°C
57
10
41
7
6
6
18
28
8
I
II
III
IV
V
C
area µm²
****
****
control 25°C
dumpy RNAi 25°C
control 29°C
dumpy RNAi 29°C

Figure 2.16 Dumpy is required for proper posterior lobe shape.

(A) Range of adult posterior lobe phenotypes produced by control (*mCherry* RNAi) and *dumpy* RNAi animals. Phenotypic classes defined from wild type (I) to most severe (V). Scale bar, 20μm. (B) Percentage of posterior lobes in each class for control, *dumpy* RNAi at 25°C, and *dumpy* RNAi at 29°C. (C) Quantification of area of adult posterior lobes of *mCherry* RNAi (control) and *dumpy* RNAi at 25°C and 29°C. All data points plotted in whisker plot. $n \geq 28$. Statistical significance between each temperature indicated (unpaired t-test; ****$p \leq 0.0001$).

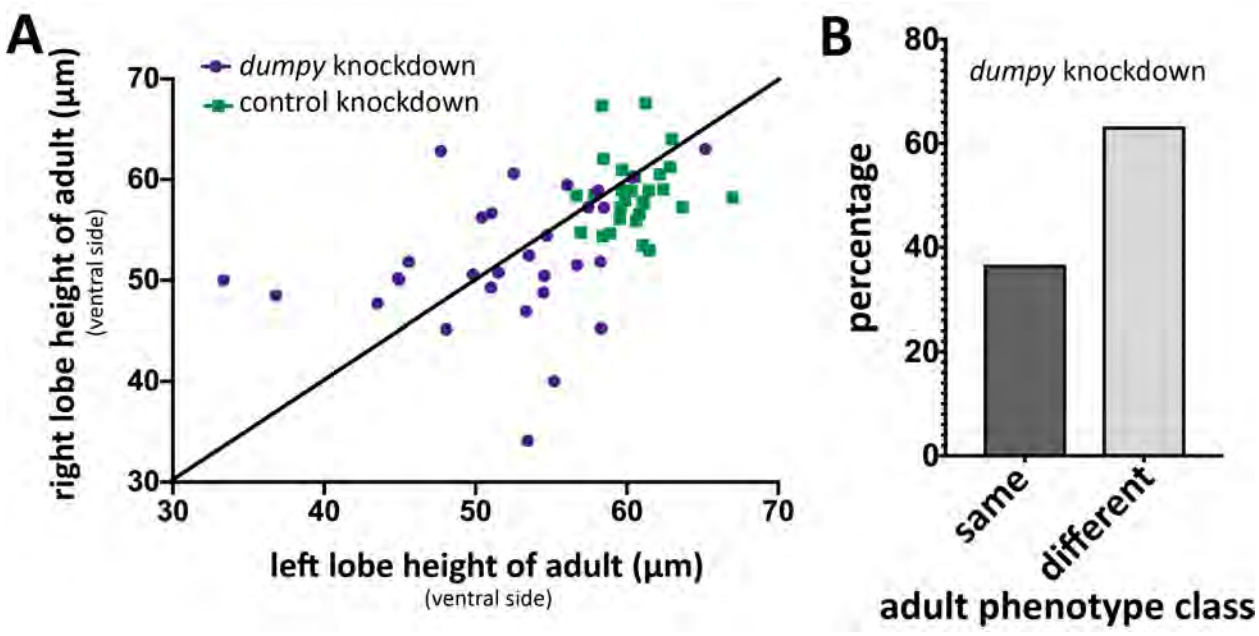

Figure 2.17 Increased left-right variability of posterior lobe phenotype upon *dumpy* knockdown.

(A) Comparison of *dumpy* knockdown (purple circles) and control knockdown (green squares) of left and right adult posterior lobes in single individuals grown at 29°C measuring height at the ventral side of the posterior lobe (single individual represented as a single dot or square). Black line represents perfect correlation in height. *dumpy* knockdown individuals stray more from perfect correlation, indicating that the height of the posterior lobe varies more in the *dumpy* knockdown. (B) Percentage of *dumpy* knockdown individuals plotted in (A) in which both posterior lobes were classified as the same phenotype or different phenotypes (defined in Figure 2.16).

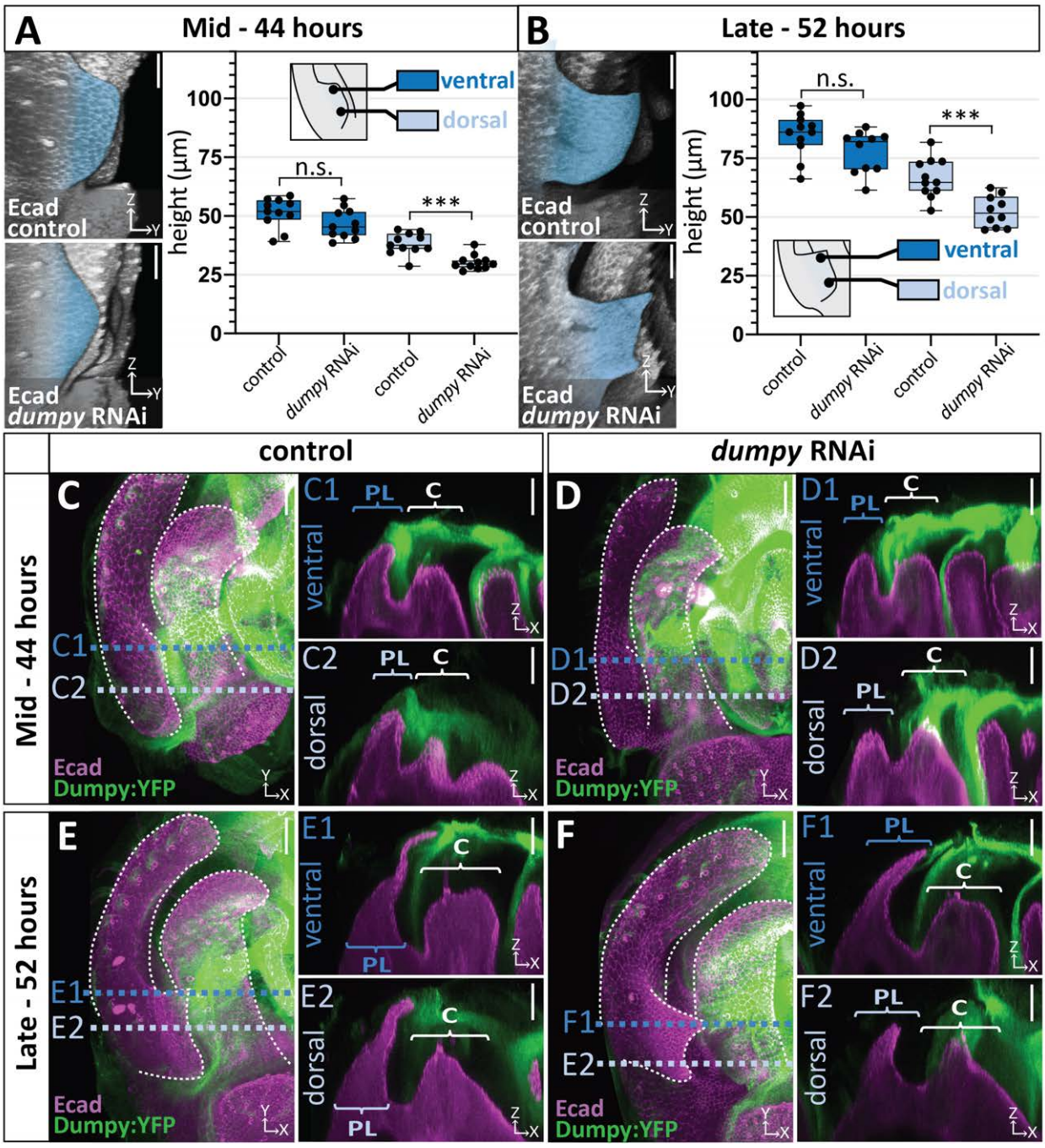

Figure 2.18 Correlation between the deposition of Dumpy and knockdown phenotype.

(A-B) Comparison of *mCherry* RNAi (control) and *dumpy* RNAi at 44 hours APF (A) and 52 hours APF (B). Images are rotated in 3D to visualize the full shape of the posterior lobe labeled with E-cadherin. Quantification of tissue height at the ventral tip (dark blue) and dorsal base (light blue) of the posterior lobe. Cartoon represents relative location of cross-section used for tissue thickness measurement. Individual data points presented; n=at least 10 per

each time point. The ventral tip is defined as the location where the posterior lobe is at its max height. The base was determined by moving 19.76μm dorsally from the ventral tip. Statistical significance for each time point indicated All data points plotted in whisker plot. (unpaired t-test; ***$p \leq 0.001$; n.s.=not significant $p \geq 0.05$). (C-F) Comparison of *mCherry* RNAi (control) (C & E) and *dumpy* RNAi (D & F) at 44 hours APF and 52 hours APF with Dumpy:YFP (Green) and Ecad (Magenta). GFP antibody was used to increase YFP signal. All cross-sections are oriented with apical side at the top and basal side at the bottom. Relevant structures labeled: Lateral plate (LP) posterior lobe (PL), and clasper (C). Cross-sections are max projections of 5.434μm sections to show full Dumpy connection. Images were independently brightened to show relevant structures. Scale bar, 20μm. n=at least 5 per experiment.

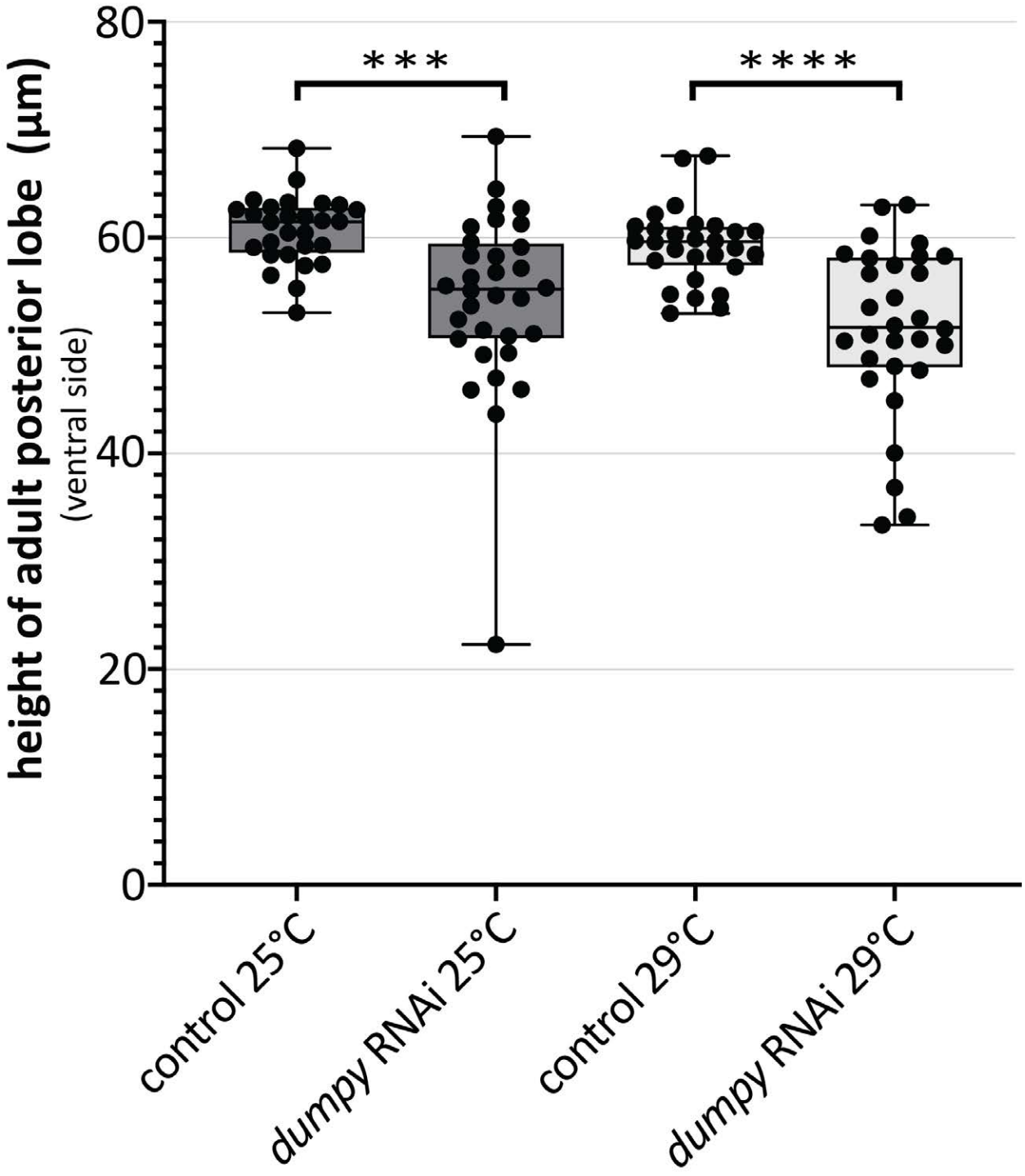

Figure 2.19 Variability in height of the adult posterior lobe in *dumpy* knockdown.

Comparison of *mCherry* RNAi (control) and *dumpy* RNAi adults. Quantification of height of cuticle at the ventral side of the posterior lobe. All data points plotted in whisker plot. n≥28. (unpaired t-test; ***p≤0.001; ****p≤0.0001; n≥28).

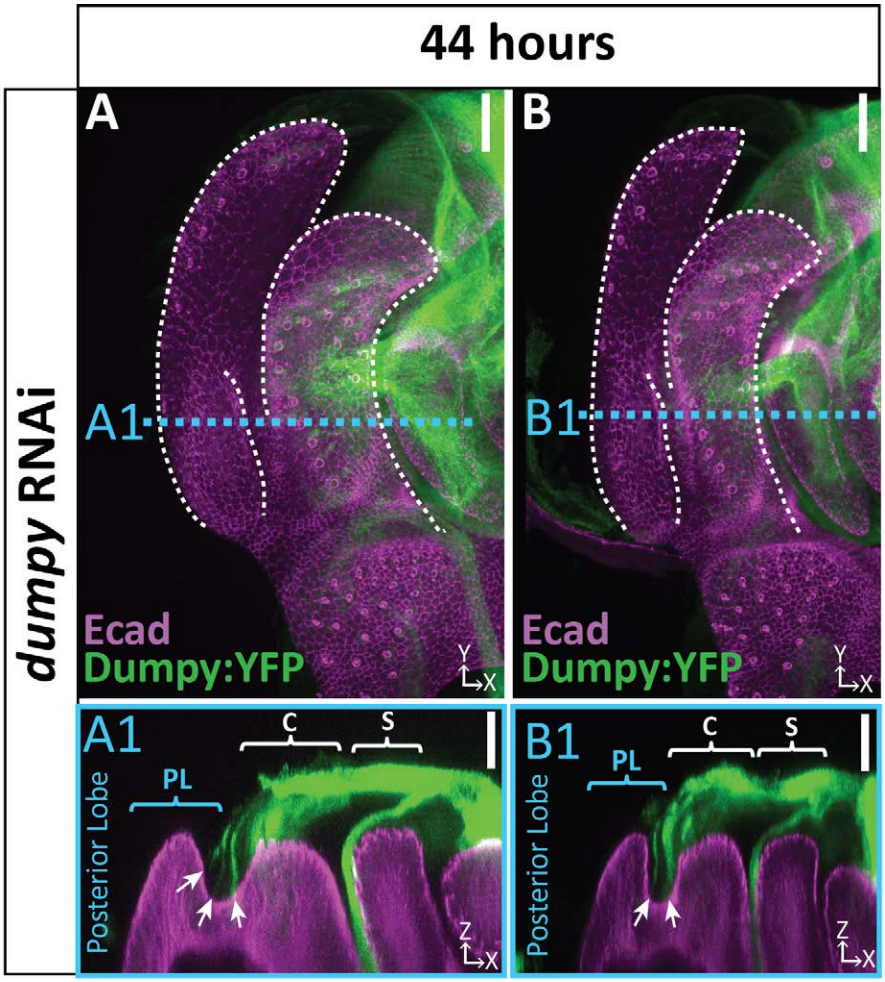

Figure 2.20 Strands of Dumpy in *dumpy* knockdown.

(A & B) *dumpy* RNAi at 44 hours APF with Dumpy:YFP showing strands of Dumpy connecting to the crevice between the lateral plate and clasper (arrow). Relevant structures labeled: Lateral plate (LP) posterior lobe (PL), and clasper (C). Cross-sections are max projection of 5.434µm section to show full Dumpy connection. Scale bar, 20µm**.**

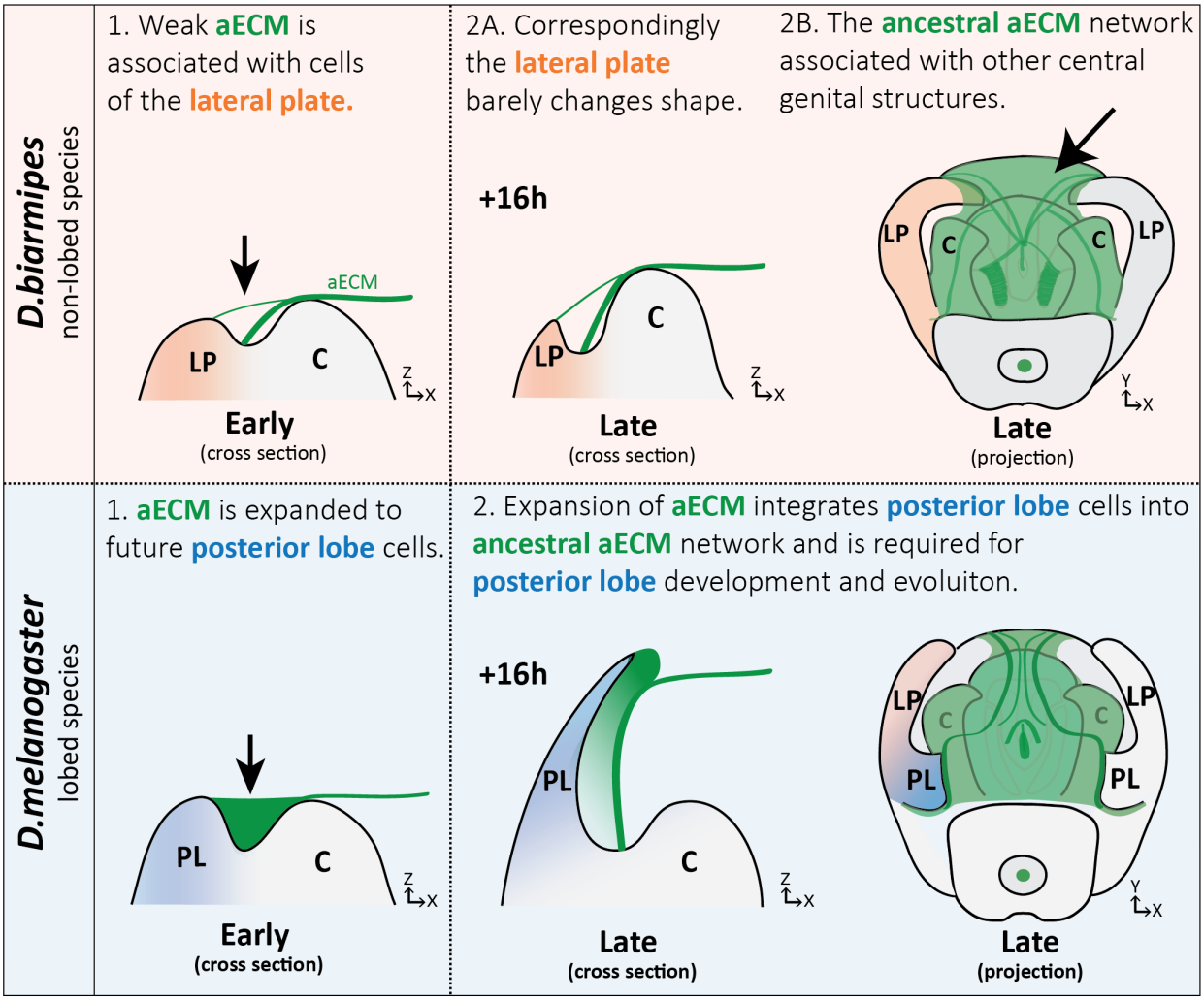

Figure 2.21 Expansion of apical extracellular matrix underlies the morphogenesis of a recently evolved structure.

(Top) Illustration of non-lobed species, *D. biarmipes*, with ancestral aECM network covering central genital structures (2B) including the clasper (C), sheath, and phallus. Weak connections of aECM span from the clasper to the lateral plate (LP) during early development (1 & 2A - top). (Bottom) Illustration of lobed species, *D. melanogaster*. The aECM network has expanded to fill the crevice between the lateral plate and clasper (1-bottom) integrating these cells into the ancestral aECM network (2-bottom). This aECM population is needed for cells to properly project from the lateral plate, forming the posterior lobe.

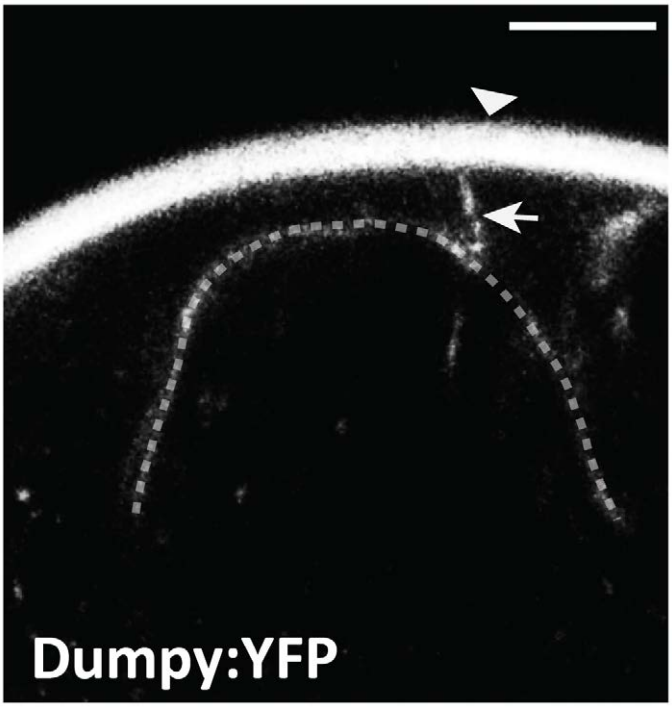

Figure 2.22 Dumpy anchors posterior spiracles to surrounding cuticle.

Live imaging of Dumpy:YFP in the embryonic posterior spiracles. Posterior spiracle (dotted line) is connected to the cuticle (arrowhead) via a tether of dumpy (arrow). Scale bar, 20μm.

3.0 Connecting the evolution of signaling pathways to cellular effectors and morphogenesis

3.1 Introduction

Key to the development of morphological structures are transcription factors and signaling pathways (collectively referred to as 'toolkit' genes), which interact with each other to pattern development (Carroll, Grenier, & Weatherbee, 2005). Of particular importance are signaling pathways, which allow for cell-cell communication through diffusion of extracellular ligands. (Perrimon, Pitsouli, & Shilo, 2012; Pires-daSilva & Sommer, 2003). Ligand diffusion creates concentration gradients, which in turn can activate different genes based on the concentration of ligand received by the cell (Barolo & Posakony, 2002; Lawrence, 2001; Perrimon et al., 2012). Remarkably, many signaling pathways are frequently reused throughout development to regulate the formation of extraordinarily diverse structures (Carroll et al., 2005). Metazoan evolution has generated an array of novel morphological structures and it is commonly believed that alteration in the regulation of these 'toolkit' genes represent a prime mechanism that generates morphological novelty during evolution (Carroll et al., 2005; E. H. Davidson, 2006). However, the genetic changes underlying these alterations remain poorly understood.

The evolution of novel morphology has frequently been associated with changes in temporal or spatial deployment of signaling pathways. For example, the venom claws in centipedes (Hayden & Arthur, 2013) and wing spots in *Drosophila guitifera* (Werner, Koshikawa, Williams, & Carroll, 2010) are correlated with the evolution of new patterns of gene expression of the ligand for Wnt signaling. Furthermore, expansion of ancestral (i.e., pre-existing) patterns of signaling pathway expression is often correlated with the evolution of novel structures. For instance,

opposing gradients of the ligands for Sonic hedgehog (Shh) and bone morphogenetic protein (BMP) signaling pathways are correlated with the development of reptile scales. However, in birds this ancestral signaling module is spatially expanded, associated with the evolution and diversification of feathers (Harris, Fallon, & Prum, 2002). In all of these examples, the initiating ligand of the signaling pathway has evolved new patterns of gene expression. This indicates that evolution of the regulatory regions of signaling pathway ligands may be crucial to the evolution of novel morphologies. However, our molecular genetic understanding of how this occurs is poorly understood because of the limited genetic tools available in most of these organisms. What is needed are systems in which morphological novelties associated with signaling pathways exist and that can be dissected at the level of their regulatory elements using transgenesis and manipulation of the genome.

Once a singling pathway is active, the details of each signal transduction process differ, but all are capable of regulating transcription of downstream genes (Barolo & Posakony, 2002); ultimately leading to the transcription of cellular effectors. Cellular effectors are genes that function to non-transcriptionally alter a cell, such as by activating or localizing actomyosin contraction, or altering cell adhesion (S. J. Smith et al., 2018). The combined activity of cellular effectors across a tissue leads to the formation of a structure. It is currently not known how the evolution of signaling pathway activity generates the expression of relevant cellular effectors that coordinate morphogenesis. One possibility is that the signaling pathway and target cellular effector could be ancestrally active in a different context, and when the signaling pathway is established in a new context, the target cellular effector is re-deployed. Alternatively, new downstream connections may evolve to connect derived signaling pathway activities to different cellular effectors.

To dissect the evolution of signaling pathways and their connections to morphogenesis, I examined the development of the posterior lobe, a recently evolved structure on the male genitalia of species in the *D. melanogaster* clade (Kopp & True, 2002). Previous research has already identified one signaling pathway, the JAK/STAT pathway, in the posterior lobe gene regulatory network (Glassford et al., 2015), which is initiated by the secretion of the ligand unpaired (upd) (Harrison, McCoon, Binari, Gilman, & Perrimon, 1998; W. X. Li, 2008). Previous research found that *upd* was temporally expanded in species with a posterior lobe compared to those without a posterior lobe and is required for proper posterior lobe formation (Figure 3.1)(Glassford et al., 2015). However, the mechanisms causing expanded expression of *upd*, and how it contributed to morphogenetic processes in the posterior lobe have remained elusive.

Here I uncover an enhancer that regulates the temporal expansion of *upd* in the posterior lobe, in addition to identifying a second potential shadow enhancer. This enhancer is ancestrally functional, requiring changes in the *trans*-regulatory environment to activate it. In addition, I identified the spectraplakin encoded by *short stop* (*shot*) as an important cellular effector during posterior lobe morphogenesis and determined that it is activated in response to JAK/STAT signaling. Together, these data provide an example of how a signaling pathway evolved expanded expression by drawing on an ancestral enhancer to deploy an important downstream cellular effector.

3.2 Results

3.2.1 Regulation of novel expression of *upd*

The JAK/STAT pathway is expanded in species with a posterior lobe (Figure 3.1). Underlying this expansion is the ligand of the JAK/STAT pathway, *unpaired* (*upd*), which persists for 24 hours longer in lobed species compared to non-lobed species (Glassford et al., 2015). To understand how this temporal difference in *upd* expression evolved, I sought to identify the enhancer that regulates *upd*. Using a reporter assay consisting of a basal promoter driving the green florescent protein (GFP) gene, short (3-5kb) overlapping fragments which spanned the entire *upd* locus were cloned and placed upstream of the reporter construct (Figure 3.2A). Each construct was transgenically inserted into *D. melanogaster* to identify regions of the locus that could drive GFP in a pattern similar to *D. melanogaster upd*. I identified a potential enhancer of *upd* (*upd* enhancer 1), which activates gene expression between the clasper and lateral plate on the dorsal side (Figure 3.2B). Given the long half-life of GFP (approximately 24 -48 hours), I performed *in situ* hybridization to localize the less stable *GFP* mRNA, allowing me to examine the full temporal pattern of gene expression driven by the enhancer. Using this approach, I found that *upd* enhancer 1 drives the full-time course of gene expression from 24 to 48 hours APF (Figure 3.3).

Because the genomic location of a reporter can affect its activity (Wilson, Bellen, & Gehring, 1990), I placed the reporter construct into a different genomic location, where I observed the same activity (Figure 3.2D). This new genomic location displayed less background expression, more accurately mimicking the pattern observed by *in situ* hybridization (Figure 3.1). To further test the ability of this enhancer to drive expression of *upd,* I used CRISPR/Cas9 to delete the enhancer. To reduce the possibility of any unpredicted effects of a large deletion, I identified

smaller regions to delete. First, based upon the location of two smaller overlapping fragments within enhancer 1, both of which drove some GFP expression in the posterior lobe, I designed a 500 base pair 'minimal' deletion corresponding to this overlap. In addition, another smaller 1500 base pair reporter drove GFP expression in a temporal and spatial pattern very similar to the full length enhancer 1, for which I also designed a deletion. Upon deletion of both the 500 base pair and the 1500 base pair regions, I observed a decrease in the size of the posterior lobe, which was more drastic in the larger deletion (Figure 3.4A). When JAK/STAT activity is observed using a GFP reporter of JAK/STAT signaling (Bach et al., 2007), I observe a qualitative decrease in activity with the 500 base pair deletion, but JAK/STAT activity still persists in the posterior lobe (Figure 3.4B & C). To assess the effects of this 500bp deletion, I deleted this same region from the full length 4.4 kb reporter for enhancer 1. This showed a mild effect on reporter activity and indicated that *upd* expression likely persisted in the deletion background (Figure 3.4D & E). Overall, these data suggest that *upd* enhancer regulates the expression of *upd* in the posterior lobe and contributes to its temporally expanded expression.

3.2.2 Novel temporal expression of *upd* evolved through co-option of a pre-existing enhancer

Two possible mechanisms could explain how enhancer 1 evolved a role in poster lobe development. One is that transcriptional activators that function upstream of the enhancer may have evolved expression in the tissue (i.e. in *trans*), or alternatively, changes to the enhancer region evolved to recruit activators (i.e. in *cis*). To distinguish between these two possibilities, I examined the orthologous enhancer regions of *upd* enhancer 1 from two non-lobed species using a reporter assay. Each reporter was transgenically inserted into the same genomic location in *D.*

melanogaster, allowing for direct comparisons of activity. If the orthologous reporter drives expanded GFP expression, this indicates that the enhancer is ancestrally functional, supporting the existence of *trans*-regulatory changes in lobed species. However, if the orthologous reporter does not drive expanded GFP this would suggest that *cis*-regulatory changes have occurred to the enhancer along the lineage of species producing a posterior lobe. Results from this experiment demonstrate that the orthologous enhancer 1 from non-lobed species drives fully expanded GFP expression (Figure 3.5A & B), similar to the *D. melanogaster* version of the enhancer (Figure 3.2B). This indicates that the temporally extended activity of enhancer 1 may have evolved through *trans*-regulatory changes, as the non-lobed enhancer is functional in the correct *trans*-regulatory context.

Given that enhancer 1 is ancestrally functional, I hypothesized that the *upd* enhancer 1 may regulate additional ancestral activities of *upd* during development, which may have facilitated the co-option of this ancestral enhancer into the posterior lobe. To test this, I screened expression of the *D. melanogaster upd* enhancer 1 reporter in regions of the embryo and larva where *upd* is known to be expressed. I found no other activities of the *upd* enhancer 1 reporter, indicating that *upd* enhancer 1 may be dedicated to genital development, and ancestrally functions to drive early *upd* expression at the base between the clasper and lateral plate, as observed in non-lobed species (Figure 3.1C & D). However, the possibility cannot be ruled out that there are unreported patterns of *upd* expression that I did not examine and could be regulated by the *upd* enhancer 1.

To test the possibility that the *upd* enhancer 1 drives early expression of *upd* in the genitalia of non-lobed species, I inserted the *D. melanogaster* enhancer 1 reporter into a random location within the non-lobed species *D. ananassae.* The *D. melanogaster upd* enhancer 1 drives faint expression at the base between the lateral plate and clasper, which mimics the early non-lobed *upd*

expression pattern (Figure 3.5 C & D). This experiment further supports a model in which the ancestral function of the *upd* enhancer 1 was to drive early expression in non-lobed species. However, additional lines, species, and time points must be tested.

3.2.3 A second shadow enhancer may contribute to novel *upd* expression in the posterior lobe

During the reporter screen of the *upd* locus, I identified a second potential enhancer of *upd* which will be referred to as "enhancer 2" (Figure 3.2C). The *upd* enhancer 2 reporter drives GFP expression during later stages of posterior lobe development, from 36 to 48 hours APF (Figure 3.3). However, when I tested enhancer 2 in a second genomic location, it did not drive expression (Figure 3.2F). Given these contrasting results, I sought to further confirm its enhancer activity by testing this reporter construct in three additional genomic locations. Enhancer 2 was able to drive weak activity in the posterior lobe in these three new genomic locations, but its patterns differed slightly in each instance (Figure 3.6A). To evaluate its endogenous function, I deleted this enhancer by CRISPR/Cas9-assisted homology directed repair, but it did not affect the size of the posterior lobe (Figure 3.6B & C). Although this alteration did show defects in other structures, such as the outstretched wing phenotype, which was previously linked to deletions in this region (L. Wang et al., 2014). Together, these data suggest that the *upd* enhancer 2 is either (1) not a regulator of *upd* in the posterior lobe, (2) that enhancer 2 may be a weak regulator of *upd,* or (3) is a redundant element which requires other genomic elements to support reproducible activity. If the second model is correct, the lack of a posterior lobe phenotype upon deletion of enhancer 1 may be due to the robust activity of enhancer to which the posterior lobe phenotype is already quite sensitive.

Similar to my investigation with enhancer 1, I tested if the potential activity of the *upd* enhancer 2 was due to changes in *cis* or *trans* regulation. Towards this end, I examined the orthologous enhancer of three non-lobed species and found that they do not drive GFP expression in lobed species (Figure 3.7E-G). Since the non-lobed *upd* enhancer 2 is non-functional in the *trans*-regulatory context of a lobed species, this indicates that *cis*-regulatory changes may have occurred along the lineage leading to the evolution of this structure. To confirm that *cis*-regulatory changes occurred within all species with a posterior lobe and not only within the *D. melanogaster* genome, I tested the orthologous *upd* enhancer 2 from the three additional lobed species and discovered they could all drive GFP expression similar to the pattern of GFP expression observed with the *D. melanogaster* enhancer 2 reporter (Figure 3.7A-D). This indicates that *cis* changes have occurred in the *upd* enhancer 2 within the lobed lineage.

I was intrigued by the potential novel activity of enhancer 2 and wanted to understand how this putative enhancer region evolved. There are several mechanisms by which an enhancer can evolve, such as transposition, *de novo* synthesis, or co-option (Glassford et al., 2015; Rebeiz, Jikomes, Kassner, & Carroll, 2011; Rebeiz et al., 2015). I examined the sequence alignment of *upd* enhancer 2 between lobed and non-lobed species and found no evidence of transposon insertion. To distinguish between *de novo* generation and co-option, I examined the enhancer 2 reporter in other tissues where *upd* has previously characterized activities. The reporter was able to drive GFP activity that mimicked the activity of *upd* in the eye disc, wing disc, and leg disc (Figure 3.6A & 3.8B-D) (Bach et al., 2007; Mukherjee, Hombría, & Zeidler, 2005; Zeidler, Perrimon, & Strutt, 1999). In addition, the orthologous *upd* enhancer 2 from non-lobed species is capable of driving expression in these tissues as well (Figure 3.7H & I).

The activity of this enhancer in wing, eye, and leg discs suggested that the putative *upd* enhancer 2 region did not form *de novo*, but instead derived its activity from one or more of these ancestral functions, and during the course of posterior lobe evolution, additional inputs evolved to generate contributions to posterior lobe expression. To further test this hypothesis, I identified three blocks of deep nucleotide conservation within the *upd* enhancer 2, which may be important for driving ancestral activity. The blocks were conserved to *D. virilis,* which *is* approximately 40 million years diverged from *D. melanogaster* (Russo, Takezaki, & Nei, 1995). To test their significance, I individually scrambled the sequence of each block within the context of the full enhancer (3.4kb) and assayed the resulting expression patterns. Disrupting blocks 1 (41 bp) and 2 (21 bp) had no effect on the posterior lobe, eye disc, or wing disc expression (leg disc not tested). However, scrambling the 41 bp block 3 ablated activity in the posterior lobe (Figure 3.8E). Interestingly, the block 3 mutant did not affect activity in the wing or eye, but greatly reduced GFP expression in the leg (Figure 3.8F-H). In addition, the block 1 mutant did not affect the posterior lobe or wing, but did ablate activity in the eye disc (Figure 3.8I-K). Together these data indicate that the *upd* enhancer 2 was ancestrally active in the imaginal discs of the leg, eye, and wing. Through the course of evolution, changes have occurred to the *upd* enhancer 2, which allowed it to drive its landing-site dependent activity in the posterior lobe, in addition to potentially sharing inputs with the leg enhancer that are required for its function.

3.2.4 *shot* is a cellular effector required for posterior lobe morphogenesis

The experiments of the previous sections suggest how the temporal expansion of *upd* resulted from a mixture of *cis* and *trans* changes to its regulatory region. However, the cellular effectors downstream of JAK/STAT signaling remain unknown. Given the high levels of

organized tubulin observed specifically in posterior lobe cells during development (S. J. Smith, Davidson, & Rebeiz, 2019), I decided to screen cellular effectors that could alter tubulin organization or change the dynamics of tubulin polymerization. I screened 24 candidates using two assays. First, I examined each candidate in *D. melanogaster* by *in situ* hybridization, looking for posterior lobe-specific patterns of mRNA accumulation that would indicate they are up-regulated in the posterior lobe. Second, when available, I completed RNAi mediated knockdown of gene expression using the *Pox neuro (Poxn)* driver which activates expression in several tissues, including the posterior lobe (Boll & Noll, 2002). During this screen, I identified a subset of candidates that had both a lobe-specific expression pattern and a knockdown phenotype in the posterior lobe (Figure 3.9). In some cases, such as *Dhc64C*, the RNAi phenotype appeared extremely disorganized, with no cuticle forming and the tissue appearing disordered, indicating that a basic cellular function may have been inhibited. This led me to consider other candidates. Of these candidates, *short stop* (*shot)* was the most promising, showing both strong RNAi phenotype and specific mRNA patterning. However, I observed decreased cuticle deposition in the posterior lobe of the *shot* knockdown, leading me to hypothesize that the tissue might have collapsed due to the lack of cuticle which may be necessary to support the posterior lobe after morphogenesis is complete. To test this, I examined development of the posterior lobe in the *shot* knockdown background and found that the phenotype manifests before cuticle secretion (Figure 3.10A & B), indicating that *shot* is actively required during posterior lobe morphogenesis.

Shot is a member of the spectraplakin family and is known to interact with many cellular proteins, such as actin, microtubules, intermediate filaments, and cell adhesion proteins, and can play a role in signaling (Voelzmann et al., 2017). To better understand what role Shot might serve during posterior lobe development, I examined Shot localization in the cells of the posterior lobe,

which uncovered posterior lobe specific localization of Shot at the apical membranes of cells on the medial face of the posterior lobe, a pattern which is absent in a *shot* knockdown background (Figure 3.10 C & D). Together, these data suggest that *shot* is an important cellular effector that contributes to posterior lobe morphogenesis.

3.2.5 *shot* is a downstream target of JAK/STAT signaling

Because *shot* is vital for posterior lobe morphogenesis, I sought to test if it is activated in response to JAK/STAT activity. I screened the *shot* locus to identify its posterior lobe enhancer region using a collection of published lines containing regions of the *shot* locus driving the GAL4 transcription factor of yeast (Pfeiffer et al., 2008). I identified a region that drove partial expression in the posterior lobe. I hypothesized that this region may be missing important regulatory information, so I cloned a larger region into the GFP reporter construct vector. This construct drives expression throughout the posterior lobe, mimicking the pattern I observed by *in situ* hybridization (Figure 3.11). To determine if *shot* is downstream of JAK/STAT signaling, I tested the *shot* reporter in the context of the *upd* enhancer 1 deletion. The activity of the *shot* enhancer is greatly reduced in the *upd* enhancer 1 deletion background, indicating that *shot* is downstream of JAK/STAT signaling (Figure 3.11).

3.3 Discussion

The novel deployment of one or multiple signaling pathways is often associated with the evolution of new structures (Harris et al., 2002; Hayden & Arthur, 2013; Werner et al., 2010).

However, few examples have demonstrating genetically how signaling pathways evolve novel patterns or how their deployment leads to morphogenetic changes. In this study, I have elucidated the regulation of JAK/STAT signaling during the evolution of the posterior lobe and connected its expansion to the activation of a vital cellular effector that contributes to the morphogenesis of this structure (Figure 3.12). These results bear upon our understanding of how signaling pathways may evolve novel patterns, and highlights the need for detailed examination of other examples of signaling pathway evolution to fully understand how they evolve. Beyond understanding the mechanisms deploying signaling pathways within novel structures, this work also highlights the need to discern the logic of how their deployment activates morphogenetic programs. The integration of these two important facets of the problem will be discussed below.

3.3.1 Temporal expansion of an ancestral signaling source

JAK/STAT signaling has evolved a temporally expanded pattern of activity in lobed species. Underlying this expansion is the extended expression of *upd*, which is potentially regulated by two enhancers. I hypothesize that *upd* enhancer 1 is the ancestral genital enhancer that was co-opted during the evolution of the posterior lobe and now drives robust expression of *upd* in this structure (Figure 3.12). Such expansions of ancestral enhancers without modification may occur due to similar *trans*-regulatory environments in two tissues, and in the case of the *upd* enhancer 1, potentially through the temporal expansion (or retraction) of an upstream factor which already regulates the element. Possibly only a limited number of upstream factor(s) may have changed to activate this enhancer in the posterior lobe cells, however, these factors remain to be identified.

3.3.2 Shadow enhancers and the evolution of novelty

In contrast to enhancer 1, *upd* enhancer 2 is not active ancestrally in the genitalia and may be a redundant element that contributes to the late expression of *upd* in the posterior lobe. The configuration of two or more enhancers which independently drive overlapping patterns of gene expression has been termed "shadow enhancers" (Hong, Hendrix, & Levine, 2008). Shadow enhancers are pervasive features found throughout the *Drosophila* genome, especially for developmental genes (Cannavò et al., 2016). However, the driving force for the evolution of shadow enhancers has remained elusive. Some experiments have pinpointed robustness, suggesting that shadow enhancers drive more resilient gene expression in the face of variable genetic or environmental conditions, compared to a single enhancer (Boettiger & Levine, 2009; Frankel et al., 2010; Perry, Boettiger, Bothma, & Levine, 2010). While work has been done to understand how shadow enhancers diverge (Wunderlich et al., 2015), currently no examples to date have examined how a shadow enhancer originates during evolution. Future experiments are needed to determine if enhancer 2 is a bonafide enhancer for the posterior lobe. Indeed, it may be that its variable activity is a latent or nascent first step towards evolving the shadow enhancer arrangement. It is also possible that this element plays more important roles in the other lobed species which have been evolving independently for 2-3 million years. Nevertheless, I have elucidated that enhancer 2 drives expression in the wing, eye, and leg and identified the location of one or more important inputs for the leg expression of *upd*. If enhancer 2 is confirmed to be an enhancer of *upd* in the posterior lobe, it will be an interesting case of co-option of an ancestral enhancer that derived modifications to expand to an additional tissue.

3.3.3 Connecting signaling pathways and cellular effectors

A missing link in the evo-devo literature is understanding how patterning by signaling pathways and transcription factors also activates terminal genes (cellular effectors), which actively contribute to morphogenesis. Specifically, what downstream targets are regulated in response to a novel signaling pathway activity? Here, I have begun to establish a system where this question can be addressed in the posterior lobe. I have found that *shot* is an important cellular effector which contributes to posterior lobe morphogenesis and is downstream JAK/STAT signaling. Given that JAK/STAT signaling is active very early in non-lobed species between the lateral plate and clasper, I hypothesize that *shot* may be a downstream target ancestrally in the genitalia. In addition, the activity I observed from the *shot* reporter was localized in another genital structure called the phallic sheath (Figure 3.13B) (Rice et al., 2019). The sheath is a flat cuticular structure which appears morphologically similar to the posterior lobe in adults (Figure 3.13A). Interestingly, Shot also localizes to the apical membrane of medial sheath cells (Figure 3.13C). It is an intriguing possibility that JAK/STAT might regulate *shot* expression in the sheath, as the JAK/STAT signaling reporter shows activity in this structure (Figure 3.1C). However, it remains to be determined if *shot* is reduced in the sheath in a JAK/STAT deficient background as the *upd* enhancer 1 deletion does not target the sheath. Nevertheless in either case, if borne out by further study, the expansion of JAK/STAT signaling would result in *shot* expression expanding to posterior lobe cells.

In addition to understanding how cellular effectors are connected to signaling pathways, future work can begin to uncover how changing levels of signaling pathway activity might alter shape of the posterior lobe. My previous work has identified the aECM protein Dumpy as a vital player during morphogenesis of the posterior lobe (S. J. Smith et al., 2019). Given that Shot

localizes to the apical membrane of medial posterior lobe cells, one may postulate a role for Shot in anchoring these cells to the aECM. The absence of *shot* leads to wing blistering phenotypes similar to what is observed in *dumpy* mutants (Prout, Damania, Soong, Fristrom, & Fristrom, 1997). In addition, it has been posited that *shot* may contribute to aECM deposition during denticle morphogenesis in *Drosophila* (Dilks & DiNardo, 2010). Potentially by altering JAK/STAT signaling, which could affect the levels of *shot* expressed within a cell or alter the cells which express it, which could ultimately lead to different configurations of aECM and different posterior lobe shapes.

3.4 Acknowledgements

Dr. Mark Rebeiz and I designed the JAK/STAT portion of the study. Winslow C. Johnson cloned *upd* constructs and Stephanie Day cloned *shot* constructs. Gavin Rice dissected and imaged the cuticle image of the sheath.

3.5 Figures

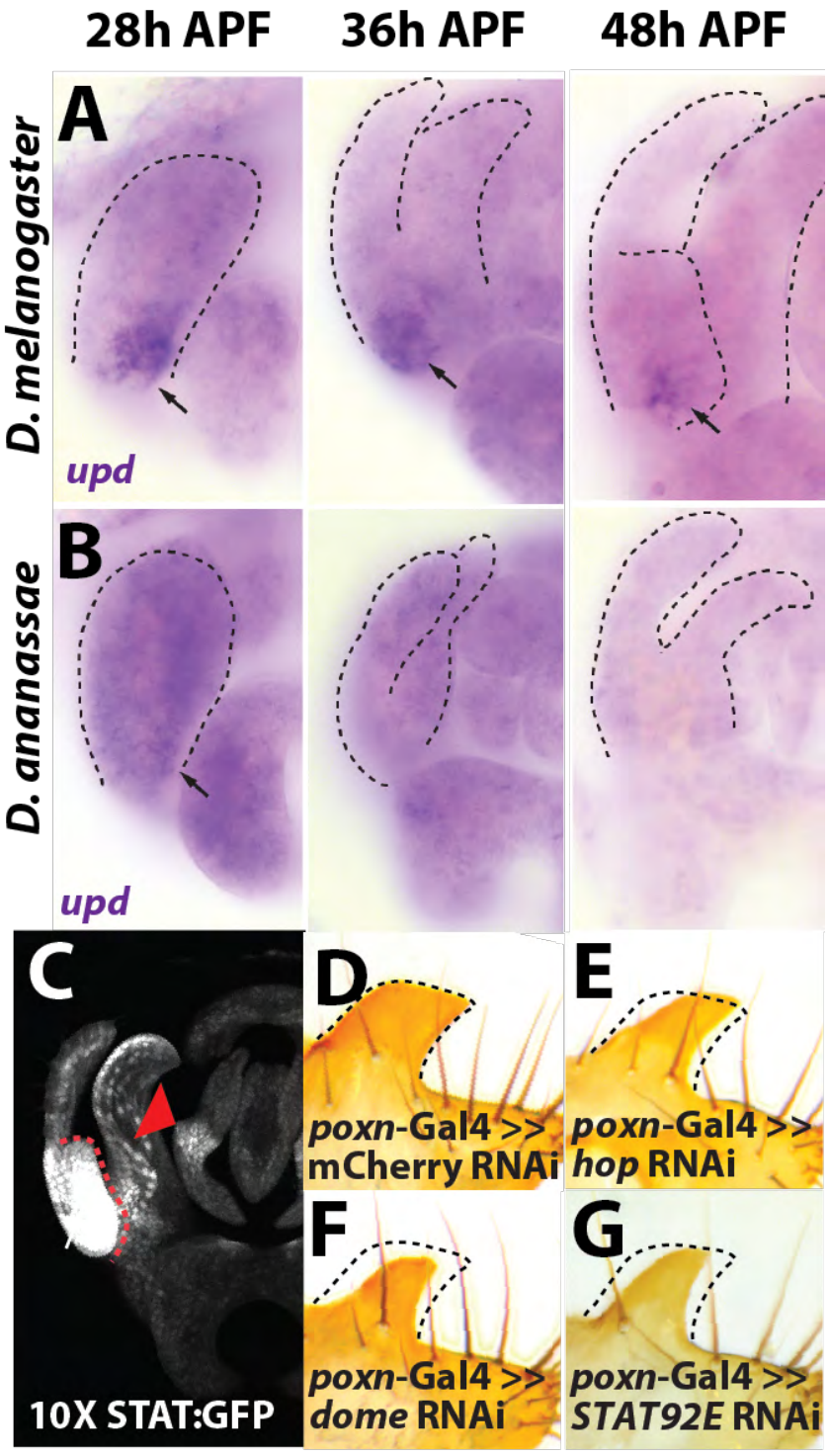
28h APF
36h APF
48h APF
D. melanogaster
D. ananassae
A
upd
B
upd
C
10X STAT:GFP
D
poxn-Gal4 >>
mCherry RNAi
E
poxn-Gal4 >>
hop RNAi
F
poxn-Gal4 >>
dome RNAi
G
poxn-Gal4 >>
STAT92E RNAi

Figure 3.1 JAK/STAT signaling is required for posterior lobe evolution.

Some images were published in (Glassford, et al. 2015). (A-B) *in situ* hybridization for the gene *upd* in the lobed species *D. melanogaster* (A) and the non-lobed species *D. ananassae* (B). Expression is present at 28 hours after pupal formation (APF) between the clasper and lateral plate on the dorsal side in both species. In *D. melanogaster*, this expression continues through 48 hours APF, but is quickly turned of in *D. ananassae.* (C) A reporter consisting of 10 STAT92E (transcription factor in the JAK/STAT pathway) binding sites connected to a basal promoter driving *green florescent protein* (*gfp*) and serves as a readout of cells activated by JAK/STAT signaling. The reporter shows high JAK/STAT activity specifically in the cells of the posterior lobe (red outline) and activity is also observed in the sheath (arrowhead). (D-G) RNAi knockdown phenotypes using the posterior lobe driver *Pox neuro* (*poxn*). As a control, RNAi directed to the *mCherry* gene was used, as the gene is not present in the *Drosophila* genome. (D) Different components of the JAK/STAT pathway were knocked down, such as the kinase (*hop*), receptor (*dome*) and the transcription factor (*Stat92e*), which all result in a smaller posterior lobe.

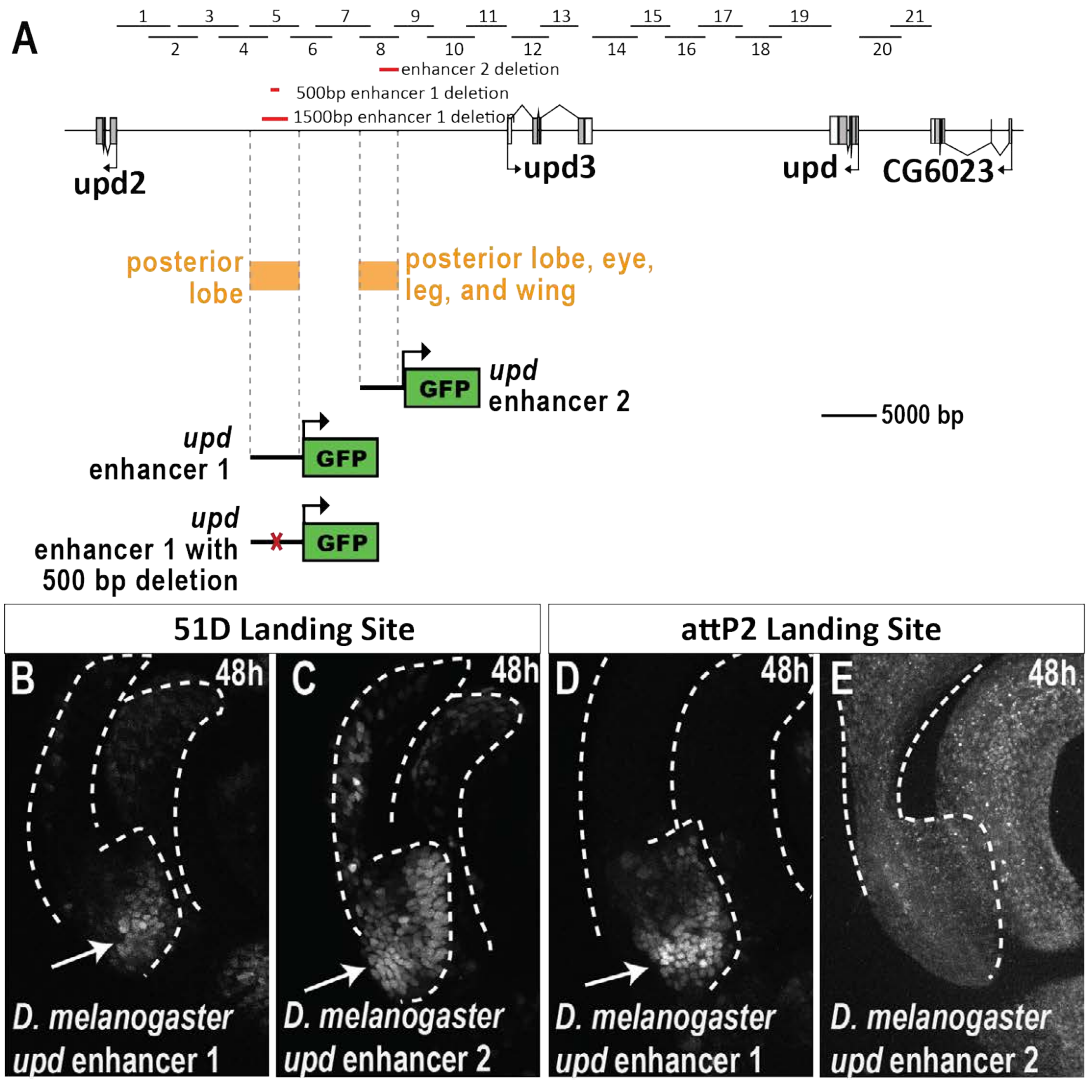

Figure 3.2 Two potential enhancers regulate expanded *upd* expression in the posterior lobe.

(A) Depiction of the *upd* locus, which consists of three *upd* genes (*upd, upd2,* and *upd3*), which are all capable of activating JAK/STAT signaling (Gilbert, Weaver, Gergen, & Reich, 2005; Hombría, Brown, Häder, & Zeidler, 2005; Wright, Vogt, Smythe, & Zeidler, 2011). The positions of 21 tested reporter constructs and representative regions of enhancer deletions are depicted in relation to the locus. Bellow in orange are the mapped regions of activity and representation of the reporter constructs for enhancer 1 and enhancer 2. (B-C) Representative images of the enhancer 1 (B) and enhancer 2 (C) reporter constructs in the original landing site 51D. (D-E) Representative images of enhancer 1 (D) and enhancer 2 (E) in the second landing site tested, attP2.

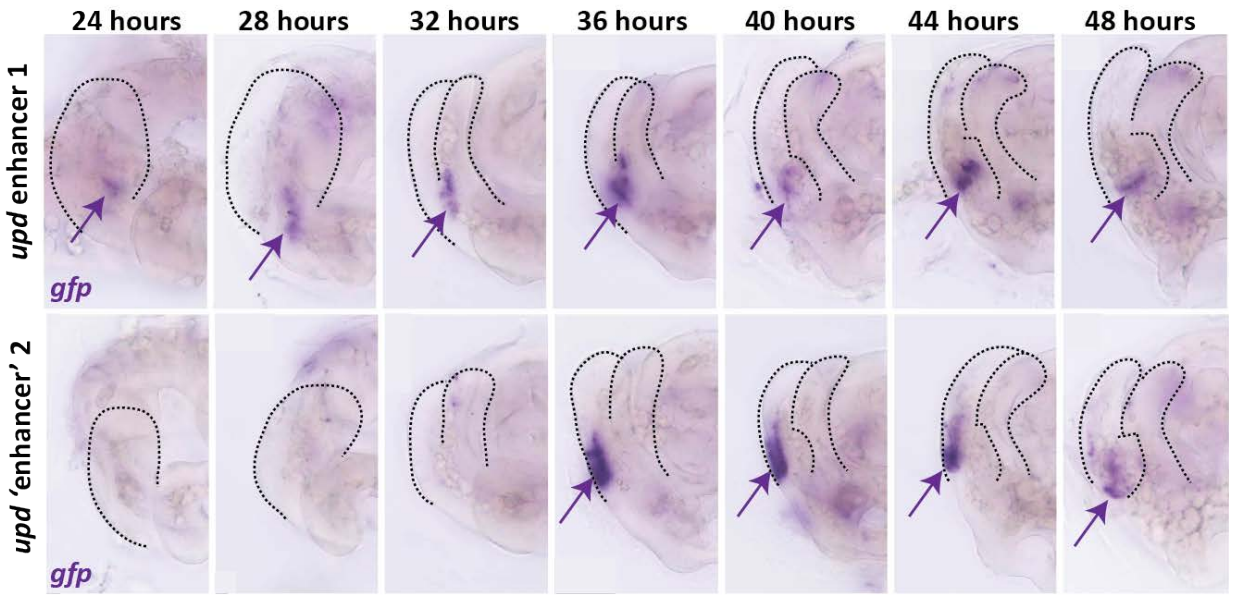

Figure 3.3 Differential temporal activities of the *upd* enhancers in the posterior lobe.

in situ hybridization for *gfp* in the enhancer 1 reporter (top) and enhancer 2 reporter (bottom), both in the 51D landing site. Enhancer 1 begins to drive activity by at least 24 hours APF and is expressed continuously through 48 hours APF while enhancer 2 does not commence expression until 36 hours and continues driving expression through 48 hours APF.

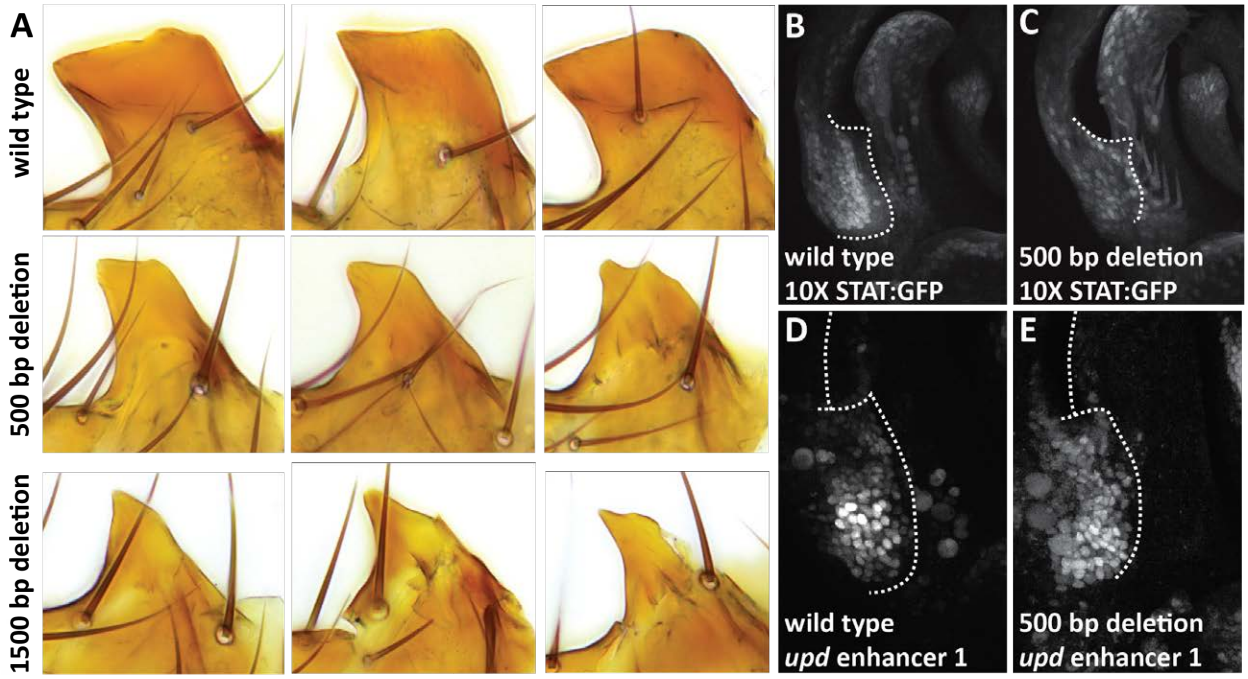

Figure 3.4 Deletion of the *upd* enhancer 1 alters posterior lobe development and JAK/STAT signaling levels.

(A) Bright-field images of adult cuticles from wild type (top), *upd* enhancer 1 500 base pair deletion (middle), and *upd* enhancer 1 1500 bp deletion (bottom). (B-C) 10X STAT:GFP reporter (Bach et al., 2007) in wild type (B) or *upd* enhancer 1 500 base pair deletion (C) background. (D-E) Wild type *upd* enhancer 1 reporter (D) and *upd* enhancer 1 reporter with same 500 base pairs removed (E), demonstrating reporter activity is not greatly decreased by the 500 base pair deletion. Larger circles of activity are fat bodies and not nuclei within the epithelial tissue.

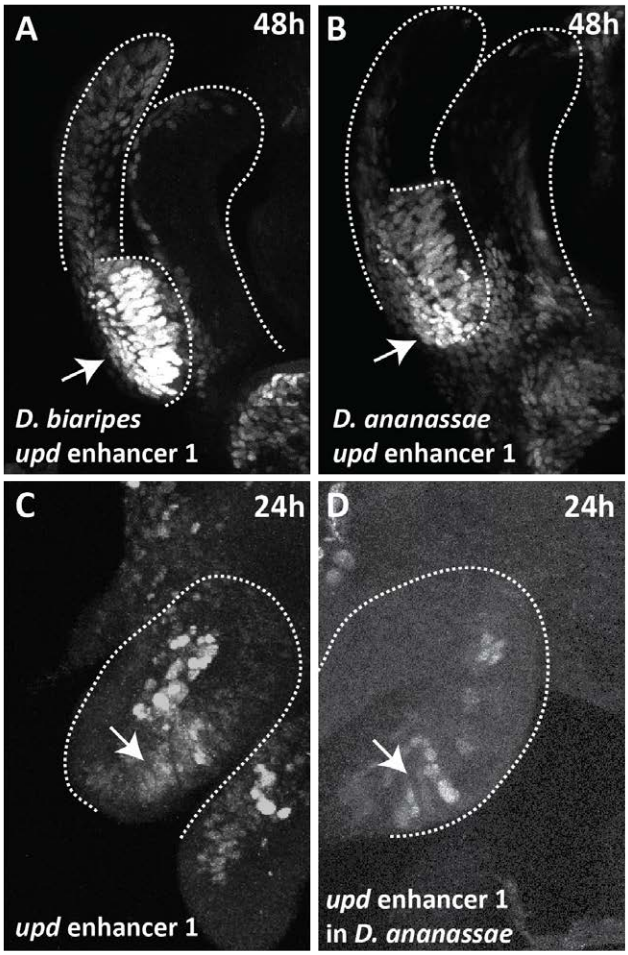

Figure 3.5 *upd* enhancer 1 is conserved in non-lobed species.

(A-B) The homologous *upd* enhancer 1 region from *D. biarmipes* (A) and *D. ananassae* (B) inserted into *D. melanogaster* drives GFP expression in the posterior lobe. Note the *D. ananasse* reporter is homologous to the smaller 1.5kb region (not the full length 4.4kb region) used in the CRISPR deletion as the larger fragment proved difficult to clone. (C) The *D. melanogaster upd* enhancer 1 reporter at 24 hours APF in *D. melanogaster* (C) and *D. ananassae* (D) driving GFP expression at the dorsal side of the future lateral plate and clasper (arrow).

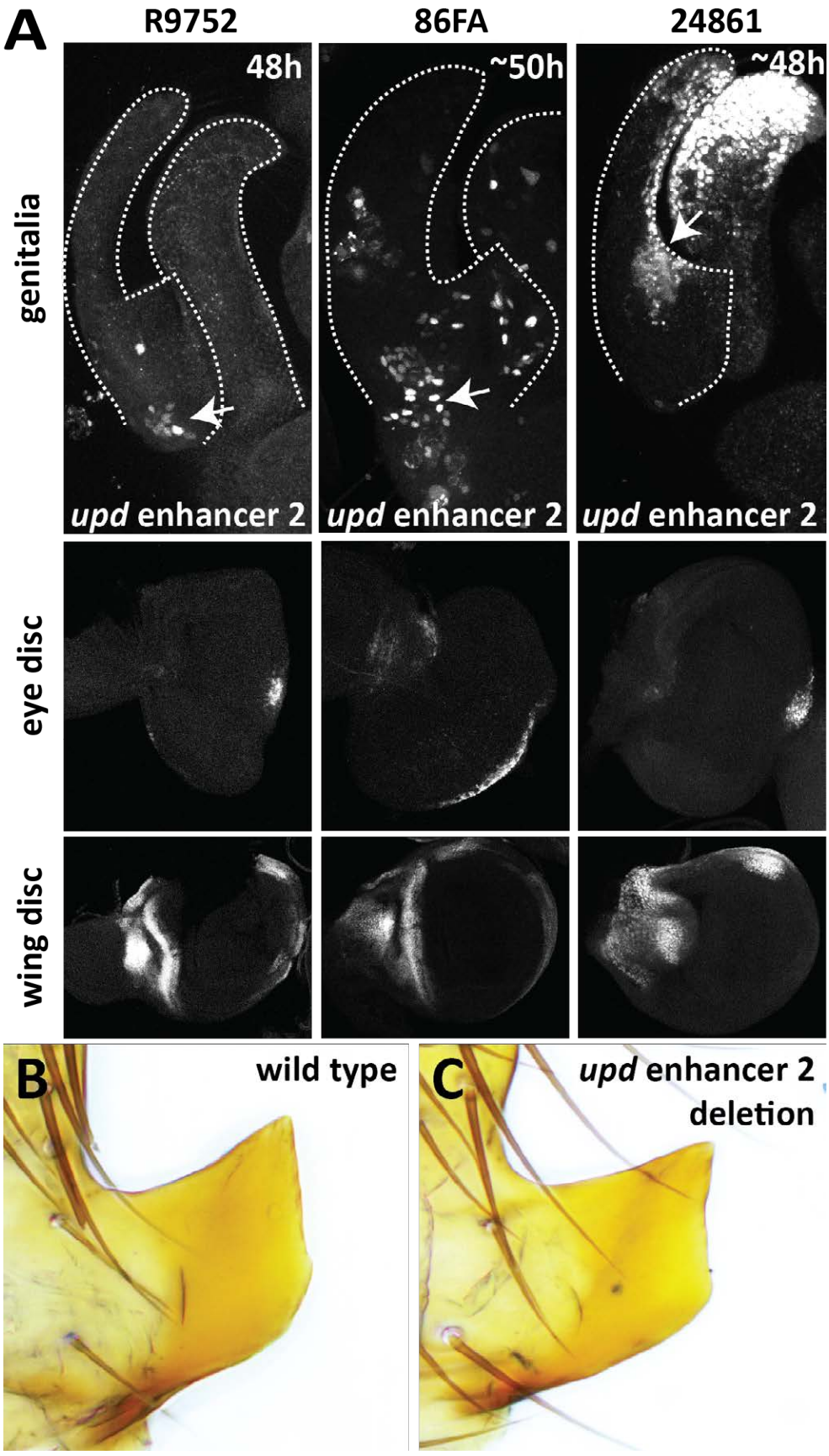
A
R9752
86FA
24861
48h
~50h
~48h
genitalia
upd enhancer 2
upd enhancer 2
upd enhancer 2
eye disc
wing disc
B
wild type
C
upd enhancer 2
deletion

Figure 3.6 enhancer 2 may be a weak shadow enhancer of *upd* in the posterior lobe.

(A) *upd* enhancer 2 inserted into 3 additional landing sites. Landing sites R9752 and 86FA drive patterns of GFP expression on the dorsal side of the posterior lobe, but 24861 drives weak expression on the ventral side of the posterior lobe. Expression patterns observed in the wing and eye disc (Figure 3.8) are also observed in the new landing sites, but are slightly expanded in the eye disc in the 86FA site. (B-C) Bright-field images from wild type (B) and *upd* enhancer 2 deletion (C), which does not alter the size of the posterior lobe.

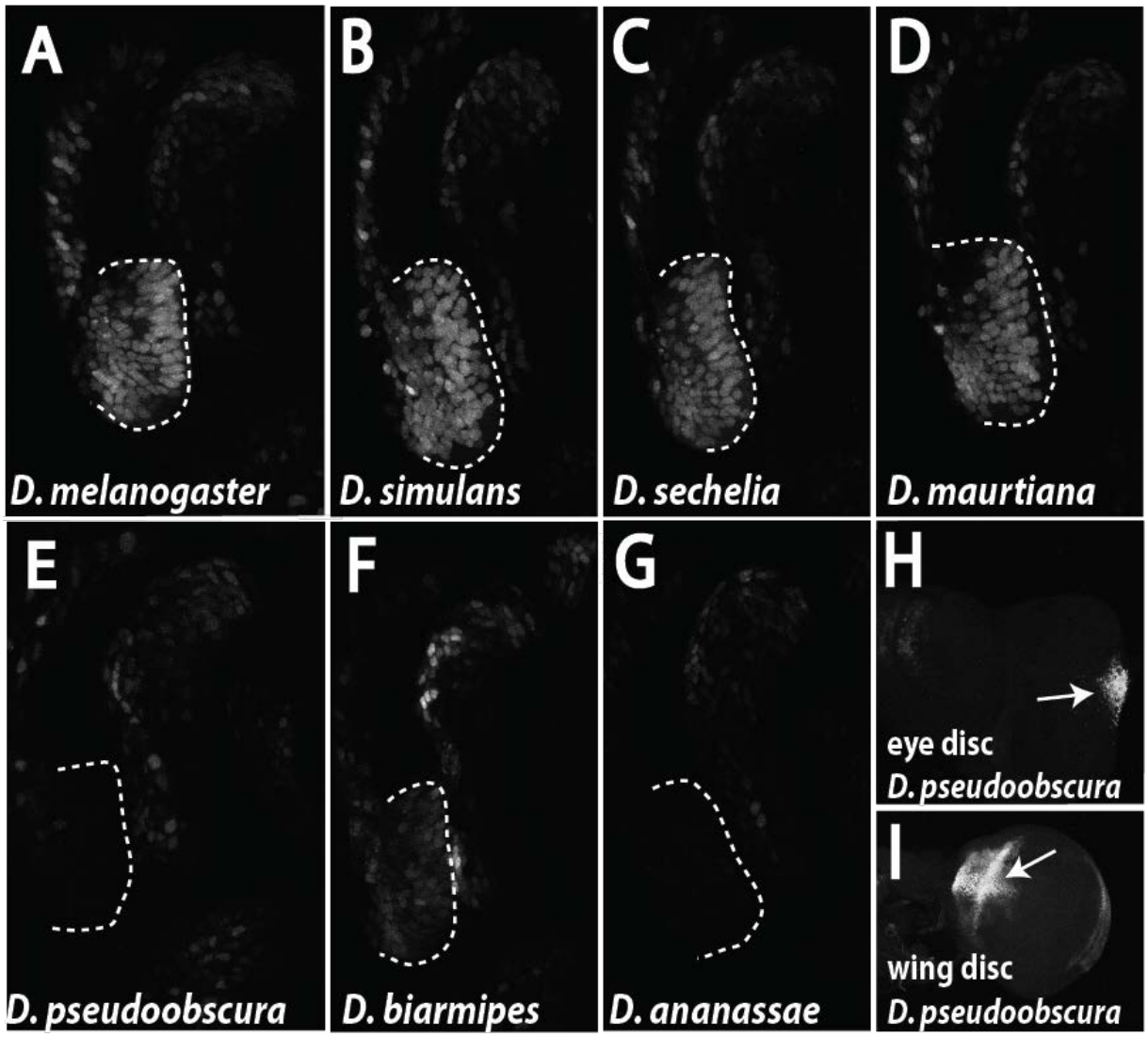

Figure 3.7 The activity of enhancer 2 likely evolved through *cis*-regulatory changes.

(A-D) The enhancer 2 reporter from *D. melanogaster* (A) and the homologous region from additional lobed species *D. simulans* (B), *D. sechellia* (C), and *D. mauritiana* (D), which all drive GFP expression in the posterior lobe when tested in the 51D landing site. (E-G) The homologous *upd* enhancer 2 region from the non-lobed species *D. pseudoobscura* (E), *D. biarmipes* (F), and *D. ananassae* (G), which all lack GFP expression in the posterior lobe when inserted into the 51D landing site. (H-I) Conserved expression of the non-lobed *D. pseudoobscura* enhancer 2 driving expression in the eye disc (H) and wing disc (I).

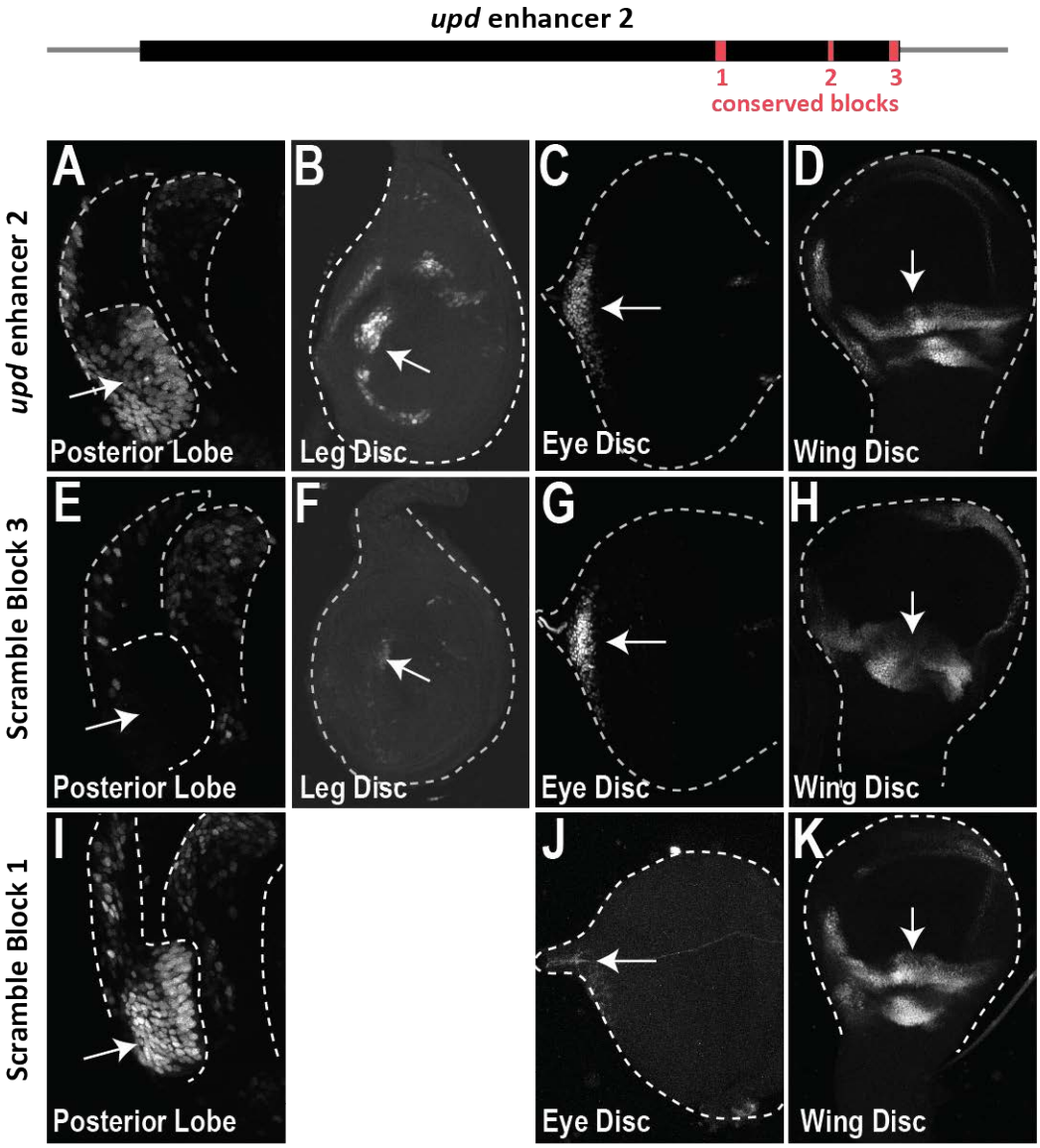

Figure 3.8 A conserved region within enhancer 2 is required for activity in the leg and posterior lobe.

(A-D) Activity of enhancer 2 in the posterior lobe (A), leg disc (B), eye disc (C), and wing disc (D). (E-H) Activity of the block 3 scramble mutant of the *upd* enhancer 2 reporter. Expression in the eye disc (G) and wing disc (H) are similar to the wild type enhancer, but expression is abolished in the posterior lobe (E) and greatly reduced in the leg disc (F). (I-K) Expression of the block 1 scramble mutant which drives a normal pattern of GFP expression in the posterior lobe (I) and wing disc (K), but ablates activity in the eye disc (J).

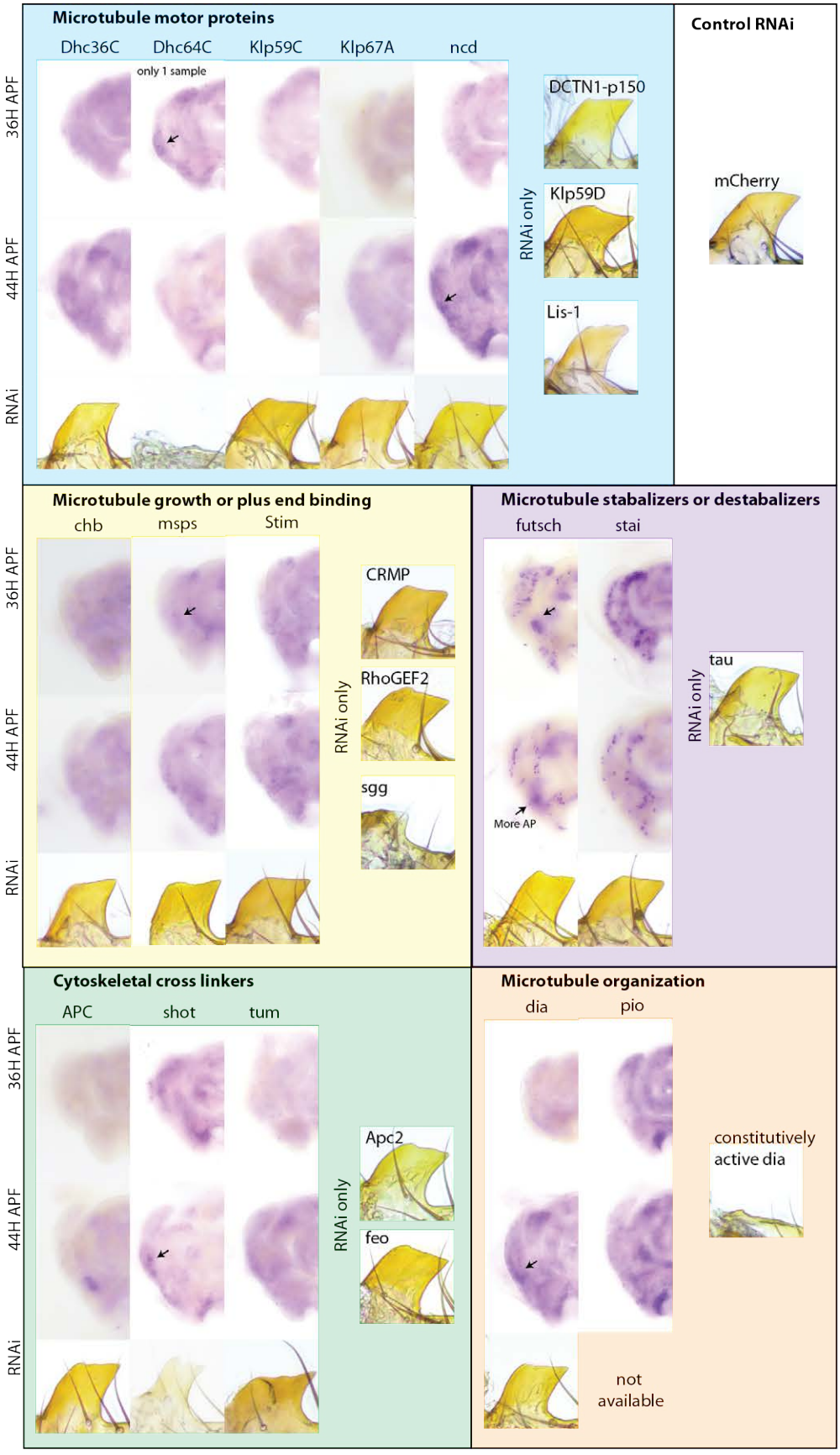
Microtubule motor proteins
Dhc36C
Dhc64C
Klp59C
Klp67A
ncd
only 1 sample
36H APF
44H APF
RNAi
RNAi only
DCTN1-p150
Klp59D
Lis-1
Control RNAi
mCherry
Microtubule growth or plus end binding
chb
msps
Stim
CRMP
RhoGEF2
sgg
Microtubule stabalizers or destabalizers
futsch
stai
More AP
tau
Cytoskeletal cross linkers
APC
shot
tum
Apc2
feo
Microtubule organization
dia
pio
constitutively active dia
not available

Figure 3.9 A screen of microtubule associated genes identified several potential downstream targets of the posterior lobe GRN.

Shown are *in situ* hybridization results at 36 hours APF and 44 hours APF, and the RNAi knockdown phenotype for each indicated gene. In bottom right corner is the *mCherry* control, a constitutively active form of dia, and 9 RNAI phenotypes for genes in which *in situ* hybridizations have not been completed.

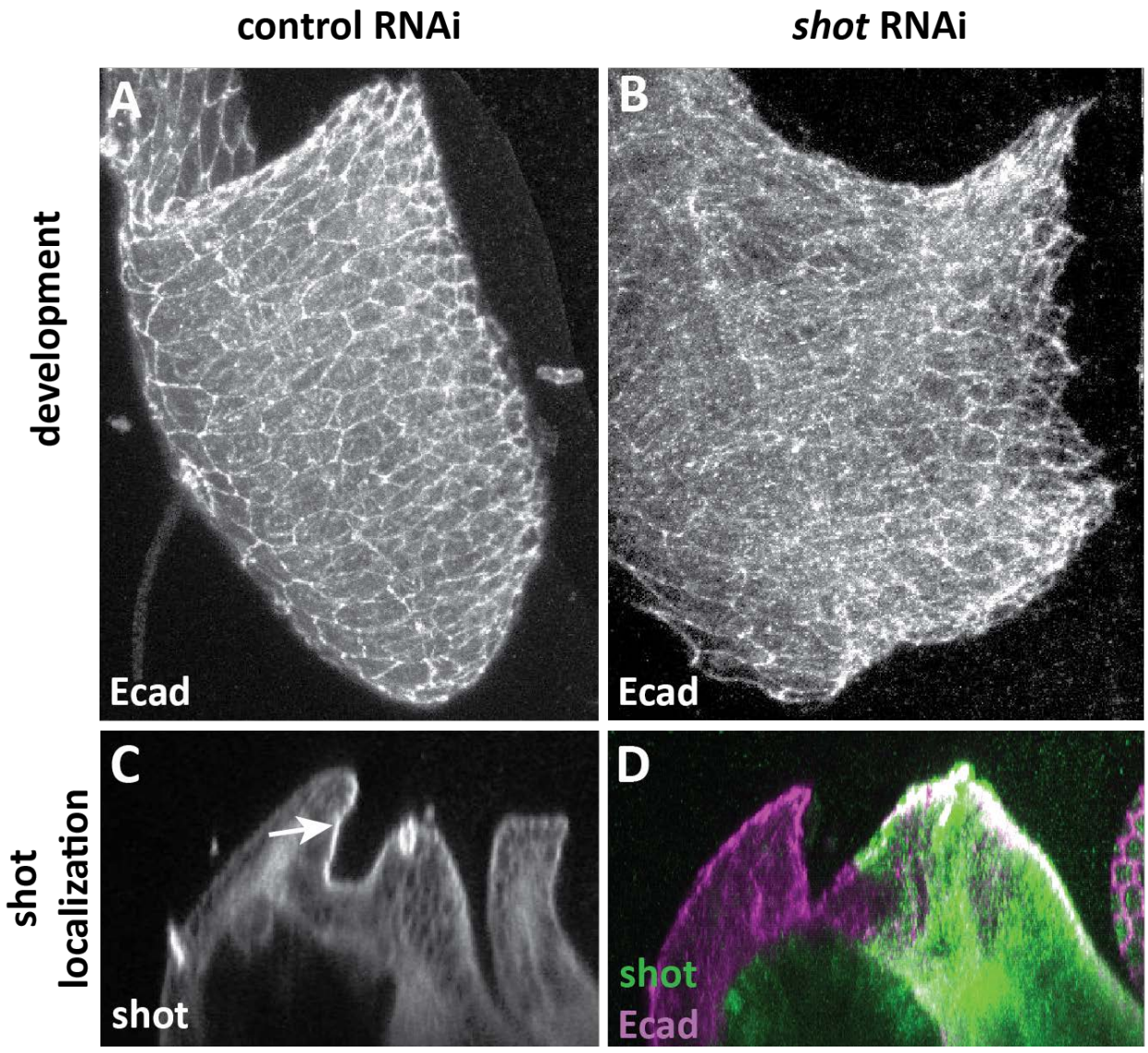

Figure 3.10 Shot is required for proper posterior lobe development.

(A-B) 48 hour APF sample with apical marker, E-cad, showing development of *mCherry* knockdown (A) and *shot* knockdown (B). The top of the lobe (right side of image) is smooth in the control, but jagged in the *shot* knockdown. (C-D) Cross-section through posterior lobe stained with Shot antibody. In a wild type animal (C), Shot localizes to apical membrane of medial posterior lobe cells. In *shot* knockdown (D), a drastic decrease in Shot is observed in posterior lobe cells. Note that Shot staining is overexposed in this image to highlight contrast between RNAi and non-RNAi tissues.

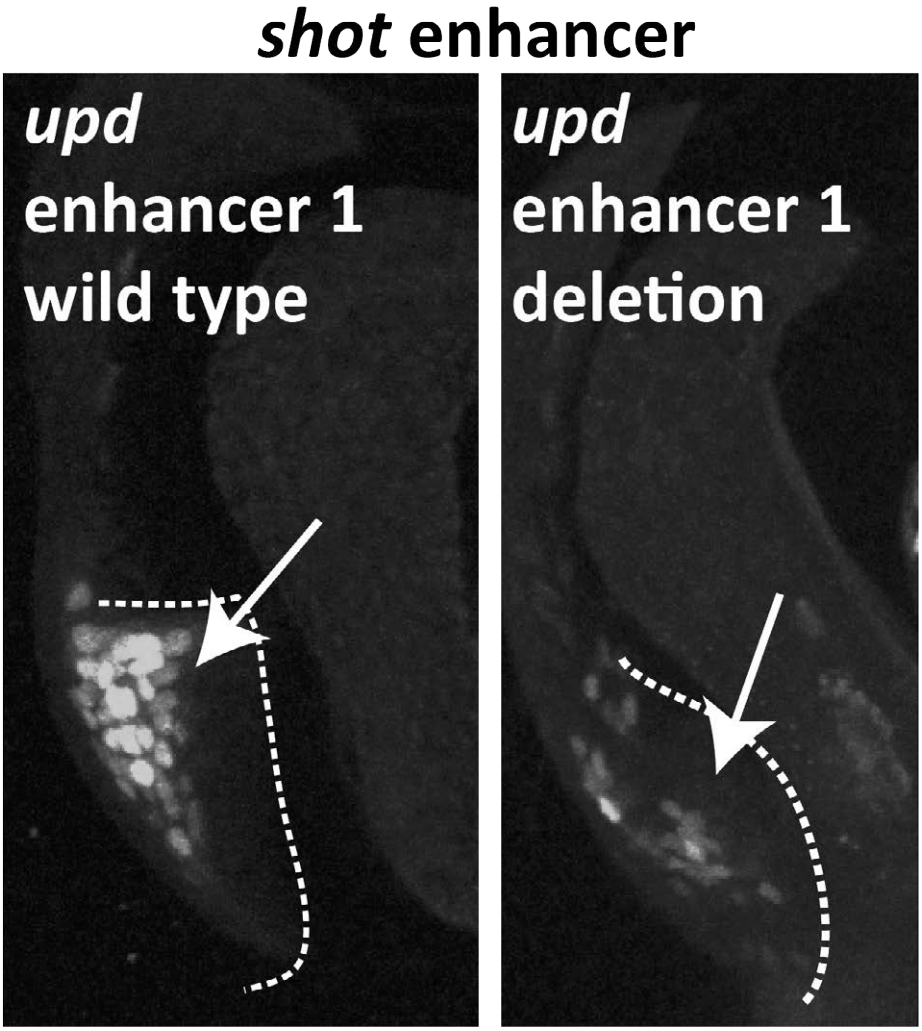

Figure 3.11 *shot* is downstream of JAK/STAT signaling.

shot enhancer in wild type (left) and in the *upd* enhancer 1 1500 bp deletion (right) which is reduced in the *upd* deletion background.

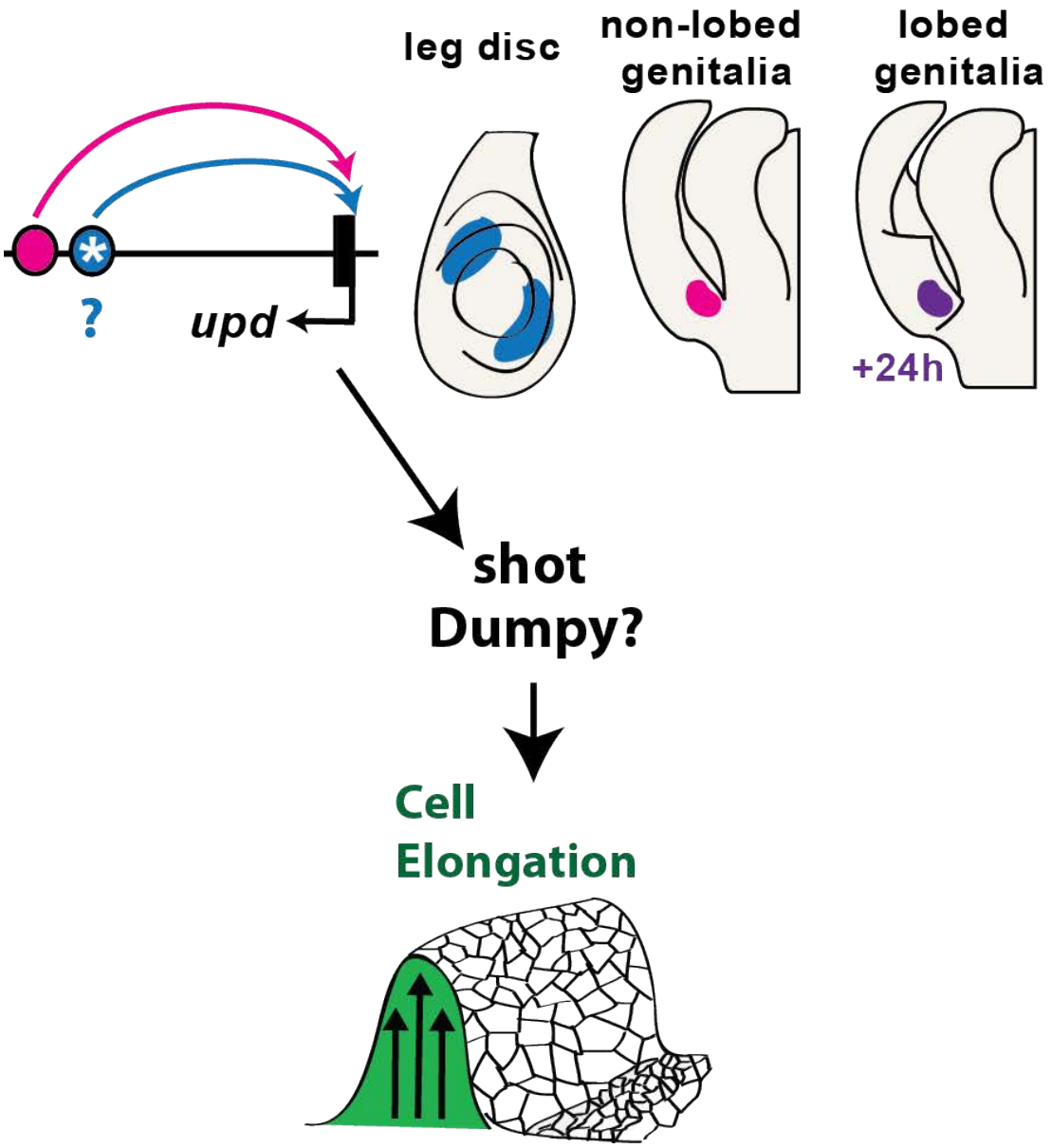

Figure 3.12 Connecting JAK/STAT signaling to morphogenesis.

(Top) The *upd* enhancer 1 (pink) drives expression ancestrally between the lateral plate and clasper on the dorsal side in non-lobed species. The *upd* enhancer 2 (blue) has not yet been confirmed to serve necessary enhancer roles in the posterior lobe, but may contribute to late expression, and may contribute to extended expression of *upd* an additional 24 hours (pink+blue enhancers = purple expression pattern) Enhancer 2 drives expression in many larval discs, including the leg disc. Data suggest that the activity of the *upd* enhancer 2 is due to *cis*-regulatory changes (indicated by *) that co-opted this enhancer to genital development. (Middle) JAK/STAT signaling activates *shot* expression and

may activate other cellular effectors genes like *dumpy*. (Bottom) *shot* and *dumpy* both are important for allowing cells of the posterior lobe to properly elongate along their apico-basal axis.

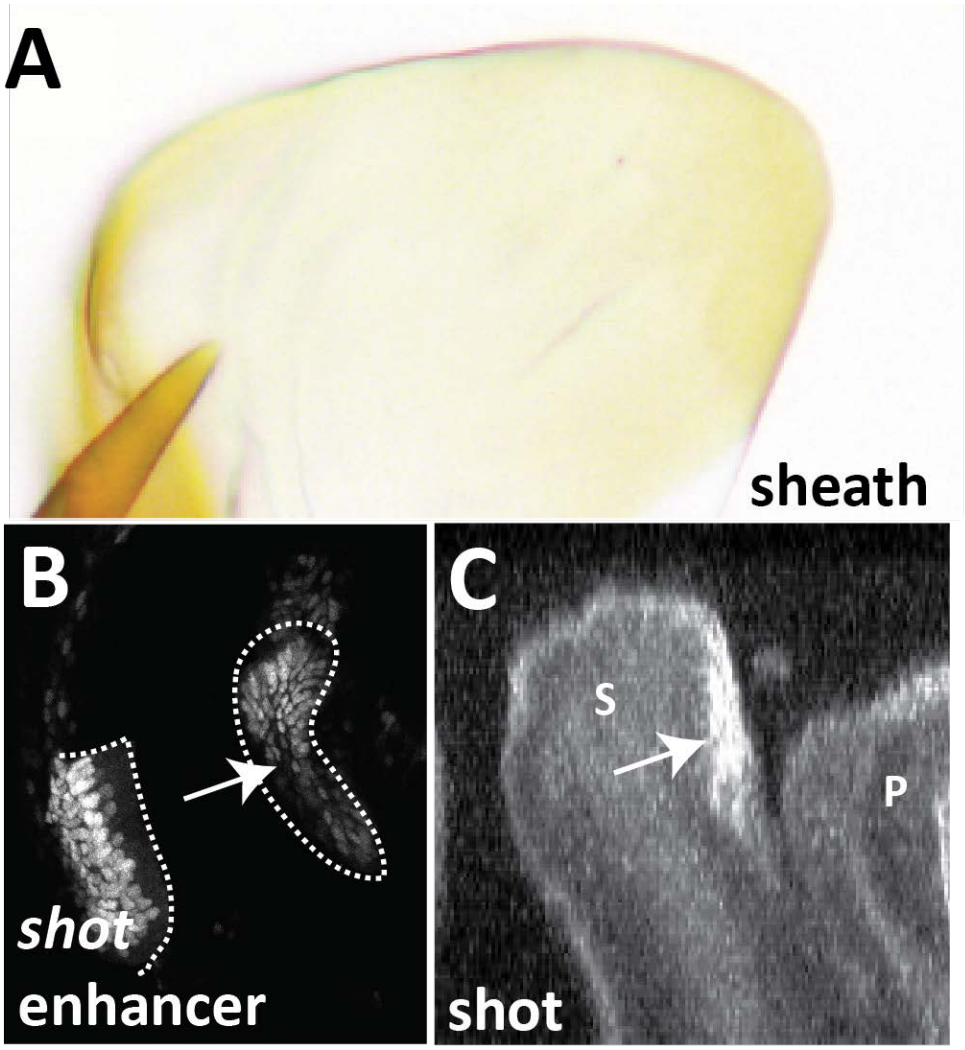

Figure 3.13 Potential regulatory and morphogenetic links to the phallic sheath.

(A) Bright-field image of the genital sheath. (B) The *shot* enhancer drives GFP expression in the posterior lobe and in the sheath (arrow). (C) Cross-section of the sheath showing Shot localized to the apical membranes of medial cells. All relevant structures labeled: sheath (S) and phallus (P).

4.0 Conclusions and future directions

4.1 Conclusion

Here, I have examined the regulation of a signaling pathway, whose expansion led to the activation of at least one cellular effector, contributing to the origination of the posterior lobe. Bridging the gap between patterning by signaling pathways and the resulting effect on morphogenesis is a complex and difficult task (Amundson, 2005). This work has begun to connect these processes, providing a stronger foundation on which future work can solidify this link. Furthermore, I have dissected the cellular processes that contribute to posterior lobe morphogenesis, and have demonstrated a role for the aECM. This highlights a potential role for extrinsic factors in evolving and shaping anatomical structures.

4.2 Future studies

4.2.1 Elucidating the expansion of JAK/STAT signaling in the posterior lobe

As discussed in chapter 3, the main enhancer that regulates *upd* expression in the posterior lobe is ancestral and likely drives early expression of *upd* in both lobed and non-lobed species. In addition to JAK/STAT, expansion of the Notch signaling pathway is vital for the evolution and morphogenesis of the posterior lobe (William J. Glassford, person communication). Preliminary evidence suggests that Delta, a ligand of the Notch signaling pathway, has potentially evolved *cis*-

regulatory changes to expand the activity of the Notch pathway during posterior lobe evolution (Donya Shodja, personal communication). Further, I have determined that the Notch signaling pathway is upstream of the JAK/STAT pathway (Figure 4.1). Future work will determine if the Notch pathway directly targets *upd* or if it is activated indirectly. In addition, further dissection of the enhancer, such as disruption of conserved sequences or identification of critical binding sites, can begin to identify regions required for activating *upd*, which can further illuminate how *upd* expression evolved in lobed species.

In addition to regulation at the enhancer level, other factors could affect signaling pathway activity that warrant exploration. For instance, Shot is known to stabilize the Notch receptor (Fuss, Josten, Feix, & Hoch, 2004) and thus could be important for proper Notch signaling in posterior lobe cells. In addition, while understudied, extrinsic forces could contribute to gene activation, as seen in feather bud patterning in chickens (Shyer et al., 2017). It is possible that evolutionary alterations to mechanical forces could lead to activation of JAK/STAT signaling or other signaling pathways and transcription factors. For instance, one could imagine a scenario in which the enhancer of *dumpy* evolves activity in the posterior lobe-forming region, increasing the level of Dumpy deposition, which could alter the mechanical environment of posterior lobe cells. The cells of the posterior lobe could detect this change in mechanical environment, and, in turn, lead to changes in gene regulation, potentially leading to activation of *upd.* While this model may appear far-fetched, it is nevertheless possible that many of the GRN features we observe result from such self-organizing processes which otherwise appear hard-wired in the genome. It will be interesting to dissect out the regulation of *dumpy* and *shot* to evaluate the possibility that "terminal nodes" of these networks represent key sites of evolutionary change. This is one of the potential great benefits of taking an evolutionary approach to GRN function and integration with cellular effectors.

4.2.2 Connecting signaling pathways to cellular effectors

In chapter 3, I demonstrated that JAK/STAT signaling activates the cellular effector, *shot*. Currently it is unknown if *dumpy* expression in the posterior lobe is also downstream of JAK/STAT signaling. To determine this, *dumpy* expression can be examined in the *upd* enhancer 1 deletion background, to determine if it is decreased. Given the strong upregulation of *dumpy* mRNA in this tissue, this experiment should provide information about the number of cells producing *dumpy* and their relative expression levels. In addition, distribution of the fusion protein Dumpy:YFP can also be examined in the *upd* deletion background. If drastic decreases in the amount of Dumpy:YFP are observed, this would indicate that *dumpy,* or a factor that can degrade Dumpy, is regulated by JAK/STAT signaling. Alternatively, levels of Dumpy:YFP may not be noticeably different, but Dumpy's association with posterior lobe cells may be altered (i.e. some cells may not be connected to the Dumpy-positive aECM). This would indicate that factors that anchor Dumpy to posterior lobe cells or factors that alter ECM organization are potential targets of JAK/STAT signaling (discussed in 4.2.3).

If it is determined that *dumpy* is activated in response to JAK/STAT activity, it will be interesting to identify the transcriptional enhancer of *dumpy*. Once an enhancer region is identified, we can begin to investigate how two cellular effectors, *dumpy* and *shot,* were integrated downstream of JAK/STAT signaling (or other signaling pathways). There are a few possible ways this could have occurred. First, these cellular effectors could ancestrally be downstream of JAK/STAT signaling in other contexts, so that once JAK/STAT is expanded in the posterior lobe, these factors are dragged along. A potential ancestral context where JAK/STAT signaling could

activate these factors is in other parts of the genitalia, specifically in the phallic sheath, which in the case of *shot*, shows signs of enhancer co-functionality (Figure 3.13B), and is also associated with dense concentrations of Dumpy (Figure 2.8). Another possibility is that the ancestral function of *upd* at very early time points in the lateral plate and clasper in non-lobed species (Figure 3.1A) may also activate *shot* and/or *dumpy*. Thus, by expanding the temporal extent of JAK/STAT signaling in lobed species (Figure 3.1A & B), *shot* and *dumpy* may be pulled along as well. Another possible ancestral context to examine are the posterior spiracles. Previous work has demonstrated that the posterior spiracle GRN was co-opted during the evolution of the posterior lobe (Glassford et al., 2015). Interestingly, I observed both Dumpy:YFP (Figure 2.22) and Shot (Figure 4.2) in the posterior spiracles. Both appear to be localized near the border between the spiracular chamber and the stigmatophore, where *upd* is expressed (Lovegrove et al., 2006). While these two observations are consistent with co-option for the posterior spiracles, *upd* is expressed in many tissues from which enhancers of either *shot* or *dumpy* could be co-opted from, which should also be explored. Indeed, these enhancers may have multiple pleiotropic functions and it may thus be difficult to pinpoint a single ancestral context from which these factors were co-opted. A second possibility is that these two cellular effectors could be recruited into posterior lobe morphogenesis through entirely independent mechanisms. While the model of co-option involving a single step that recruits all components is the simplest scenario for the evolutionary origin of a structure, this may yet not be how it occurred. The signaling pathways, transcription factors, and cellular effectors required for posterior lobe morphogenesis could be recruited to the posterior lobe gene regulatory network via several steps, and thus regulation of *shot* and *dumpy* may occur through different upstream regulators and associated ancestral developmental contexts. Finally, as mentioned earlier, evolution at the enhancer level could have occurred to either of these cellular

effectors, which would suggest a more piecemeal assembly of the network, and future work could examine potential mechanical contributions to gene expression in the posterior lobe.

In addition to understanding how signaling pathways are linked to cellular effectors, future work will also focus on understanding what components in a GRN are targets for diversification. The posterior lobe is remarkably diverse across species (Coyne, 1993) and it will be interesting to determine what factors were targets during its diversification (i.e. signaling pathways, transcription factors, or cellular effectors). Specifically, it will be fascinating to determine whether factors involved in diversification were the same factors that evolved during its origination.

4.2.3 The mechanical role of the aECM during posterior lobe morphogenesis

The work presented here demonstrates a vital role for the aECM during posterior lobe morphogenesis. However, what is currently not known is how and if the aECM mechanically contributes to lobe formation. As mentioned in chapter 2, there are three potential roles the aECM could serve, all of which could contribute to its morphogenesis. First, the aECM could contribute to the production of tensile stress in the posterior lobe, leading to elongation of the cells in the direction of that force. This could occur by the aECM pulling on the cells of the lobe through an active process or 'holding' the cells of the lobe in place while a different active force pulls the lateral plate tissue down (Figure 4.3). Preliminary evidence suggests a pulling force may be possible. When Dumpy:YFP is examined during posterior lobe development, 'shrinking' of the aECM towards the center of the genitalia can be observed (Video 4.1) and preliminary quantification, based on morphological features of the aECM, support this observation (Figure 4.4). To more accurately determine if the aECM is 'shrinking' (i.e. becoming more compact) small regions of the aECM can be photobleached in the Dumpy:YFP background and length

measurements of the photobleached area over time can then be completed to determine if the photobleached area is 'shrinking'. Work in the trachea suggests that Dumpy does not diffuse (Dong, Hannezo, & Hayashi, 2014b), which is consistent with our results that show a stable organization of Dumpy:YFP over time in the genitalia, so recovery due to diffusion should not present a major concern. There is concern that nascent expression of Dumpy could affect these results, but this can be avoided by completing the test in regions where *dumpy* is not actively being expressed (based on *in situ* hybridization results). These results, combined with the measurements based on morphological features of the aECM, could together provide support for processes involving progressive aECM compaction.

However, what remains unclear is if the aECM is actively constricting or whether it is being 'pushed' together due to its association with the cells of the genitalia. One way to determine if the aECM could actively be constricting is to utilize laser ablation to cut the aECM, which would release the aECM from its attached cells. If the aECM constricts in response, this would indicate that the aECM is under tension and suggests that it could be exerting a pulling force on the cells of the posterior lobe. However, if no response is observed, this would suggest that tissue level forces could be causing the aECM to become more compact.

Alternative to actively pulling the cells, the aECM could be 'holding' the cells of the posterior lobe while other forces pull the tissue down. If the aECM is holding the cells of the posterior lobe, a drop in the lateral plate would be expected over long periods of genital development when the aECM is removed, similar to what is observed in non-lobed species (Figure 2.2). To begin to test this idea, a full removal of the aECM associated with posterior lobe cells would need to be completed, which is currently not possible with RNAi. Alternatively, trypsin digest could be completed to remove the aECM at different time points in development, as

previously demonstrated in the wing (Ray et al., 2015). If a drop is observed, this would indicate the presence of downward forces that are normally 'resisted' by the aECM. Future work can begin to dissect out what those forces are, which could potentially be due to the neighboring abdominal tissue or the cleavage of the lateral plate and clasper.

A second role the aECM could be serving is a support role while active processes within the lobe are responsible for the force that drives apico-basal elongation. It is possible that due to the extreme height of these cells additional support may be needed during posterior lobe morphogenesis (Figure 4.3). The cytoskeleton is difficult disrupt, due the requirement for these components in other cellular functions, especially for the microtubules, which are needed to shuttle cargo along the long distances of the apico-basal axis in elongated cells. Disentangling whether this is the major role of the aECM will be difficult, but if the other two hypotheses are disproven, that may indicate that a support role for the aECM is important.

Finally, the aECM could affect signaling pathway activity during posterior lobe morphogenesis (Figure 4.3). Here I have shown a role for JAK/STAT signaling, but the Notch signaling pathway is also active and contributes to posterior lobe morphogenesis (personal communication with Bill Glassford and Donya Shodja). To determine if aECM contributes to signaling pathway activity, the 10X STAT GFP reporter and the mbeta:GFP reporter (made by Donya Shodja as a readout of Notch activity) could be examined in a *dumpy* RNAi background to determine if levels of activity are altered when the aECM is perturbed. If this is demonstrated, it will be interesting to dissect out the cause of this. Does the aECM simply affect diffusion or does it play a mechanical role that is required to activate gene expression?

If it is determined that the aECM plays a mechanical role in posterior lobe morphogenesis, it will be interesting to determine which connections are most vital (Figure 4.3). As shown in

chapter 2, the aECM on the developing genitalia forms an intricate network. A strong deposition of aECM is correlated with the ventral side of the posterior lobe, which forms a sharp point, while the dorsal side is rounded. Potentially, the levels of dumpy connected to the ventral side of the lobe is important for forming this sharp point. This increase of dumpy associated with the ventral side spans over the clasper and appears to connect to the sheath and phallus, which reside centrally within the genitalia. This raises the hypothesis that connections to other structures might be important for its function during posterior lobe morphogenesis. It will be interesting to perturb the aECM, either by RNAi or laser ablation, at different points in the genitalia to determine which connections are important, if any, for posterior lobe morphogenesis.

In addition to a potential direct role during posterior lobe morphogenesis, the aECM could also play an indirect role. In chapter 2, I observed a tether of aECM spanning from the anal plate and connecting to the surrounding pupal cuticle (Figure 2.11). This attachment could contribute indirectly to posterior lobe morphogenesis, and if so, I would hypothesize that altering it would disrupt morphogenesis of most genital structures. A quick way to test if the tether is required is to grow the genitalia *ex vivo* with and without the cuticle. I have grown the genitalia *ex vivo* with the cuticle still attached, as have others (Sato et al., 2015), and the posterior lobe develops normally (not shown). If this experiment demonstrates a requirement for the surrounding cuticle, then laser ablation could be completed on the tether to determine whether and how its disruption leads to defects in development. If it is important for genital development, then identifying the role of the tether would be important to understanding posterior lobe morphogenesis. The tether could play a role in creating tension in the aECM or be important for the structural organization of the aECM over the genitalia.

Finally, a missing link in understanding how the aECM controls morphogenesis of the posterior lobe is understanding if it is directly connected to posterior lobe cells and how it is attached. Dumpy is a ZP domain protein which can form homo- and hetero-dimers (Gupta et al., 2012). In addition, there are numerous transmembrane ZP proteins that could be important for anchoring Dumpy to posterior lobe cells (Jaźwińska & Affolter, 2004; Jaźwińska, Ribeiro, & Affolter, 2003; Roch, 2003). Through *in situ* hybridization, antibody stains, and RNAi knockdown experiments, we can explore what these factors are, if they are specific to the posterior lobe, and how they evolved a role in posterior lobe morphogenesis.

4.2.4 Elucidate potential interactions between Shot and Dumpy

While both Shot and Dumpy play a role in posterior lobe morphogenesis, what remains to be determined is how *shot* functions during posterior lobe morphogenesis. Shot plays a role in stabilizing or localization of other proteins at the apical membrane (Voelzmann et al., 2017). This stimulates the hypothesis that Shot could stabilize a transmembrane protein with a ZP domain to bind to Dumpy (also a ZP protein). By examining Dumpy:YFP in a *shot* RNAi background, we can determine if Dumpy localization is altered in the absence of *shot*. In addition, identification of these other ZP proteins (proposed in 4.2.3) could further help elucidate if Shot is important for their localization in the posterior lobe.

It is possible that Shot and Dumpy function independently. Another potential role for *shot* during posterior lobe morphogenesis is that it may contribute to tubulin organization. It is known that Shot can bind to both microtubules and actin independently or by linking them together (Voelzmann et al., 2017). Given the localization of Shot to the apical membrane in posterior lobe cells, one may hypothesize that Shot anchors microtubules to the actin cortex, where it would

create a microtubule organizing center, as has been observed in other instances (Applewhite et al., 2010; Nashchekin, Fernandes, & St Johnston, 2016). Future work can analyze the numerous domains of Shot, which have been analyzed in great detail, to determine which are required for posterior lobe formation (Voelzmann et al., 2017).

In conclusion, this work has begun to bridge the gap between signaling pathways and cellular effectors and their resulting influence on morphogenesis. The experiments proposed here will help focus future research on the vital morphogenetic processes and interactions between signaling pathways and cellular effectors that contribute to posterior lobe development. By examining evolutionary changes in these relationships, the field can move towards a genetic perspective regarding how these processes are constructed together.

4.3 Figures and videos

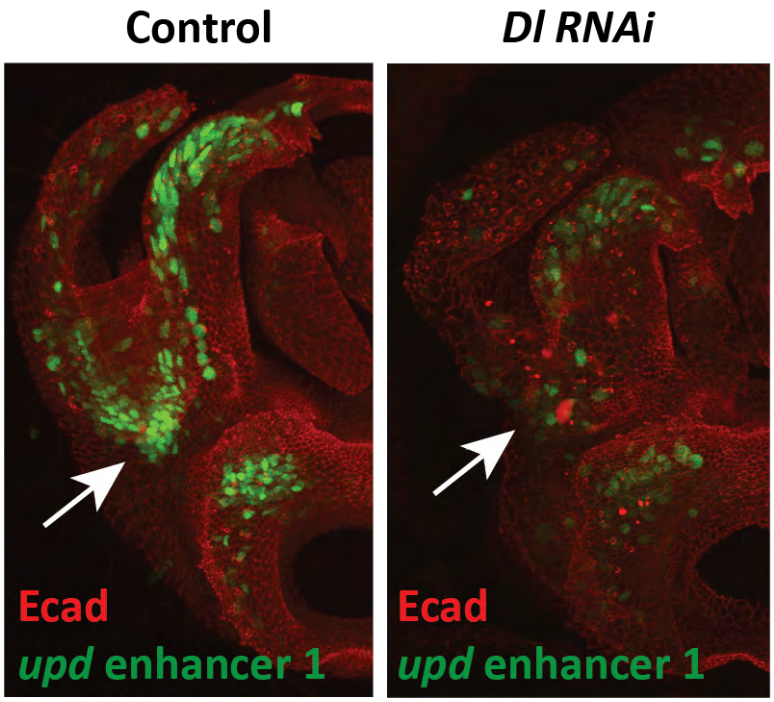

Figure 4.1 *upd* enhancer 1 of the JAK/STAT pathway is downstream of Notch signaling.

Activity of *upd* enhancer 1 (inserted into 51D) in *mCherry* (control) RNAi knockdown (left) and *Delta* (*Dl*) RNAi knockdown (right). Reduction in *upd* enhancer 1 activity is observed in the *Dl* knockdown.

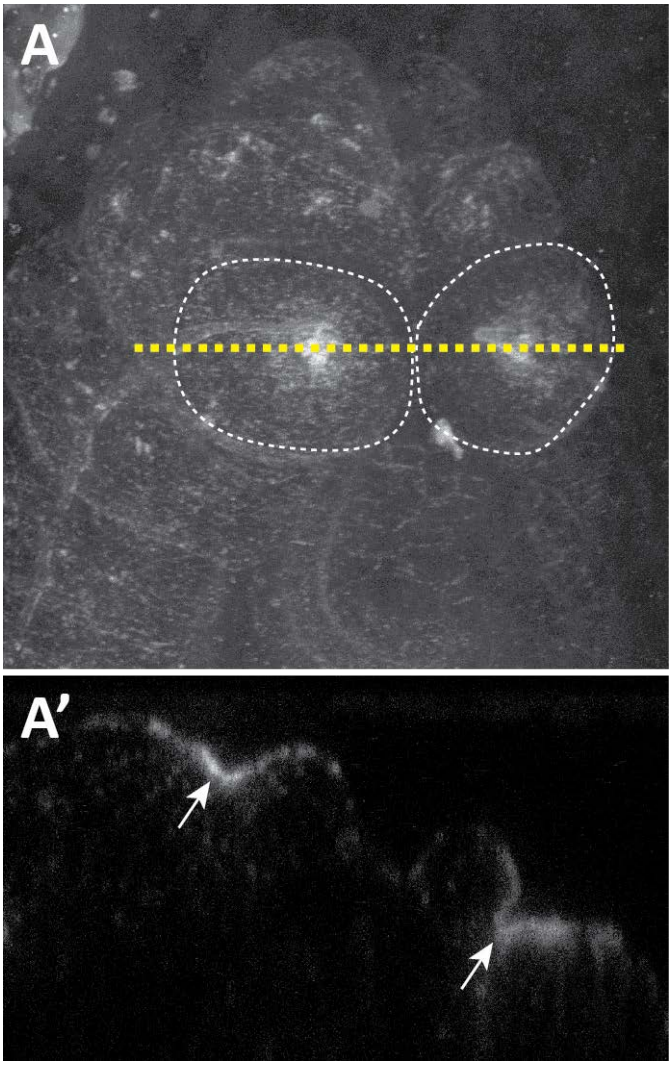

Figure 4.2 Shot localizes to the apical membrane in the posterior spiracles.

(A) Shot antibody in a late stage embryo (~stage 16) with posterior spiracles outlined. Yellow line represents location of respective cross-section in A'. Shot is localized to apical membrane in posterior spiracles (A' arrows) near the border between the spiracular chamber (inner structure) and the stigmatophore (outer structure).

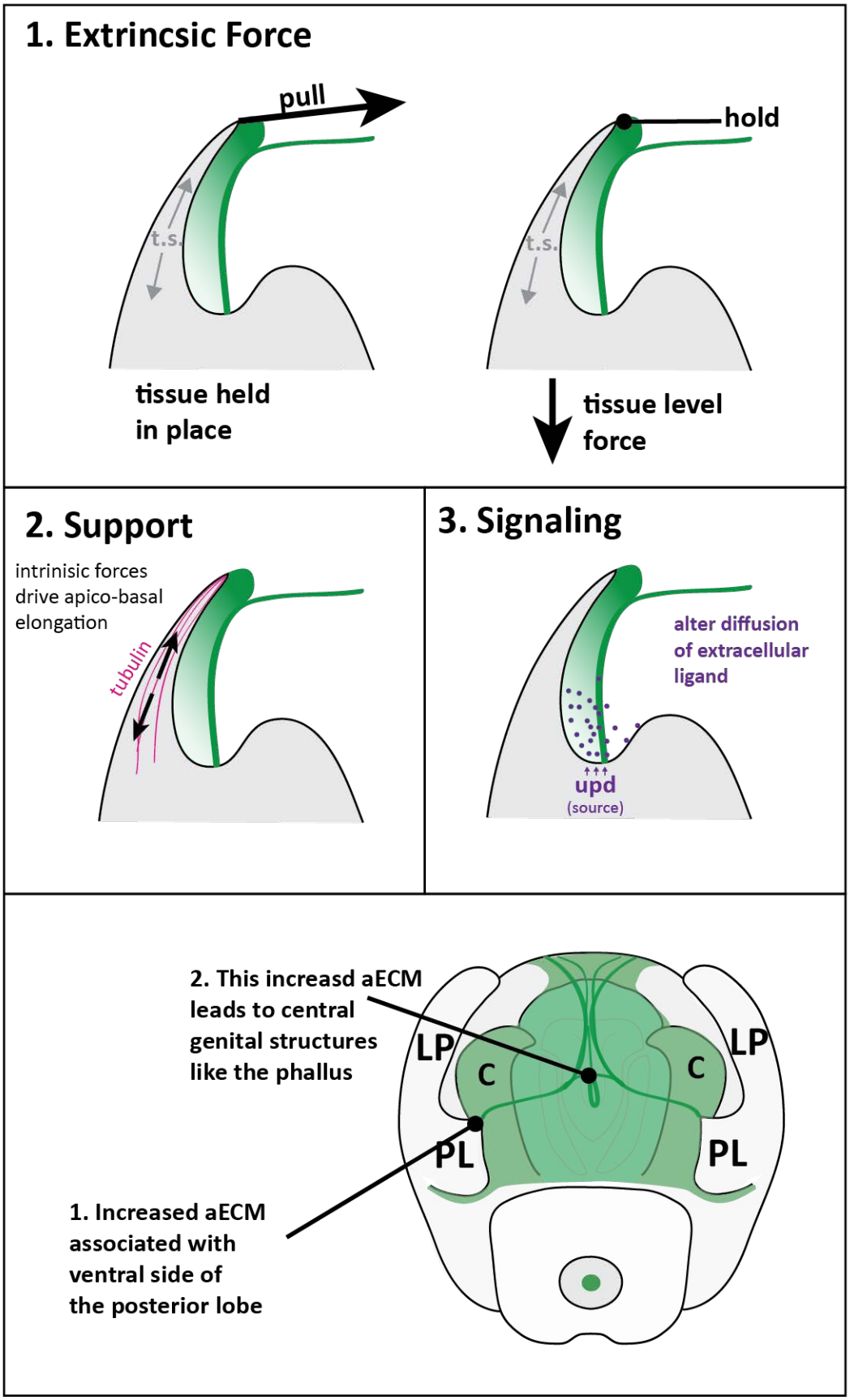
1. Extrincsic Force
pull
hold
t.s.
t.s.
tissue held
in place
tissue level
force
2. Support
intrinisic forces
drive apico-basal
elongation
tubulin
3. Signaling
alter diffusion
of extracellular
ligand
upd
(source)
2. This increasd aECM
leads to central
genital structures
like the phallus
LP
C
C
LP
PL
PL
1. Increased aECM
associated with
ventral side of
the posterior lobe

Figure 4.3 Hypothetical models for aECM function role during posterior lobe morphogenesis.

(1) The aECM could provide extrinsic forces which contribute to tensile stress (t.s.) production in the posterior lobe. This could occur through an active pulling force (left) or by holding the cells of the posterior lobe while other forces pull on the posterior lobe cells in the opposite direction (right). (2) The aECM could support the cells of the posterior lobe as intrinsic forces drive them to elongate along their apico-basal axis. (3) The aECM could affect signaling dynamics, such as the ability or localization of extracellular ligand diffusion. (Bottom - 1) An increase in Dumpy:YFP is observed associated with the ventral side of the posterior lobe. This localized increase connects to central genital structures (Bottom – 2).

Video 4.1 Dumpy (aECM) 'shrinks' during posterior lobe morphogenesis.

Time-lapse cross-section movie of Dumpy:YFP (green) and the epithelial cells (magenta) during genital development. Both posterior lobes can be observed in the movie and are the two most outer (left and right) structures in the movie.

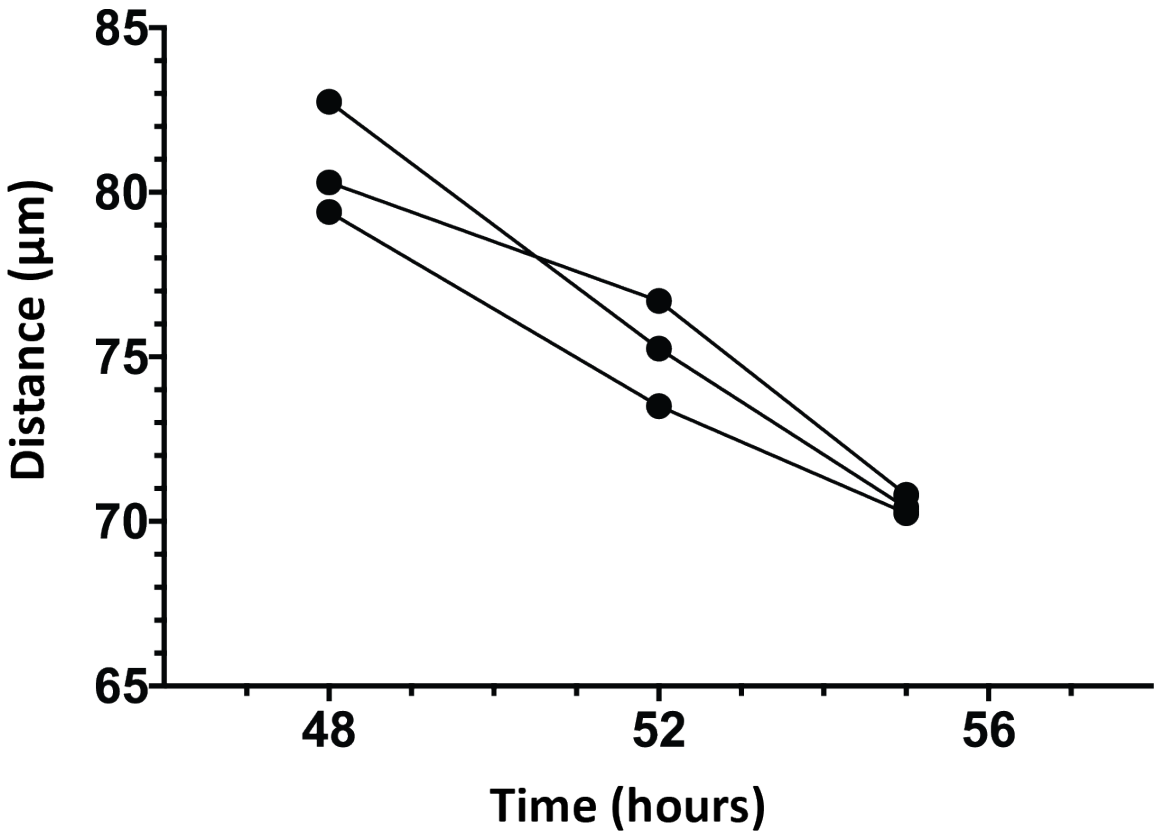

Figure 4.4 Quantification of aECM 'shrinking' during posterior lobe morphogenesis.

The Distance between the aECM localized near the posterior lobe and aECM associated with the phallus during posterior lobe development is plotted over time. Each line represents 1 sample which was live-imaged. Time points are not comparable to others in this document as these sample were observed under uncontrolled temperature settings. p=0.0093 for 48 vs 55 hours.1

Appendix A Key resource and methods

A.1 Key resources

Table A.1 Key Resources

Reagent type (species) or resource	Designation	Source or reference	Identifiers	Additional Information
Antibody	rat anti-alpha tubulin (tyrosinated)	MilliporeSigma	Millipore Cat# MAB1864-I	IHC (1:500)
Antibody	mouse anti-alpha tubulin (acetylated)	Sigma-Aldrich	Sigma-Aldrich Cat# T6793, RRID:AB_477585	IHC (1:500)
Antibody	rat anti-Ecadherin	DSHB	DSHB Cat# DCAD2, RRID:AB_528120	IHC (1:500)
Antibody	mouse anti-fasciclin III	DSHB	DSHB Cat# 7G10 anti-Fasciclin III, RRID:AB_528238	IHC (1:500)
Antibody	rabbit anti-histone H3 (phospho S10)	Abcam	Abcam Cat# ab5176, RRID:AB_304763	IHC (1:50)
Antibody	goat anti-GFP	Abcam	Abcam Cat# ab6662, RRID:AB_305635	IHC (1:300)
Antibody	fluorescein Vicia Villosa Lectin (VVA)	Vector Laboratories	Vector Laboratories Cat# FL-1231, RRID:AB_2336856	IHC (1:200)
Antibody	mouse anti-Shot	DSHB	DSHB Cat# anti-Shot mABRod1, RRID:AB_ 528467	
Chemical compound, drug	rhodamine phalloidin	Thermo Fisher Scientific	Thermo Fisher Scientific Cat# R415, RRID:AB_2572408	IHC (1:200)

Strain, strain background (*Drosophila melanogaster*)	y^1w^1 *Drosophila melanogaster*	Bloomington Drosophila Stock Center	BDSC Cat# 1495, RRID:BDSC_1495	
Strain, strain background (*Drosophila biarmipes*)	wild type	National Drosophila Species Stock Center (NDSSC)	NDSSC Stock #: 14023-0361.10 RRID:FlyBase_FBst 0203870	
Strain, strain background (*Drosophila ananassae*)	wild type	National Drosophila Species Stock Center (NDSSC)	NDSSC Stock #: 14024-0371.13 RRID:FlyBase_FBst 0201380	No longer available
Strain, strain background (*Drosophila pseudoobscura*)	wild type	National Drosophila Species Stock Center (NDSSC)	NDSSC Stock #: 14011-0121.87 RRID:FlyBase_FBst 0200074	No longer available
Genetic reagent (*Drosophila melanogaster*)	*UAS*-Raeppli-CAAX	Bloomington Drosophila Stock Center (BDSC)	BDSC Cat# 55084, RRID:BDSC_55084	
Genetic reagent (*Drosophila melanogaster*)	*pox neuro-Gal4*	(Boll & Noll, 2002)	Construct #13	
Genetic reagent (*Drosophila melanogaster*)	*D. simulans pox neuro*-Gal4	This paper	N/A	
Genetic reagent (*Drosophila melanogaster*)	hs – flippase^{122}	Gift from Erika A. Bach	Flybase: FBtp0001101	
Genetic reagent (*Drosophila melanogaster*)	*armadillo-GFP*	Bloomington Drosophila stock center	BDSC Cat# 8556, RRID:BDSC_8556	
Genetic reagent (*Drosophila melanogaster*)	Dumpy:YFP	Drosophila Genomics and Genetic Resources	DGGR Cat# 115238, RRID:DGGR_115238	
Genetic reagent (*Drosophila melanogaster*)	E-cadherin:mCherry	Bloomington Drosophila stock center	BDSC Cat# 59014, RRID:BDSC_59014	
Genetic reagent (*Drosophila melanogaster*)	*UAS*-dumpyRNAi	Vienna Drosophila Resource Center	VDRC Cat#44029, RRID:FlyBase_FBst 0465370	
Genetic reagent	*UAS*-mCherryRNAi	Bloomington	BDSC Cat# 35785,	

(*Drosophila melanogaster*)		Drosophila stock center	RRID:BDSC_35785	
Genetic reagent (*Drosophila melanogaster*)	*UAS-apcRNAi*	Bloomington Drosophila stock center	BDSC Cat# 28582 RRID:BDSC_28582	
Genetic reagent (*Drosophila melanogaster*)	*UAS-apcRNAi*	Bloomington Drosophila stock center	BDSC Cat# 34869, RRID:BDSC_34869	
Genetic reagent (*Drosophila melanogaster*)	*UAS-apc2RNAi*	Bloomington Drosophila stock center	BDSC Cat# 28585, RRID:BDSC_28585	
Genetic reagent (*Drosophila melanogaster*)	*UAS-apc2RNAi*	Bloomington Drosophila stock center	BDSC Cat# 34875, RRID:BDSC_34875	
Genetic reagent (*Drosophila melanogaster*)	*UAS-chbRNAi*	Bloomington Drosophila stock center	BDSC Cat# 35442, RRID:BDSC_35442	
Genetic reagent (*Drosophila melanogaster*)	*UAS-chbRNAi*	Bloomington Drosophila stock center	BDSC Cat# 34669, RRID:BDSC_34669	
Genetic reagent (*Drosophila melanogaster*)	*UAS-crmpRNAi*	Bloomington Drosophila stock center	BDSC Cat# 53354, RRID:BDSC_53354	
Genetic reagent (*Drosophila melanogaster*)	*UAS-crmpRNAi*	Bloomington Drosophila stock center	BDSC Cat# 62479, RRID:BDSC_62479	
Genetic reagent (*Drosophila melanogaster*)	*UAS-dhc36cRNAi*	Bloomington Drosophila stock center	BDSC Cat# 51726, RRID:BDSC_51726	
Genetic reagent (*Drosophila melanogaster*)	*UAS-dhc64cRNAi*	Bloomington Drosophila stock center	BDSC Cat# 36698, RRID:BDSC_36698	
Genetic reagent (*Drosophila melanogaster*)	*UAS-diaRNAi*	Bloomington Drosophila stock center	BDSC Cat# 28541, RRID:BDSC_28541	
Genetic reagent (*Drosophila melanogaster*)	*UAS-diaRNAi*	Bloomington Drosophila stock center	BDSC Cat# 33424, RRID:BDSC_33424	
Genetic reagent (*Drosophila*	*UAS-dia constitutively active*	Bloomington Drosophila	BDSC Cat# 27616, RRID:BDSC_27616	

melanogaster)		stock center		
Genetic reagent (*Drosophila melanogaster*)	*UAS-dia constitutively active*	Bloomington Drosophila stock center	BDSC Cat# 56753, RRID:BDSC_56753	
Genetic reagent (*Drosophila melanogaster*)	*UAS-feoRNAi*	Bloomington Drosophila stock center	BDSC Cat# 35467, RRID:BDSC_35467	
Genetic reagent (*Drosophila melanogaster*)	*UAS-feoRNAi*	Bloomington Drosophila stock center	BDSC Cat# 28926, RRID:BDSC_28926	
Genetic reagent (*Drosophila melanogaster*)	*UAS-futschRNAi*	Bloomington Drosophila stock center	BDSC Cat# 40834, RRID:BDSC_40834	
Genetic reagent (*Drosophila melanogaster*)	*UAS-glRNAi*	Bloomington Drosophila stock center	BDSC Cat# 24761, RRID:BDSC_24761	
Genetic reagent (*Drosophila melanogaster*)	*UAS-glRNAi*	Bloomington Drosophila stock center	BDSC Cat# 24760, RRID:BDSC_24760	
Genetic reagent (*Drosophila melanogaster*)	*UAS-klp59cRNAi*	Bloomington Drosophila stock center	BDSC Cat# 35596, RRID:BDSC_35596	
Genetic reagent (*Drosophila melanogaster*)	*UAS-klp59dRNAi*	Bloomington Drosophila stock center	BDSC Cat# 35474, RRID:BDSC_35474	
Genetic reagent (*Drosophila melanogaster*)	*UAS-klp67aRNAi*	Bloomington Drosophila stock center	BDSC Cat# 62383, RRID:BDSC_62383	
Genetic reagent (*Drosophila melanogaster*)	*UAS-klp67aRNAi*	Bloomington Drosophila stock center	BDSC Cat# 27549, RRID:BDSC_27549	
Genetic reagent (*Drosophila melanogaster*)	*UAS-lis1RNAi*	Bloomington Drosophila stock center	BDSC Cat# 35043, RRID:BDSC_35043	
Genetic reagent (*Drosophila melanogaster*)	*UAS-lis1RNAi*	Bloomington Drosophila stock center	BDSC Cat# 28663, RRID:BDSC_28663	
Genetic reagent (*Drosophila melanogaster*)	*UAS-mspsRNAi*	Bloomington Drosophila stock center	BDSC Cat# 38990, RRID:BDSC_38990	
Genetic reagent	*UAS-mspsRNAi*	Bloomington	BDSC Cat# 31138,	

(*Drosophila melanogaster*)		Drosophila stock center	RRID:BDSC_31138	
Genetic reagent (*Drosophila melanogaster*)	*UAS-ncdRNAi*	Bloomington Drosophila stock center	BDSC Cat# 58144, RRID:BDSC_58144	
Genetic reagent (*Drosophila melanogaster*)	*UAS-rhogef2RNAi*	Bloomington Drosophila stock center	BDSC Cat# 34643, RRID:BDSC_34643	
Genetic reagent (*Drosophila melanogaster*)	*UAS-sggRNAi*	Bloomington Drosophila stock center	BDSC Cat# 38293, RRID:BDSC_38293	
Genetic reagent (*Drosophila melanogaster*)	*UAS-sggRNAi*	Bloomington Drosophila stock center	BDSC Cat# 31308, RRID:BDSC_31308	
Genetic reagent (*Drosophila melanogaster*)	*UAS-shotRNAi*	Bloomington Drosophila stock center	BDSC Cat# 64041, RRID:BDSC_64041	
Genetic reagent (*Drosophila melanogaster*)	*UAS-staiRNAi*	Bloomington Drosophila stock center	BDSC Cat# 36902, RRID:BDSC_36902	
Genetic reagent (*Drosophila melanogaster*)	*UAS-staiRNAi*	Bloomington Drosophila stock center	BDSC Cat# 53925, RRID:BDSC_53925	
Genetic reagent (*Drosophila melanogaster*)	*UAS-stimRNAi*	Bloomington Drosophila stock center	BDSC Cat# 52911, RRID:BDSC_52911	
Genetic reagent (*Drosophila melanogaster*)	*UAS-stimRNAi*	Bloomington Drosophila stock center	BDSC Cat# 27263, RRID:BDSC_27263	
Genetic reagent (*Drosophila melanogaster*)	*UAS-tauRNAi*	Bloomington Drosophila stock center	BDSC Cat# 28891, RRID:BDSC_28891	
Genetic reagent (*Drosophila melanogaster*)	*UAS-tauRNAi*	Bloomington Drosophila stock center	BDSC Cat# 40875, RRID:BDSC_40875	
Genetic reagent (*Drosophila melanogaster*)	*UAS-tumRNAi*	Bloomington Drosophila stock center	BDSC Cat# 35007, RRID:BDSC_35007	
Genetic reagent (*Drosophila melanogaster*)	*UAS-tumRNAi*	Bloomington Drosophila stock center	BDSC Cat# 28982, RRID:BDSC_28982	

Genetic reagent (*Drosophila melanogaster*)	*shot-gal4*	Bloomington Drosophila stock center	BDSC Cat# 47350, RRID:BDSC_47350	
Genetic reagent (*Drosophila melanogaster*)	*shot-gal4*	Bloomington Drosophila stock center	BDSC Cat# 47921, RRID:BDSC_47921	
Genetic reagent (*Drosophila melanogaster*)	*shot-gal4*	Bloomington Drosophila stock center	BDSC Cat# 49958, RRID:BDSC_49958	
Genetic reagent (*Drosophila melanogaster*)	*shot-gal4*	Bloomington Drosophila stock center	BDSC Cat# 49964, RRID:BDSC_49964	
Genetic reagent (*Drosophila melanogaster*)	*shot-gal4*	Bloomington Drosophila stock center	BDSC Cat# 46521, RRID:BDSC_46521	
Genetic reagent (*Drosophila melanogaster*)	*shot-gal4*	Bloomington Drosophila stock center	BDSC Cat# 49537, RRID:BDSC_49537	
Genetic reagent (*Drosophila melanogaster*)	*shot-gal4*	Bloomington Drosophila stock center	BDSC Cat# 49542, RRID:BDSC_49542	
Genetic reagent (*Drosophila melanogaster*)	*shot-gal4*	Bloomington Drosophila stock center	BDSC Cat# 50014, RRID:BDSC_50014	Posterior lobe enhancer
Genetic reagent (*Drosophila melanogaster*)	*shot-gal4*	Bloomington Drosophila stock center	BDSC Cat# 50020, RRID:BDSC_50020	
Recombinant DNA reagent	pS3aG4	Gift from Benjamin Prud'homme	N/A	Gal4 vector used to make *D. simulans pox neuro* gal4 line
Recombinant DNA reagent	pS3aG	(Williams et al., 2008)	N/A	GFP vector
Recombinant DNA reagent	pBAC	(Horn & Wimmer, 2000a)	N/A	PiggyBAC vector
Recombinant DNA reagent	attp dsRED attp homology arm vector	Gift from Thomas Williams.	N/A	Homology arm vector
Recombinant DNA reagent	pCFD3: U6:3-gRNA	(Port, Chen, Lee, & Bullock, 2014) Addgene	RRID:Addgene_49410	gRNA vector for enhancer 2 deletion

Recombinant DNA reagent	pNos-cas9	Addgene	RRID:Addgene_62208	Cas9 source for enhancer 2 deletion
Sequence-based reagent	GCCACTAACAATCCATGCGGTT	N/A	N/A	*dumpy* probe forward primer
Sequence-based reagent	TAATACGACTCACTATAGGGAGAAATAGCCCTGTCCTTGGAATCC	N/A	N/A	*dumpy* probe reverse primer with T7 primer
Sequence-based reagent	TTCCGGGCGCGCCTCGGTGGCTTAACACGCGCATT	N/A	N/A	*D. simulans pox neuro* forward primer for gal 4 line
Sequence-based reagent	TTGCCCCTGCAGGATCGCTGATTCCATGGCCCAGT	N/A	N/A	*D. simulans pox neuro* reverse primer for gal 4 line
Sequence-based reagent	TTCCGggcgcgccCGTATCAGTTTGCAATGGGTGGTG	N/A	N/A	*upd* locus screen reporter 1F
Sequence-based reagent	TTGCCcctgcaggCACCACCCATTGCAAACTGATACG	N/A	N/A	*upd* locus screen reporter 1R
Sequence-based reagent	TTCCGggcgcgccTTGCGTCACAATGCCGTACAACTC	N/A	N/A	*upd* locus screen reporter 2F
Sequence-based reagent	TTGCCcctgcaggGAGTTGTACGGCATTGTGACGCAA	N/A	N/A	*upd* locus screen reporter 2R
Sequence-based reagent	TTCCGggcgcgccCCAACGCGTTCCAGTTCCAAT	N/A	N/A	*upd* locus screen reporter 3F
Sequence-based reagent	TTGCCcctgcaggATTGGAACTGGAACGCGTTGG	N/A	N/A	*upd* locus screen reporter 3R
Sequence-based reagent	TTCCGggcgcgccCCAGCAAATGGAGCATCTGAAACG	N/A	N/A	*upd* locus screen reporter 4F
Sequence-based reagent	TTGCCcctgcaggCGTTTCAGATGCTCCATTTGCTGG	N/A	N/A	*upd* locus screen reporter 4R
Sequence-based reagent	TTCCGggcgcgccGCTCGTCTTATCGCAGCAACA	N/A	N/A	*upd* locus screen reporter 5/enhancer 1F also used for pBAC

Sequence-based reagent	TTGCCcctgcaggTGTTGCTGCGATAAGACGAGC	N/A	N/A	*upd* locus screen reporter 5/enhancer 1R also used for pBAC
Sequence-based reagent	TTCCGggcgcgccAGCAGGCGCTTGTGATTATCCTTTC	N/A	N/A	*upd* locus screen reporter 6F
Sequence-based reagent	TTGCCcctgcaggGAAAGGATAATCACAAGCGCCTGCT	N/A	N/A	*upd* locus screen reporter 6R
Sequence-based reagent	TTCCGggcgcgccATTGTCCCGATCCTGATCCATGGTG	N/A	N/A	*upd* locus screen reporter 7F
Sequence-based reagent	TTGCCcctgcaggCACCATGGATCAGGATCGGGACAAT	N/A	N/A	*upd* locus screen reporter 7R
Sequence-based reagent	TTCCGggcgcgccATTCATTGAGCGCTGGCCAAGTGTC	N/A	N/A	*upd* locus screen reporter 8/enhancer 2F used for all lobed species and *pseudoobscura*
Sequence-based reagent	TTGCCcctgcaggGACACTTGGCCAGCGCTCAATGAAT	N/A	N/A	*upd* locus screen reporter 8/enhancer 2R used for all lobed species and *pseudoobscura*
Sequence-based reagent	TTCCGggcgcgccATCCTGATCCGCTGAGCCATTGTTC	N/A	N/A	*upd* locus screen reporter 9F
Sequence-based reagent	TTGCCcctgcaggGAACAATGGCTCAGCGGATCAGGAT	N/A	N/A	*upd* locus screen reporter 9R
Sequence-based reagent	TTCCGggcgcgccCTTGTCTGTTGGCTGCGTGTAAGAC	N/A	N/A	*upd* locus screen reporter 10F
Sequence-based reagent	TTGCCcctgcaggGTCTTACACGCAGCCAACAGACAAG	N/A	N/A	*upd* locus screen reporter 10R
Sequence-based reagent	TTCCGggcgcgccTACCCGGTGATCATCACGCATTTGC	N/A	N/A	*upd* locus screen reporter 11F

Sequence-based reagent	TTGCCcctgcaggGCAAATGCGTGATGATCACCGGGTA	N/A	N/A	*upd* locus screen reporter 11R
Sequence-based reagent	TTCCGggcgcgccGGTAAGTACAAGTAACTACCGCAGG	N/A	N/A	*upd* locus screen reporter 12F
Sequence-based reagent	TTGCCcctgcaggCCTGCGGTAGTTACTTGTACTTACC	N/A	N/A	*upd* locus screen reporter 12R
Sequence-based reagent	TTCCGggcgcgccAGCACCAAGACTCTGGACATTGTCG	N/A	N/A	*upd* locus screen reporter 13F
Sequence-based reagent	TTGCCcctgcaggCGACAATGTCCAGAGTCTTGGTGCT	N/A	N/A	*upd* locus screen reporter 13R
Sequence-based reagent	TTCCGggcgcgccTCCTGGCGCCATATCAATTACACTC	N/A	N/A	*upd* locus screen reporter 14F
Sequence-based reagent	TTGCCcctgcaggGAGTGTAATTGATATGGCGCCAGGA	N/A	N/A	*upd* locus screen reporter 14R
Sequence-based reagent	TTCCGggcgcgccCTCTTGACCTTTTGCGGCTATTTGG	N/A	N/A	*upd* locus screen reporter 15F
Sequence-based reagent	TTGCCcctgcaggCCAAATAGCCGCAAAAGGTCAAGAG	N/A	N/A	*upd* locus screen reporter 15R
Sequence-based reagent	TTCCGggcgcgccCTTTCGTCGTCAGCTCGTCAGTTTG	N/A	N/A	*upd* locus screen reporter 16F
Sequence-based reagent	TTGCCcctgcaggCAAACTGACGAGCTGACGACGAAAG	N/A	N/A	*upd* locus screen reporter 16R
Sequence-based reagent	TTCCGggcgcgccGTTCACCTTGTTTATGGACTCGCTG	N/A	N/A	*upd* locus screen reporter 17F
Sequence-based reagent	TTGCCcctgcaggCAGCGAGTCCATAAACAAGGTGAAC	N/A	N/A	*upd* locus screen reporter 17R
Sequence-based reagent	TTCCGggcgcgccATGCATCAATTAG	N/A	N/A	*upd* locus screen reporter 18F

	CTCCCACTGAGC			
Sequence-based reagent	TTGCCcctgcaggGCTCAGTGGGAGCTAATTGATGCAT	N/A	N/A	*upd* locus screen reporter 18R
Sequence-based reagent	TTCCGggcgcgccAACGCATCCCTGAGTTGTCGATCC	N/A	N/A	*upd* locus screen reporter 19F
Sequence-based reagent	TTGCCcctgcaggGGATCGACAACTCAGGGATGCGTT	N/A	N/A	*upd* locus screen reporter 19R
Sequence-based reagent	TTCCGggcgcgccACGACCAACGATCAACTGCTATCAC	N/A	N/A	*upd* locus screen reporter 20F
Sequence-based reagent	TTGCCcctgcaggGTGATAGCAGTTGATCGTTGGTCGT	N/A	N/A	*upd* locus screen reporter 20R
Sequence-based reagent	TTCCGggcgcgccCTTTCGAGGGCTTGCACAATTGACG	N/A	N/A	*upd* locus screen reporter 21F
Sequence-based reagent	TTGCCcctgcaggCGTCAATTGTGCAAGCCCTCGAAAG	N/A	N/A	*upd* locus screen reporter 21R
Sequence-based reagent	TTCCGggcgcgccCCAATACAGCTGCTCAACTGGA	N/A	N/A	*upd* enhancer 1 cutdown 3F (used to identify minimal region)
Sequence-based reagent	TTGCCcctgcaggGAGGAGAATGAGTATGCGGATG	N/A	N/A	*upd* enhancer 1 cutdown 3R (used to identify minimal region)
Sequence-based reagent	TTCCGggcgcgccGGCCAGCACCAGAGAATCAACT	N/A	N/A	*upd* enhancer 1 cutdown 4F (used to identify minimal region)
Sequence-based reagent	TTGCCcctgcaggTCGCACATTTTGTGGCATGAGG	N/A	N/A	*upd* enhancer 1 cutdown 4R (used to identify minimal region)
Sequence-based reagent	TTCCGggcgcgccAATTATGGCCAGCACCAGTGGA	N/A	N/A	*upd* enhancer 1 *ananassae* F
Sequence-based	TTGCCcctgcaggTC	N/A	N/A	*upd* enhancer 1

reagent	TCGTCCACTCAACAAGATGC			*ananassae* R
Sequence-based reagent	TTCCGggcgcgccTTGCTGATGCAACAAGGTCGTC	N/A	N/A	*upd* enhancer 1 *biarmipes* F
Sequence-based reagent	TTGCCcctgcaggTCTTTTGTCGTGGCCCAAA	N/A	N/A	*upd* enhancer 1 *biarmipes* R
Sequence-based reagent	AACGCTCTTCCTCCTGACTTCGCATCCGCATACTCATTCTCCTC	N/A	N/A	*upd* enhancer 1 500 bp deletion F
Sequence-based reagent	GAGGAGAATGAGTATGCGGATGCGAAGTCAGGAGGAAGAGCGTT	N/A	N/A	*upd* enhancer 1 500 bp deletion R
Sequence-based reagent	TTCCGggcgcgccCTGCCAGCTAAATGAGCAACAC	N/A	N/A	*upd* enhancer 2 *ananassae* F
Sequence-based reagent	TTCCGggcgcgccTGGCGCTATCGCATTTGATCTC	N/A	N/A	*upd* enhancer 2 *biarmipes* F
Sequence-based reagent	TTCCGggcgcgccCCTAACGCAGTTATCAAAAGCG	N/A	N/A	*upd* enhancer 2 all non-lobed species R
Sequence-based reagent	tAgTtAcTgTaAaAaGgGtCgTcGgGgCaGaCaGaAgTcAtCACGCTCCGACGAGCCGCA	N/A	N/A	*upd* enhancer 2 scramble 1F
Sequence-based reagent	aTgAcTtCtGtCtGcCcCgAcGaCcCtTtTtAcAgTaAcTaACCAACTCAGCCAGCCGGC	N/A	N/A	*upd* enhancer 2 scramble 1R
Sequence-based reagent	aTtCtTcTtAcTtAtTgAgTgCGGACCTAATCGCTCCGTTT	N/A	N/A	*upd* enhancer 2 scramble 2F
Sequence-based reagent	cAcTcAaTaAgTaAgAaGaAtAGACGGCCAGAGGAATGGAAT	N/A	N/A	*upd* enhancer 2 scramble 2R
Sequence-based	gGgCaTaCcTgTtAg	N/A	N/A	*upd* enhancer 2

reagent	TtAcCgGaTaAcTtAcAgAgGaAcAgTTGTTGCCGCCGCTTAATC			scramble 3F
Sequence-based reagent	cTgTtCcTcTgTaAgTtAtCcGgTaAcTaAcAgGtAtGcCcGCCCAAAGAGCCTGGCTGG	N/A	N/A	*upd* enhancer 2 scramble 3R
Sequence-based reagent	TTCCGggcgcgccGTGCATTCTGCAGCATATGGAA	N/A	N/A	*shot* enhancer 3F
Sequence-based reagent	TTGCCcctgcaggGGTATCTCGCTAATTGCAACTC	N/A	N/A	*shot* enhancer 3R
Sequence-based reagent	TTCCGggcgcgccGGCTACCAAATTTGGATGTGC	N/A	N/A	*upd* enhancer 1 left homology arm 1500bp F
Sequence-based reagent	TTGCCcctgcaggTACCGGCAACAACAACAGCAA	N/A	N/A	*upd* enhancer 1 left homology arm 1500bp R
Sequence-based reagent	TTGCCccgcggAGCTGCATCCTTGCCATTCTC	N/A	N/A	*upd* enhancer 1 right homology arm 1500bp F
Sequence-based reagent	TTCCAagatctTGTCTCTGTGGAAATAGCCCA	N/A	N/A	*upd* enhancer 1 right homology arm 1500bp R
Sequence-based reagent	CAAGATTAACTCGACGATAC	N/A	N/A	*upd* enhancer 1 left crRNA
Sequence-based reagent	TGGCAGCTGAAACACTTTGG	N/A	N/A	*upd* enhancer 1 right crRNA
Sequence-based reagent	TTCCGggcgcgccGCTATTCTGGTGCTCCTGGCTT	N/A	N/A	*upd* enhancer 1 left homology arm 500bp F
Sequence-based reagent	TTGCCcctgcaggGCTGAATGTCCTGCCACAAGGT	N/A	N/A	*upd* enhancer 1 left homology arm 500bp R
Sequence-based reagent	TTGCCccgcggCACCGATCTTGGCCATTCCTGG	N/A	N/A	*upd* enhancer 1 right homology arm 500bp F
Sequence-based reagent	TTCCAagatctTTGCTGTTGTTGTTGC	N/A	N/A	*upd* enhancer 1 right homology arm

	CCACTC			500bp R
Sequence-based reagent	GTGGCAGGACATTCAGCAGT	N/A	N/A	*upd* enhancer 1 left crRNA
Sequence-based reagent	AATGGCCAAGATCGGTGAAC	N/A	N/A	*upd* enhancer 1 right crRNA
Sequence-based reagent	GTCGCTAGGAGATACCTTGATGCC	N/A	N/A	*upd* enhancer 2 left gRNA Sense version A
Sequence-based reagent	AAACGGCATCAAGGTATCTCCTAG	N/A	N/A	*upd* enhancer 2 left gRNA antisense version A
Sequence-based reagent	GTCGAATCATAGGGCGTTTGCTGG	N/A	N/A	*upd* enhancer 2 left gRNA Sense version B
Sequence-based reagent	AAACCCAGCAAACGCCCTATGATT	N/A	N/A	*upd* enhancer 2 left gRNA antisense version B
Sequence-based reagent	GTCGCTGTCGACTTCTTTTGAGCC	N/A	N/A	*upd* enhancer 2 right gRNA Sense version A
Sequence-based reagent	AAACGGCTCAAAAGAAGTCGACAG	N/A	N/A	*upd* enhancer 2 right gRNA antisense version A
Sequence-based reagent	GTCGCTTCAGCACTCCGCACTACC	N/A	N/A	*upd* enhancer 2 right gRNA Sense version B
Sequence-based reagent	AAACGGTAGTGCGGAGTGCTGAAG	N/A	N/A	*upd* enhancer 2 right gRNA antisense version B
Sequence-based reagent	TTCCGggcgcgccCGTCTTCTTAACCAGTCACCGG	N/A	N/A	*upd* enhancer 2 left homology arm version A & B F
Sequence-based reagent	TTGCCcctgcaggGCCTGGCAGAACTTTTATTAAA	N/A	N/A	*upd* enhancer 2 left homology arm version A R
Sequence-based reagent	TTGCCcctgcaggGCAAACGCCCTATGATTATCAG	N/A	N/A	*upd* enhancer 2 left homology arm version B R
Sequence-based reagent	TTCCAagatctATACATCGTGATCCGCATCTGC	N/A	N/A	*upd* enhancer 2 right homology arm version A & B R

Sequence-based reagent	TTGCCccgcggTCAAAAGAAGTCGACAGTTGCA	N/A	N/A	*upd* enhancer 2 right homology arm version A F
Sequence-based reagent	TTGCCccgcggACCCGGCTCAAAAGAAGTCGAC	N/A	N/A	*upd* enhancer 2 right homology arm version B F
Sequence-based reagent	atttaggtgacactatagaCCACCATGGTGAGCAAGGGCGAGG	N/A	N/A	*gfp* probe F
Sequence-based reagent	taatacgactcactataggTTAGCGTCTTCGTTCACTGCTGCG	N/A	N/A	*gfp* probe R
Sequence-based reagent	GTAGCTTAAGTAAATTATTTGATTG	N/A	N/A	*upd* probe F *ananassae*
Sequence-based reagent	taatacgactcactatagggagaGCGGTTGCTCTTATGTGACTAGAA	N/A	N/A	*upd* probe R *ananassae*
Sequence-based reagent	TTCTAGTCACATAAGAGCAACCGC	N/A	N/A	*upd* probe F *melanogaster*
Sequence-based reagent	taatacgactcactatagggagaTCAAGCACTATATCACAGAT	N/A	N/A	*upd* probe R *melanogaster*
Sequence-based reagent	GACTACTGCTCCTTCCTGAAG	N/A	N/A	*apc* probe F
Sequence-based reagent	taatacgactcactatagggagaTCAGGGCCATCAAAGCGTATC	N/A	N/A	*apc* probe R
Sequence-based reagent	GGACATAAGGTCCACACTGTG	N/A	N/A	*chb* probe F
Sequence-based reagent	taatacgactcactatagggagaAATGCGGGATACAGTGCGTCT	N/A	N/A	*chb* probe R
Sequence-based reagent	ACAGGTGCAAACGTACGACAC	N/A	N/A	*dhc36c* probe F
Sequence-based reagent	taatacgactcactatagggagaACTGGGATAGATCCCAGCCAT	N/A	N/A	*dhc36c* probe R

Sequence-based reagent	TGACATCAAGCA ATCGCGCAC	N/A	N/A	*dhc64c* probe F
Sequence-based reagent	taatacgactcactataggg agaATGAAGCTCA CGGCATCCGAT	N/A	N/A	*dhc64c* probe R
Sequence-based reagent	TGCCAGCTACGA GAAGATCGA	N/A	N/A	*dia* probe F
Sequence-based reagent	taatacgactcactataggg agaAGGATGTGGC TGCAATAGTGG	N/A	N/A	*dia* probe R
Sequence-based reagent	TCCGCTCCTCCC TCTAAAGAA	N/A	N/A	*futsch* probe F
Sequence-based reagent	taatacgactcactataggg agaATACCGATTC TGGTCGGGAAG	N/A	N/A	*futsch* probe R
Sequence-based reagent	AAGCCAGGACTC GTCTAGATC	N/A	N/A	*klp59c* probe F
Sequence-based reagent	taatacgactcactataggg agaCAGGAACTTG ACCAGGTTCAC	N/A	N/A	*klp59c* probe R
Sequence-based reagent	CAACTCTCATCG CACTCAGCA	N/A	N/A	*klp67a* probe F
Sequence-based reagent	taatacgactcactataggg agaTTCAGGATGC GTGTCAGGTTC	N/A	N/A	*klp67a* probe R
Sequence-based reagent	CAATGAGGACG ATGATGGTGG	N/A	N/A	*msps* probe F
Sequence-based reagent	taatacgactcactataggg agaAGCTGCTCGC AAATGGCAAGT	N/A	N/A	*msps* probe R
Sequence-based reagent	GAGAACCGTATG TGTTGCACC	N/A	N/A	*ncd* probe F
Sequence-based reagent	taatacgactcactataggg agaACTCCGTCCA TTGTGTAGGTC	N/A	N/A	*ncd* probe R
Sequence-based reagent	AACGCTTGCCAC ATGTTGAGC	N/A	N/A	*shot* probe F
Sequence-based reagent	taatacgactcactataggg agaCCACCAAGCG ACCACTAGAAA	N/A	N/A	*shot* probe R

Sequence-based reagent	CTCTAGAAGCCAAGAAGATGG	N/A	N/A	*stai* probe F
Sequence-based reagent	taatacgactcactatagggagaGCTTCTCCTTCATGTCACTGA	N/A	N/A	*stai* probe R
Sequence-based reagent	GAGCTAGTAGACAACTGCTGG	N/A	N/A	*stim* probe F
Sequence-based reagent	taatacgactcactatagggagaCTCCAAGTAGGGCAGACCATT	N/A	N/A	*stim* probe R
Sequence-based reagent	AGAGATCGCGATTGAGCACTG	N/A	N/A	*tum* probe F
Sequence-based reagent	taatacgactcactatagggagaTCTCGTTGCCGGCAATTACAG	N/A	N/A	*tum* probe R
Software algorithm	Fiji (ImageJ v2.0)	(Schindelin et al., 2012)	RRID:SCR_002285	
Software algorithm	GenePalette	(Rebeiz & Posakony, 2004; A. F. Smith, Posakony, & Rebeiz, 2017)	N/A	
Software algorithm	Leica Application Suite X	Leica	RRID:SCR_013673)	
Software algorithm	Microsoft Excel	Microsoft	RRID:SCR_016137	
Software algorithm	MorphoGraphX	(Barbier de Reuille et al., 2015)	N/A	
Software algorithm	Prism 8	GraphPad	N/A	

A.2 Methods

Fly stocks and genetics

Fly stocks were reared using standard culture conditions. Wild type species used in this study were obtained from the University of California, San Diego *Drosophila* Stock Center (now known as The National Drosophila Species Stock Center at Cornell University)(*Drosophila biarmipes* #14024-0361.10, *Drosophila ananassae* #14024-0371.13, *Drosophila pseudoobscura* #14011-0121.87) and from the Bloomington Drosophila Stock Center (*Drosophila melanogaster* [y^1w^1] #1495). *pox neuro*-Gal4 (construct #13) was obtained from Werner Boll (Boll & Noll, 2002). The following were obtained from the Bloomington Drosophila stock center: *UAS*-Raeppli-CAAX (#55084), *armadillo-GFP* (#8556), Ecadherin:mCherry (#59014), and *UAS*-mCherryRNAi (control for RNAi experiments, as mCherry is not present in the *Drosophila* genome)(35785). *UAS*-dumpyRNAi was obtained from the Vienna Drosophila Resource Center (#44029) and Dumpy:YFP was obtained from the Drosophila Genomics and Genetic Resources (#115238).

For the Raeppli experiments, stable lines of hs-flippase;;*UAS*-Raeppli-CAAX/*UAS*-Raeppli-CAAX and *D. simulans pox neuro*-gal4/*D. simulans pox neuro*-gal4;*UAS*-Raeppli-CAAX/*UAS*-Raeppli-CAAX were generated. *D. simulans pox neuro* posterior lobe enhancer-\gal4 was used as opposed to *pox neuro*-gal4 because a gal4 driver on the second chromosome was required. Virgin females from the first line were crossed to males from the second line to ensure hs-flippase was inherited by all offspring. Offspring were collected and grown as normal, heat shocked at 37°C for 1 hour around 24 to 28 hours APF, and allowed to finish development at 25°C.

Sample preparation

Pupal samples were prepared following the protocol in Glassford, et al., 2015. Briefly, samples were incubated at 25°C unless otherwise noted. Dissections were performed in cold PBS, pupae were cut in half, removed from their pupal cases, and fat bodies removed by flushing. Larval samples were dissected in cold PBS by cutting the larva in half, and flipping the posterior end of the larva inside out. All samples were fixed for 30 minutes at room temperature in PBS with 0.1% Triton-X and 4% paraformaldehyde. Samples stained with phalloidin had Triton-X concentrations increased to 0.3%. Samples used for VVA staining were removed from pupal cuticle before being fixed in PBS with 0.1% Triton-x, 4% paraformaldehyde, and 1% trichloroacetic acid on ice for 1 hour followed by 30 minutes at room temperature. The trichloroacetic acid method causes some slight tissue distortion, as the precipitation treatment utilized to refine the VVA signal causes the posterior lobe to become slightly deformed and curve in towards the clasper. However, similar defects were not observed in the other structures such as the lateral plate or in *D. biarmipes*. Samples were stored in PBT for immunostaining at 4°C for up to two days. For *in situ* hybridization, samples were rinsed twice in methanol and rinsed twice in ethanol. Samples were stored at -20°C in ethanol.

Immunostaining and *in situ* hybridization

For immunostaining, genital samples were removed from the surrounding pupal cuticle and incubated overnight at 4°C with primary antibodies diluted in PBS with 0.1% Triton-X (PBT). VVA and phalloidin samples were placed on a rocker. The following primary antibodies were used: rat anti-alpha tubulin (tyrosinated) 1:500 (MAB 1864-I, MilliporeSigma), mouse anti-alpha tubulin (acetylated) 1:500 (T6793, Sigma-Aldrich), rat anti-Ecadherin 1:500 (DCAD2, DSHB),

mouse anti-fasciclin III 1:500 (7G10, DSHB), rabbit anti-histone H3 (phospho S10) 1:50 (ab5176, Abcam), goat anti-GFP 1:300 (ab6662, Abcam), fluorescein Vicia Villosa Lectin (VVA) 1:200 (FL-1231, Vector Laboratories), mouse anti-Shot (anti-Shot mAbRod1, DSHB) 1:500. The goat anti-GFP was used to increase signal of Dumpy:YFP in the knockdown experiments only. Primary antibody was removed by performing two quick rinses and two long washes (at least 5 minutes) in PBT. Samples were incubated overnight at 4°C in secondary antibodies diluted in PBT. The following secondary antibodies were used: donkey anti-rat Alexa 594 1:500 (A21209, Invitrogen), donkey anti-mouse Alexa 488 1:500 (A21202, Thermo Fisher Scientific), donkey anti-rat Alexa 488 1:500 (A21208, Thermo Fisher Scientific), goat anti-mouse Alexa 594 1:500 (A-11005, Thermo Fisher Scientific), goat anti-rabbit Alexa 594 1:500 (A-11012, Thermo Fisher Scientific), donkey anti-goat Cy2 1:500 (705-225-147, Jackson ImmunoResearch). Rhodamine phalloidin (R415, Thermo Fisher Scientific) stain was performed with secondary antibody. Samples were washed out of secondary antibody by performing two quick rinses and two long washes (at least 5 minutes) in PBT. Samples were then incubated in 50% PBT/50% glycerol solution for at least 5 minutes. Pupal samples were mounted on glass slides coated with Poly-L-Lysine Solution. Glass slides had 1 to 2 layers of double side tape with a well cut out in which the sample was placed and covered with a cover slip

in situ hybridization was performed following the protocol in Rebeiz et al., 2009 with modifications to perform *in situs* in the InsituPro VSi robot (Intavis Bioanalytical Instruments) as done by Glassford et al., 2015 (Rebeiz, Pool, Kassner, Aquadro, & Carroll, 2009).

Microscopy and live imaging

Cuticles of adult posterior lobes and in situ hybridization samples were imaged on Leica

DM2000 with a 40x objective for cuticles and a 10x objective for in situ samples. Samples with fluorescent antibodies and fluorescently tagged proteins were imaged using a Leica TCS SP5 Confocal microscope using either a 40x or 63x oil immersion objective or using a 40X oil immersion objective on an Olympus Fluoview 1000 confocal microscope.

To live image genital development, a 2% agar solution was poured into a small petri dish filling the dish half way. A 0.1-10µL pipette tip was used to make small wells in the agar for pupal samples. Timed pupal samples were inserted head first into the small well and a 5-300µL pipette tip was used to push sample into agar by placing the tip around the posterior spiracles on the pupal case. To better image the developing genitalia the pupal case at the posterior end was removed with forceps. Deionized water was used to cover the samples and imaged on a Leica TCS SP5 Confocal microscope using a 63x water objective.

To live image embryos, Dumpy:YFP flies were grown in egg-laying chamber with grape agar plates (Genesee Scientific). Embryos were removed from plates using forceps and rolled on a piece of double sided tape to remove the chorion. Embryos then were positioned on a glass coverslip coated with embryo glue. A glass slide was covered with double sided tape and a well was made and filled with halocarbon 27 oil. The cover slip with the embryos was then placed on the glass slide, submerging the embryos in halocarbon oil. Embryos were imaged on a Leica TCS SP8 confocal with a 63x oil objective.

Image analysis

Images were processed with Fiji (Schindelin et al., 2012) and Photoshop. Three-dimensional views were obtained with MorphoGraphX (Barbier de Reuille et al., 2015) or Leica Application Suite X. Movies were processed in Fiji and cell rearrangements were tracked using

the manual tracking plugin. Tissue thickness/cell height during development was measured in cross-section view by drawing a line centered between the two sides (based on apical membrane) of the lobe until the basal side was reached. Area of adult posterior lobe cuticles and height of the adult lobe were measured by using the lateral plate as a guide for determining the bottom boundary of the posterior lobe. To prevent any possible bias for one lobe vs the other (i.e. left vs right) which lobe was used in statistical analysis was randomly decided, except for Figure 6 - supplement 1 where both sides of the posterior lobe were considered.

Transgenic constructs

GFP reporters were cloned using primers listed in key resources table using genomic DNA purified with the DNeasy Blood and Tissue Kit (QIAGEN). Primers were designed using sequence conservation with the GenePalette software tool (Rebeiz and Posakony 2004; Smith et al., 2017). Enhancer 2 scramble block mutants were generated by changing every other nucleotide to non-complimentary transversions. Scramble block mutants and enhancer 1 min deletion were created using mutant primers in key resource table and performing overlap PCR. *AscI* and *SbfI* restriction sites were added to primers to amplify DNA and inserted into pS3AG vector (GFP reporters in *D. melanogaster*) or pBAC vector (GFP reporter in non-lobed species), or pS3aG4 (gal4 vector) using *AscI* and *SbfI* restriction sites(Horn & Wimmer, 2000b; Williams et al., 2008). All constructs were inserted into the indicated landing site by Rainbow Transgenics, except for the pBAC vector which inserts itself randomly into the genome (Groth, Fish, Nusse, & Calos, 2004).

CRISPR/Cas9 enhancer deletions

Crispr deletions were designed to cut outside of the identified enhancer regions with two

separate gRNAs. A homology directed repair vector was supplied that would insert a 3xpP3 promoter driving dsRED in place of the deletion to facilitate screening. The homology arms consisted of about 1000 base pairs that aligned with the surround DNA region that was not cut. The homology arms were cloned using the primers in the key resources table and then insterted into the attp dsRED atpp vector using *AscI*, *SbfI*, SacII, and *BglII* restriction sites.

For the enhancer 1, deletions were done utilizing the IDT (Integrated DNA Technologies) Alt-R CRISPR-Cas9 system in which the gRNA is complexed with Cas9 and injected into the embryos with the homology arm vector. Briefly the crRNA (CRISPR RNA that is target specific) and tracrRNA (universal gRNA sequence) are annealed together by combining 10.0µl of 100µM crRNA, 10.0µl of 100µM tracrRNA, and 70µl of nuclease free duplex buffer and heated for 5 minutes at 95°C and then allowed to cool to room temperature. To complex the gRNA to the Cas9 protien 8.0µl of the assembled gRNA, 1.5µl of the cas9 protein (15.0µg total) and 0.5µl of nuclease free duplex buffer are incublated at 37°C for ten minutes and then allowed to cool to room temperature. The injection mixture consisted of 10.0µl of each RNP complexed with the gRNA (for each cut site), 500ng/µl of homology arm vector, and then nuclease free duplex buffer to bring the mixture to a total of 10.0µl.

For the enhancer 2 deletions all components were delivered by vector. To insert the gRNA 1 µl of the sense and antisense oligos were allowed to anneal with 0.5 µl of T4 Polynucleotide Kinase (NEB) and 1.0µl of 10X T4 ligation buffer (NEB) and 6.5µl deionized water for 30minutes at 37°C, the 95°C for 5 minutes, and then the temperature was ramped down to 25°C at a rate of 5°C per minute. This reaction anneals the oligos together and can then be inserted into the gRNA vector digested with *BbsI* by T4 ligation. The injection mxiture consists of 250ng/µl nos-cas9, 100ng/µl of each gRNA vector, and 500ng/µl of the homology arm vector.

Bibliography

Amundson, R. (2005). *The changing role of the embryo in evolutionary thought : roots of evo-devo*. Cambridge University Press.

Applewhite, D. A., Grode, K. D., Keller, D., Zadeh, A. D., Zadeh, A., Slep, K. C., & Rogers, S. L. (2010). The spectraplakin Short stop is an actin-microtubule cross-linker that contributes to organization of the microtubule network. *Molecular Biology of the Cell*, *21*(10), 1714–1724. https://doi.org/10.1091/mbc.e10-01-0011

Atallah, J., Liu, N. H., Dennis, P., Hon, A., & Larsen, E. W. (2009). Developmental constraints and convergent evolution in *Drosophila* sex comb formation. *Evolution & Development*, *11*(2), 205–218. https://doi.org/10.1111/j.1525-142X.2009.00320.x

Bach, E. A., Ekas, L. A., Ayala-Camargo, A., Flaherty, M. S., Lee, H., Perrimon, N., & Baeg, G.-H. (2007). GFP reporters detect the activation of the Drosophila JAK/STAT pathway in vivo. *Gene Expression Patterns : GEP*, *7*(3), 323–331. https://doi.org/10.1016/j.modgep.2006.08.003

Bainbridge, S. P., & Bownes, M. (1981). Staging the metamorphosis of Drosophila melanogaster. *Journal of Embryology and Experimental Morphology*, *66*, 57–80. Retrieved from http://www.ncbi.nlm.nih.gov/pubmed/6802923

Barbier de Reuille, P., Routier-Kierzkowska, A.-L., Kierzkowski, D., Bassel, G. W., Schüpbach, T., Tauriello, G., … Smith, R. S. (2015). MorphoGraphX: A platform for quantifying morphogenesis in 4D. *ELife*, *4*, 05864. https://doi.org/10.7554/eLife.05864

Barolo, S., & Posakony, J. W. (2002). Three habits of highly effective signaling pathways: principles of transcriptional control by developmental cell signaling. *Genes & Development*, *16*(10), 1167–1181. https://doi.org/10.1101/gad.976502

Bergqvist, L. P. (2015). The role of teeth in mammal History. *Brazilian Journal of Oral Sciences*, *2*(6), 249–257. https://doi.org/10.20396/bjos.v2i6.8641693

Bernadskaya, Y., & Christiaen, L. (2016). Transcriptional Control of Developmental Cell Behaviors. *Annual Review of Cell and Developmental Biology*, *32*(1), 77–101. https://doi.org/10.1146/annurev-cellbio-111315-125218

Biggs, L. C., & Mikkola, M. L. (2014). Early inductive events in ectodermal appendage morphogenesis. *Seminars in Cell & Developmental Biology*, *25–26*, 11–21. https://doi.org/10.1016/j.semcdb.2014.01.007

Boettiger, A. N., & Levine, M. (2009). Synchronous and stochastic patterns of gene activation in the Drosophila embryo. *Science (New York, N.Y.)*, *325*(5939), 471–473.

https://doi.org/10.1126/science.1173976

Boll, W., & Noll, M. (2002). The Drosophila Pox neuro gene: control of male courtship behavior and fertility as revealed by a complete dissection of all enhancers. *Development (Cambridge, England)*, *129*(24), 5667–5681. Retrieved from http://www.ncbi.nlm.nih.gov/pubmed/12421707

Brown, N. H. (2011). Extracellular Matrix in Development: Insights from Mechanisms Conserved between Invertebrates and Vertebrates. *Cold Spring Harbor Perspectives in Biology*, *3*(12), a005082–a005082. https://doi.org/10.1101/cshperspect.a005082

Cannavò, E., Khoueiry, P., Garfield, D. A., Geeleher, P., Zichner, T., Gustafson, E. H., … Furlong, E. E. M. (2016). Shadow Enhancers Are Pervasive Features of Developmental Regulatory Networks. *Current Biology*, *26*(1), 38–51. https://doi.org/10.1016/j.cub.2015.11.034

Carroll, S. B., Grenier, J. K., & Weatherbee, S. D. (2005). *From DNA to diversity : molecular genetics and the evolution of animal design*. Retrieved from https://www.wiley.com/en-us/From+DNA+to+Diversity%3A+Molecular+Genetics+and+the+Evolution+of+Animal+Design%2C+2nd+Edition-p-9781405119504

Chan, C. J., Heisenberg, C.-P., & Hiiragi, T. (2017). Coordination of Morphogenesis and Cell-Fate Specification in Development. *Current Biology*, *27*(18), R1024–R1035. https://doi.org/10.1016/j.cub.2017.07.010

Chanet, S., Miller, C. J., Vaishnav, E. D., Ermentrout, B., Davidson, L. A., & Martin, A. C. (2017). Actomyosin meshwork mechanosensing enables tissue shape to orient cell force. *Nature Communications*, *8*, 15014. https://doi.org/10.1038/ncomms15014

Chanut-Delalande, H., Fernandes, I., Roch, F., Payre, F., & Plaza, S. (2006). Shavenbaby Couples Patterning to Epidermal Cell Shape Control. *PLoS Biology*, *4*(9), 1549–1561. https://doi.org/10.1371/journal.pbio.0040290

Charles, C., Lazzari, V., Tafforeau, P., Schimmang, T., Tekin, M., Klein, O., & Viriot, L. (2009). Modulation of *Fgf3* dosage in mouse and men mirrors evolution of mammalian dentition. *Proceedings of the National Academy of Sciences*, *106*(52), 22364–22368. https://doi.org/10.1073/pnas.0910086106

Coyne, J. A. (1993). THE GENETICS OF AN ISOLATING MECHANISM BETWEEN TWO SIBLING SPECIES OF *DROSOPHILA*. *Evolution*, *47*(3), 778–788. https://doi.org/10.1111/j.1558-5646.1993.tb01233.x

Daley, W. P., & Yamada, K. M. (2013). ECM-modulated cellular dynamics as a driving force for tissue morphogenesis. *Current Opinion in Genetics & Development*, *23*(4), 408–414. https://doi.org/10.1016/j.gde.2013.05.005

Davidson, E. H. (2006). *The Regulatory Genome : Gene Regulatory Networks In Development And Evolution.* Elsevier.

Davidson, L. A. (2012). Epithelial machines that shape the embryo. *Trends in Cell Biology*, *22*(2), 82–87. https://doi.org/10.1016/j.tcb.2011.10.005

Delon, I., Chanut-Delalande, H., & Payre, F. (2003). The Ovo/Shavenbaby transcription factor specifies actin remodelling during epidermal differentiation in Drosophila. *Mechanisms of Development*, *120*(7), 747–758. https://doi.org/10.1016/S0925-4773(03)00081-9

Devenport, D. (2016). Tissue morphodynamics: Translating planar polarity cues into polarized cell behaviors. *Seminars in Cell & Developmental Biology*, *55*, 99–110. https://doi.org/10.1016/j.semcdb.2016.03.012

Diaz-de-la-Loza, M.-D.-C., Ray, R. P., Ganguly, P. S., Alt, S., Davis, J. R., Hoppe, A., … Thompson, B. J. (2018). Apical and Basal Matrix Remodeling Control Epithelial Morphogenesis. *Developmental Cell*, *46*(1), 23-39.e5. https://doi.org/10.1016/j.devcel.2018.06.006

Dickinson, W. J., & Thatcher, J. W. (1997). Morphogenesis of denticles and hairs in Drosophila embryos: Involvement of actin-associated proteins that also affect adult structures. *Cell Motility and the Cytoskeleton*, *38*(1), 9–21. https://doi.org/10.1002/(SICI)1097-0169(1997)38:1<9::AID-CM2>3.0.CO;2-4

Dilks, S. A., & DiNardo, S. (2010). Non-cell-autonomous control of denticle diversity in the Drosophila embryo. *Development (Cambridge, England)*, *137*(8), 1395–1404. https://doi.org/10.1242/dev.045450

Dinwiddie, A., Null, R., Pizzano, M., Chuong, L., Leigh Krup, A., Ee Tan, H., & Patel, N. H. (2014). Dynamics of F-actin prefigure the structure of butterfly wing scales. *Developmental Biology*, *392*(2), 404–418. https://doi.org/10.1016/J.YDBIO.2014.06.005

Dong, B., Hannezo, E., & Hayashi, S. (2014a). Balance between apical membrane growth and luminal matrix resistance determines epithelial tubule shape. *Cell Reports*, *7*(4), 941–950. https://doi.org/10.1016/j.celrep.2014.03.066

Dong, B., Hannezo, E., & Hayashi, S. (2014b). Balance between Apical Membrane Growth and Luminal Matrix Resistance Determines Epithelial Tubule Shape. *Cell Reports*, *7*(4), 941–950. https://doi.org/10.1016/J.CELREP.2014.03.066

Duffy, J. B. (2002). GAL4 system in Drosophila: a fly geneticist's Swiss army knife. *Genesis (New York, N.Y. : 2000)*, *34*(1–2), 1–15. https://doi.org/10.1002/gene.10150

Eberhard, W. G. (1985). *Sexual Selection and Animal Genitalia*. Cambridge: Harvard University Press.

Etournay, R., Popović, M., Merkel, M., Nandi, A., Blasse, C., Aigouy, B., … Eaton, S. (2015). Interplay of cell dynamics and epithelial tension during morphogenesis of the Drosophila pupal wing. *ELife*, *4*, e07090. https://doi.org/10.7554/eLife.07090

Fernandes, I., Chanut-Delalande, H., Ferrer, P., Latapie, Y., Waltzer, L., Affolter, M., … Plaza, S.

(2010). Zona pellucida domain proteins remodel the apical compartment for localized cell shape changes. *Developmental Cell*, *18*(1), 64–76. https://doi.org/10.1016/j.devcel.2009.11.009

Frankel, N., Davis, G. K., Vargas, D., Wang, S., Payre, F., & Stern, D. L. (2010). Phenotypic robustness conferred by apparently redundant transcriptional enhancers. *Nature*, *466*(7305), 490–493. https://doi.org/10.1038/nature09158

Frazee, S. R., & Masly, J. P. (2015). Multiple sexual selection pressures drive the rapid evolution of complex morphology in a male secondary genital structure. *Ecology and Evolution*, *5*(19), 4437–4450. https://doi.org/10.1002/ece3.1721

Fuss, B., Josten, F., Feix, M., & Hoch, M. (2004). Cell movements controlled by the Notch signalling cascade during foregut development in Drosophila. *Development*, *131*(7), 1587–1595. https://doi.org/10.1242/dev.01057

Gallant, J. R., Imhoff, V. E., Martin, A., Savage, W. K., Chamberlain, N. L., Pote, B. L., … Mullen, S. P. (2014). Ancient homology underlies adaptive mimetic diversity across butterflies. *Nature Communications*, *5*, 4817. https://doi.org/10.1038/ncomms5817

Gilbert, M. M., Weaver, B. K., Gergen, J. P., & Reich, N. C. (2005). A novel functional activator of the Drosophila JAK/STAT pathway, unpaired2, is revealed by an in vivo reporter of pathway activation. *Mechanisms of Development*, *122*(7–8), 939–948. https://doi.org/10.1016/j.mod.2005.03.004

Gilmour, D., Rembold, M., & Leptin, M. (2017). From morphogen to morphogenesis and back. *Nature*, *541*(7637), 311–320. https://doi.org/10.1038/nature21348

Glassford, W. J., Johnson, W. C., Dall, N. R., Smith, S. J., Liu, Y., Boll, W., … Rebeiz, M. (2015). Co-option of an Ancestral Hox-Regulated Network Underlies a Recently Evolved Morphological Novelty. *Developmental Cell*, *34*(5), 520–531. https://doi.org/10.1016/j.devcel.2015.08.005

Green, J. E., Cavey, M., Médina Caturegli, E., Aigouy, B., Gompel, N., & Prud'homme, B. (2019). Evolution of Ovipositor Length in Drosophila suzukii Is Driven by Enhanced Cell Size Expansion and Anisotropic Tissue Reorganization. *Current Biology*, *29*(12), 2075-2082.e6. https://doi.org/10.1016/J.CUB.2019.05.020

Groth, A. C., Fish, M., Nusse, R., & Calos, M. P. (2004). Construction of transgenic Drosophila by using the site-specific integrase from phage phiC31. *Genetics*, *166*(4), 1775–1782. Retrieved from http://www.ncbi.nlm.nih.gov/pubmed/15126397

Guirao, B., & Bellaïche, Y. (2017). Biomechanics of cell rearrangements in Drosophila. *Current Opinion in Cell Biology*, *48*, 113–124. https://doi.org/10.1016/j.ceb.2017.06.004

Gupta, S. K., Bhandari, B., Shrestha, A., Biswal, B. K., Palaniappan, C., Malhotra, S. S., & Gupta, N. (2012). Mammalian zona pellucida glycoproteins: structure and function during fertilization. *Cell and Tissue Research*, *349*(3), 665–678. https://doi.org/10.1007/s00441-

011-1319-y

Harjunmaa, E., Seidel, K., Häkkinen, T., Renvoisé, E., Corfe, I. J., Kallonen, A., … Jernvall, J. (2014). Replaying evolutionary transitions from the dental fossil record. *Nature*, *512*(7512), 44–48. https://doi.org/10.1038/nature13613

Harris, M. P., Fallon, J. F., & Prum, R. O. (2002). Shh-Bmp2 signaling module and the evolutionary origin and diversification of feathers. *Journal of Experimental Zoology*, *294*(2), 160–176. https://doi.org/10.1002/jez.10157

Harrison, D. A., McCoon, P. E., Binari, R., Gilman, M., & Perrimon, N. (1998). Drosophila unpaired encodes a secreted protein that activates the JAK signaling pathway. *Genes & Development*, *12*(20), 3252–3263. Retrieved from http://www.pubmedcentral.nih.gov/articlerender.fcgi?artid=317220&tool=pmcentrez&rendertype=abstract

Hayden, L., & Arthur, W. (2013). Expression patterns of *Wnt* genes in the venom claws of centipedes. *Evolution & Development*, *15*(5), 365–372. https://doi.org/10.1111/ede.12044

Heer, N. C., & Martin, A. C. (2017). Tension, contraction and tissue morphogenesis. *Development (Cambridge, England)*, *144*(23), 4249–4260. https://doi.org/10.1242/dev.151282

Heer, N. C., Miller, P. W., Chanet, S., Stoop, N., Dunkel, J., & Martin, A. C. (2017). Actomyosin-based tissue folding requires a multicellular myosin gradient. *Development*, *144*(10), 1876–1886. https://doi.org/10.1242/dev.146761

Heiman, M. G., & Shaham, S. (2009). DEX-1 and DYF-7 establish sensory dendrite length by anchoring dendritic tips during cell migration. *Cell*, *137*(2), 344–355. https://doi.org/10.1016/j.cell.2009.01.057

Heisenberg, C.-P., & Bellaïche, Y. (2013). Forces in Tissue Morphogenesis and Patterning. *Cell*, *153*(5), 948–962. https://doi.org/10.1016/j.cell.2013.05.008

Heller, E., & Fuchs, E. (2015). Tissue patterning and cellular mechanics. *The Journal of Cell Biology*, *211*(2), 219–231. https://doi.org/10.1083/jcb.201506106

Hombría, J. C.-G., Brown, S., Häder, S., & Zeidler, M. P. (2005). Characterisation of Upd2, a Drosophila JAK/STAT pathway ligand. *Developmental Biology*, *288*(2), 420–433. https://doi.org/10.1016/j.ydbio.2005.09.040

Hong, J.-W., Hendrix, D. A., & Levine, M. S. (2008). Shadow enhancers as a source of evolutionary novelty. *Science (New York, N.Y.)*, *321*(5894), 1314. https://doi.org/10.1126/science.1160631

Horn, C., & Wimmer, E. A. (2000a). A versatile vector set for animal transgenesis. *Development Genes and Evolution*, *210*(12), 630–637. Retrieved from http://www.ncbi.nlm.nih.gov/pubmed/11151300

Horn, C., & Wimmer, E. A. (2000b). A versatile vector set for animal transgenesis. *Development Genes and Evolution*, *210*(12), 630–637. Retrieved from http://www.ncbi.nlm.nih.gov/pubmed/11151300

Irvine, K. D., & Wieschaus, E. (1994). Cell intercalation during Drosophila germband extension and its regulation by pair-rule segmentation genes. *Development (Cambridge, England)*, *120*(4), 827–841. Retrieved from http://www.ncbi.nlm.nih.gov/pubmed/7600960

Jagadeeshan, S., & Singh, R. S. (2006). A time-sequence functional analysis of mating behaviour and genital coupling in Drosophila: role of cryptic female choice and male sex-drive in the evolution of male genitalia. *Journal of Evolutionary Biology*, *19*(4), 1058–1070. https://doi.org/10.1111/j.1420-9101.2006.01099.x

Jaźwińska, A., & Affolter, M. (2004). A family of genes encoding zona pellucida (ZP) domain proteins is expressed in various epithelial tissues during Drosophila embryogenesis. *Gene Expression Patterns*, *4*(4), 413–421. https://doi.org/10.1016/j.modgep.2004.01.003

Jaźwińska, A., Ribeiro, C., & Affolter, M. (2003). Epithelial tube morphogenesis during Drosophila tracheal development requires Piopio, a luminal ZP protein. *Nature Cell Biology*, *5*(10), 895–901. https://doi.org/10.1038/ncb1049

Jernvall, J., & Thesleff, I. (2012). Tooth shape formation and tooth renewal: evolving with the same signals. *Development (Cambridge, England)*, *139*(19), 3487–3497. https://doi.org/10.1242/dev.085084

Kamimura, Y. (2010). Copulation anatomy of Drosophila melanogaster (Diptera: Drosophilidae): wound-making organs and their possible roles. *Zoomorphology*, *129*(3), 163–174. https://doi.org/10.1007/s00435-010-0109-5

Kanca, O., Caussinus, E., Denes, A. S., Percival-Smith, A., & Affolter, M. (2014). Raeppli: a whole-tissue labeling tool for live imaging of Drosophila development. *Development (Cambridge, England)*, *141*(2), 472–480. https://doi.org/10.1242/dev.102913

Kim, R., Green, J. B. A., & Klein, O. D. (2017). From snapshots to movies: Understanding early tooth development in four dimensions. *Developmental Dynamics*, *246*(6), 442–450. https://doi.org/10.1002/dvdy.24501

Kirkpatrick, C. A., Dimitroff, B. D., Rawson, J. M., & Selleck, S. B. (2004). Spatial Regulation of Wingless Morphogen Distribution and Signaling by Dally-like Protein. *Developmental Cell*, *7*(4), 513–523. https://doi.org/10.1016/j.devcel.2004.08.004

Kopp, A., & True, J. R. (2002). Evolution of male sexual characters in the Oriental Drosophila melanogaster species group. *Evolution and Development*, *4*(4), 278–291. https://doi.org/10.1046/j.1525-142X.2002.02017.x

Kreuger, J., Perez, L., Giraldez, A. J., & Cohen, S. M. (2004). Opposing activities of Dally-like glypican at high and low levels of Wingless morphogen activity. *Developmental Cell*, *7*(4), 503–512. https://doi.org/10.1016/j.devcel.2004.08.005

Lawrence, P. A. (2001). Morphogens: how big is the big picture? *Nature Cell Biology*, *3*(7), E151–E154. https://doi.org/10.1038/35083096

Lecuit, T., & Lenne, P.-F. (2007). Cell surface mechanics and the control of cell shape, tissue patterns and morphogenesis. *Nature Reviews Molecular Cell Biology*, *8*(8), 633–644. https://doi.org/10.1038/nrm2222

Lecuit, T., Lenne, P.-F., & Munro, E. (2011). Force Generation, Transmission, and Integration during Cell and Tissue Morphogenesis. *Annual Review of Cell and Developmental Biology*, *27*(1), 157–184. https://doi.org/10.1146/annurev-cellbio-100109-104027

Leptin, M. (1995). *Drosophila* Gastrulation: From Pattern Formation to Morphogenesis. *Annual Review of Cell and Developmental Biology*, *11*(1), 189–212. https://doi.org/10.1146/annurev.cb.11.110195.001201

LeVasseur-Viens, H., Polak, M., & Moehring, A. J. (2015). No evidence for external genital morphology affecting cryptic female choice and reproductive isolation in Drosophila. *Evolution; International Journal of Organic Evolution*. https://doi.org/10.1111/evo.12685

Levine, M. (2010). Transcriptional enhancers in animal development and evolution. *Current Biology : CB*, *20*(17), R754-63. https://doi.org/10.1016/j.cub.2010.06.070

Li, L., Tang, Q., Nakamura, T., Suh, J.-G., Ohshima, H., & Jung, H.-S. (2016). Fine tuning of Rac1 and RhoA alters cuspal shapes by remolding the cellular geometry. *Scientific Reports*, *6*(1), 37828. https://doi.org/10.1038/srep37828

Li, W. X. (2008). Canonical and non-canonical JAK-STAT signaling. *Trends in Cell Biology*, *18*(11), 545–551. https://doi.org/10.1016/j.tcb.2008.08.008

Lim, B., Levine, M., & Yamazaki, Y. (2017). Transcriptional Pre-patterning of Drosophila Gastrulation. *Current Biology : CB*, *27*(2), 286–290. https://doi.org/10.1016/j.cub.2016.11.047

Linde-Medina, M., & Marcucio, R. (2018). Living tissues are more than cell clusters: The extracellular matrix as a driving force in morphogenesis. *Progress in Biophysics and Molecular Biology*, *137*, 46–51. https://doi.org/10.1016/j.pbiomolbio.2018.01.009

Liu, Y., Ramos-Womack, M., Han, C., Reilly, P., Brackett, K. L., Rogers, W., … Rebeiz, M. (2019). Changes throughout a Genetic Network Mask the Contribution of Hox Gene Evolution. *Current Biology : CB*, *29*(13), 2157-2166.e6. https://doi.org/10.1016/j.cub.2019.05.074

Loganathan, R., Rongish, B. J., Smith, C. M., Filla, M. B., Czirok, A., Bénazéraf, B., & Little, C. D. (2016). Extracellular matrix motion and early morphogenesis. *Development*, *143*(12), 2056–2065. https://doi.org/10.1242/dev.127886

Lovegrove, B., Simões, S., Rivas, M. L., Sotillos, S., Johnson, K., Knust, E., … Hombría, J. C.-G. (2006). Coordinated control of cell adhesion, polarity, and cytoskeleton underlies Hox-

induced organogenesis in Drosophila. *Current Biology : CB*, *16*(22), 2206–2216. https://doi.org/10.1016/j.cub.2006.09.029

Low, I. I. C., Williams, C. R., Chong, M. K., McLachlan, I. G., Wierbowski, B. M., Kolotuev, I., & Heiman, M. G. (2019). Morphogenesis of neurons and glia within an epithelium. *Development*, *146*(4), dev171124. https://doi.org/10.1242/dev.171124

Martin, A. C., & Goldstein, B. (2014). Apical constriction: themes and variations on a cellular mechanism driving morphogenesis. *Development (Cambridge, England)*, *141*(10), 1987–1998. https://doi.org/10.1242/dev.102228

Martin, A., Papa, R., Nadeau, N. J., Hill, R. I., Counterman, B. A., Halder, G., … Reed, R. D. (2012). Diversification of complex butterfly wing patterns by repeated regulatory evolution of a Wnt ligand. *Proceedings of the National Academy of Sciences of the United States of America*, *109*(31), 12632–12637. https://doi.org/10.1073/pnas.1204800109

Martin, A., & Reed, R. D. (2014). Wnt signaling underlies evolution and development of the butterfly wing pattern symmetry systems. *Developmental Biology*, *395*(2), 367–378. https://doi.org/10.1016/J.YDBIO.2014.08.031

Matsuoka, Y., & Monteiro, A. (2018). Melanin Pathway Genes Regulate Color and Morphology of Butterfly Wing Scales. *Cell Reports*, *24*(1), 56–65. https://doi.org/10.1016/j.celrep.2018.05.092

Mazo-Vargas, A., Concha, C., Livraghi, L., Massardo, D., Wallbank, R. W. R., Zhang, L., … Martin, A. (2017). Macroevolutionary shifts of *WntA* function potentiate butterfly wing-pattern diversity. *Proceedings of the National Academy of Sciences*, *114*(40), 10701–10706. https://doi.org/10.1073/pnas.1708149114

Moczek, A. P. (2008). On the origins of novelty in development and evolution. *BioEssays*, *30*(5), 432–447. https://doi.org/10.1002/bies.20754

Mukherjee, T., Hombría, J. C.-G., & Zeidler, M. P. (2005). Opposing roles for Drosophila JAK/STAT signalling during cellular proliferation. *Oncogene*, *24*(15), 2503–2511. https://doi.org/10.1038/sj.onc.1208487

Nashchekin, D., Fernandes, A. R., & St Johnston, D. (2016). Patronin/Shot Cortical Foci Assemble the Noncentrosomal Microtubule Array that Specifies the Drosophila Anterior-Posterior Axis. *Developmental Cell*, *38*(1), 61–72. https://doi.org/10.1016/J.DEVCEL.2016.06.010

Nelson, W. J. (2003). Adaptation of core mechanisms to generate cell polarity. *Nature*, *422*(6933), 766–774. https://doi.org/10.1038/nature01602

O'Hanlon, K. N., Dam, R. A., Archambeault, S. L., & Berg, C. A. (2017). Two Drosophilids exhibit distinct EGF pathway patterns in oogenesis. *Development Genes and Evolution*, *228*(1), 31–48. Retrieved from http://www.ncbi.nlm.nih.gov/pubmed/29264645

Osterfield, M., Schupbach, T., Wieschaus, E., & Shvartsman, S. Y. (2015). Diversity of epithelial

morphogenesis during eggshell formation in drosophilids. *Development*, *142*(11), 1971–1977. https://doi.org/10.1242/dev.119404

Osterfield, Miriam, Berg, C. A., & Shvartsman, S. Y. (2017). Epithelial Patterning, Morphogenesis, and Evolution: Drosophila Eggshell as a Model. *Developmental Cell*, *41*(4), 337–348. https://doi.org/10.1016/j.devcel.2017.02.018

Paluch, E., & Heisenberg, C.-P. (2009). Biology and physics of cell shape changes in development. *Current Biology : CB*, *19*(17), R790-799. https://doi.org/10.1016/j.cub.2009.07.029

Peluffo, A. E., Nuez, I., Debat, V., Savisaar, R., Stern, D. L., & Orgogozo, V. (2015). A Major Locus Controls a Genital Shape Difference Involved in Reproductive Isolation Between Drosophila yakuba and Drosophila santomea. *G3 (Bethesda, Md.)*, *5*(12), 2893–2901. https://doi.org/10.1534/g3.115.023481

Perrimon, N., Pitsouli, C., & Shilo, B.-Z. (2012). Signaling Mechanisms Controlling Cell Fate and Embryonic Patterning. *Cold Spring Harbor Perspectives in Biology*, *4*(8), a005975–a005975. https://doi.org/10.1101/cshperspect.a005975

Perry, M. W., Boettiger, A. N., Bothma, J. P., & Levine, M. (2010). Shadow enhancers foster robustness of Drosophila gastrulation. *Current Biology : CB*, *20*(17), 1562–1567. https://doi.org/10.1016/j.cub.2010.07.043

Peter, I. S., & Davidson, E. H. (2011). Evolution of Gene Regulatory Networks Controlling Body Plan Development. *Cell*, *144*(6), 970–985. https://doi.org/10.1016/j.cell.2011.02.017

Peter, I. S., & Davidson, E. H. (2015). *Genomic control process : development and evolution*. Academic Press.

Pfeiffer, B. D., Jenett, A., Hammonds, A. S., Ngo, T.-T. B., Misra, S., Murphy, C., … Rubin, G. M. (2008). Tools for neuroanatomy and neurogenetics in Drosophila. *Proceedings of the National Academy of Sciences of the United States of America*, *105*(28), 9715–9720. https://doi.org/10.1073/pnas.0803697105

Pires-daSilva, A., & Sommer, R. J. (2003). The evolution of signalling pathways in animal development. *Nature Reviews. Genetics*, *4*(1), 39–49. https://doi.org/10.1038/nrg977

Port, F., Chen, H.-M., Lee, T., & Bullock, S. L. (2014). Optimized CRISPR/Cas tools for efficient germline and somatic genome engineering in Drosophila. *Proceedings of the National Academy of Sciences of the United States of America*, *111*(29), E2967-76. https://doi.org/10.1073/pnas.1405500111

Price, M. H., Roberts, D. M., McCartney, B. M., Jezuit, E., & Peifer, M. (2006). Cytoskeletal dynamics and cell signaling during planar polarity establishment in the Drosophila embryonic denticle. *Journal of Cell Science*, *119*(3), 403–415. https://doi.org/10.1242/jcs.02761

Prout, M., Damania, Z., Soong, J., Fristrom, D., & Fristrom, J. W. (1997). Autosomal mutations affecting adhesion between wing surfaces in Drosophila melanogaster. *Genetics*, *146*(1),

275–285. Retrieved from http://www.ncbi.nlm.nih.gov/pubmed/9136017

Pyrowolakis, G., Veikkolainen, V., Yakoby, N., & Shvartsman, S. Y. (2017). Gene regulation during Drosophila eggshell patterning. *Proceedings of the National Academy of Sciences of the United States of America*, *114*(23), 5808–5813. https://doi.org/10.1073/pnas.1610619114

Ray, R. P., Matamoro-Vidal, A., Ribeiro, P. S., Tapon, N., Houle, D., Salazar-Ciudad, I., & Thompson, B. J. (2015). Patterned Anchorage to the Apical Extracellular Matrix Defines Tissue Shape in the Developing Appendages of Drosophila. *Developmental Cell*, *34*(3), 310–322. https://doi.org/10.1016/j.devcel.2015.06.019

Rebeiz, M., Jikomes, N., Kassner, V. A., & Carroll, S. B. (2011). Evolutionary origin of a novel gene expression pattern through co-option of the latent activities of existing regulatory sequences. *Proceedings of the National Academy of Sciences of the United States of America*, *108*(25), 10036–10043. https://doi.org/10.1073/pnas.1105937108

Rebeiz, M., Patel, N. H., & Hinman, V. F. (2015). Unraveling the Tangled Skein: The Evolution of Transcriptional Regulatory Networks in Development. *Annual Review of Genomics and Human Genetics*, *16*(1), 103–131. https://doi.org/10.1146/annurev-genom-091212-153423

Rebeiz, M., Pool, J. E., Kassner, V. A., Aquadro, C. F., & Carroll, S. B. (2009). Stepwise modification of a modular enhancer underlies adaptation in a Drosophila population. *Science (New York, N.Y.)*, *326*(5960), 1663–1667. https://doi.org/10.1126/science.1178357

Rebeiz, M., & Posakony, J. W. (2004). GenePalette: a universal software tool for genome sequence visualization and analysis. *Developmental Biology*, *271*(2), 431–438. https://doi.org/10.1016/j.ydbio.2004.04.011

Renvoisé, E., Kavanagh, K. D., Lazzari, V., Häkkinen, T. J., Rice, R., Pantalacci, S., … Jernvall, J. (2017). Mechanical constraint from growing jaw facilitates mammalian dental diversity. *Proceedings of the National Academy of Sciences of the United States of America*, *114*(35), 9403–9408. https://doi.org/10.1073/pnas.1707410114

Rice, G., David, J., Kamimura, Y., Masly, J., Mcgregor, A., Nagy, O., … Yassin, A. (2019). *A Standardized Nomenclature and Atlas of the Male Terminalia of Drosophila melanogaster*. https://doi.org/10.20944/PREPRINTS201906.0071.V1

Rizzo, N. P., & Bejsovec, A. (2017). SoxNeuro and Shavenbaby act cooperatively to shape denticles in the embryonic epidermis of Drosophila. *Development (Cambridge, England)*, *144*(12), 2248–2258. https://doi.org/10.1242/dev.150169

Roch, F. (2003). Drosophila miniature and dusky encode ZP proteins required for cytoskeletal reorganisation during wing morphogenesis. *Journal of Cell Science*, *116*(7), 1199–1207. https://doi.org/10.1242/jcs.00298

Roll-Mecak, A. (2019). How cells exploit tubulin diversity to build functional cellular microtubule mosaics. *Current Opinion in Cell Biology*, *56*, 102–108. https://doi.org/10.1016/j.ceb.2018.10.009

Russo, C. A., Takezaki, N., & Nei, M. (1995). Molecular phylogeny and divergence times of drosophilid species. *Molecular Biology and Evolution*, *12*(3), 391–404. https://doi.org/10.1093/oxfordjournals.molbev.a040214

Sato, K., Hiraiwa, T., Maekawa, E., Isomura, A., Shibata, T., & Kuranaga, E. (2015). Left–right asymmetric cell intercalation drives directional collective cell movement in epithelial morphogenesis. *Nature Communications*, *6*(1), 10074. https://doi.org/10.1038/ncomms10074

Schindelin, J., Arganda-Carreras, I., Frise, E., Kaynig, V., Longair, M., Pietzsch, T., … Cardona, A. (2012). Fiji: an open-source platform for biological-image analysis. *Nature Methods*, *9*(7), 676–682. https://doi.org/10.1038/nmeth.2019

Schnatwinkel, C., & Niswander, L. (2013). Multiparametric image analysis of lung-branching morphogenesis. *Developmental Dynamics : An Official Publication of the American Association of Anatomists*, *242*(6), 622–637. https://doi.org/10.1002/dvdy.23961

Schwartz, S. (2003). For Good. [Recorded by K. Chenoweth & I. Menzel]. On *Wicked: a New Musical: Original Broadway Cast Recording* [CD]. New York, NY: Decca Broadway.

Shawkey, M. D., Morehouse, N. I., & Vukusic, P. (2009). A protean palette: colour materials and mixing in birds and butterflies. *Journal of the Royal Society, Interface*, *6*(Suppl 2), S221-231. https://doi.org/10.1098/rsif.2008.0459.focus

Shyer, A. E., Rodrigues, A. R., Schroeder, G. G., Kassianidou, E., Kumar, S., & Harland, R. M. (2017). Emergent cellular self-organization and mechanosensation initiate follicle pattern in the avian skin. *Science (New York, N.Y.)*, *357*(6353), 811–815. https://doi.org/10.1126/science.aai7868

Smith, A. F., Posakony, J. W., & Rebeiz, M. (2017). Automated tools for comparative sequence analysis of genic regions using the GenePalette application. *Developmental Biology*, *429*(1), 158–164. https://doi.org/10.1016/j.ydbio.2017.06.033

Smith, S. J., Davidson, L. A., & Rebeiz, M. (2019). Expansion of apical extracellular matrix underlies the morphogenesis of a recently evolved structure. *BioRxiv*, 686089. https://doi.org/10.1101/686089

Smith, S. J., Rebeiz, M., & Davidson, L. (2018). From pattern to process: studies at the interface of gene regulatory networks, morphogenesis, and evolution. *Current Opinion in Genetics and Development*, *51*. https://doi.org/10.1016/j.gde.2018.08.004

Stavenga, D. G., Leertouwer, H. L., & Wilts, B. D. (2014). Coloration principles of nymphaline butterflies - thin films, melanin, ommochromes and wing scale stacking. *Journal of Experimental Biology*, *217*(12), 2171–2180. https://doi.org/10.1242/jeb.098673

Tada, M., Heisenberg, C.-P., Arboleda-Estudillo, Y., Krieg, M., Stühmer, J., Licata, N. A., … Wieschaus, E. (2012). Convergent extension: using collective cell migration and cell intercalation to shape embryos. *Development*, *139*(21), 3897–3904.

https://doi.org/10.1242/dev.073007

Tanaka, K., Barmina, O., & Kopp, A. (2009). Distinct developmental mechanisms underlie the evolutionary diversification of Drosophila sex combs. *Proceedings of the National Academy of Sciences*, *106*(12), 4764–4769. https://doi.org/10.1073/pnas.0807875106

Tian, E., & Hagen, K. G. Ten. (2007). O-linked glycan expression during Drosophila development. *Glycobiology*, *17*(8), 820–827. https://doi.org/10.1093/glycob/cwm056

Voelzmann, A., Liew, Y.-T., Qu, Y., Hahn, I., Melero, C., Sánchez-Soriano, N., & Prokop, A. (2017). Drosophila Short stop as a paradigm for the role and regulation of spectraplakins. *Seminars in Cell & Developmental Biology*, *69*, 40–57. https://doi.org/10.1016/J.SEMCDB.2017.05.019

Vukusic, P., Sambles, J. R., Lawrence, C. R., & Wootton, R. J. (1999). Quantified interference and diffraction in single Morpho butterfly scales. *Proceedings of the Royal Society of London. Series B: Biological Sciences*, *266*(1427), 1403–1411. https://doi.org/10.1098/rspb.1999.0794

Wagner, Günter P. (2014). *Homology, genes, and evolutionary innovation*. Princeton University Press.

Wagner, Günter P., & Lynch, V. J. (2010). Evolutionary novelties. *Current Biology*, *20*(2), R48–R52. https://doi.org/10.1016/j.cub.2009.11.010

Walck-Shannon, E., & Hardin, J. (2014). Cell intercalation from top to bottom. *Nature Reviews. Molecular Cell Biology*, *15*(1), 34–48. https://doi.org/10.1038/nrm3723

Wang, L., Sexton, T. R., Venard, C., Giedt, M., Guo, Q., Chen, Q., & Harrison, D. A. (2014). Pleiotropy of the Drosophila JAK pathway cytokine Unpaired 3 in development and aging. *Developmental Biology*, *395*(2), 218–231. https://doi.org/10.1016/j.ydbio.2014.09.015

Wang, X., Harris, R. E., Bayston, L. J., & Ashe, H. L. (2008). Type IV collagens regulate BMP signalling in Drosophila. *Nature*, *455*(7209), 72–77. https://doi.org/10.1038/nature07214

Wasik, B. R., Liew, S. F., Lilien, D. A., Dinwiddie, A. J., Noh, H., Cao, H., & Monteiro, A. (2014). Artificial selection for structural color on butterfly wings and comparison with natural evolution. *Proceedings of the National Academy of Sciences of the United States of America*, *111*(33), 12109–12114. https://doi.org/10.1073/pnas.1402770111

Webster, D. R., Gundersen, G. G., Bulinski, J. C., & Borisy, G. G. (1987). Differential turnover of tyrosinated and detyrosinated microtubules. *Proceedings of the National Academy of Sciences*, *84*(24), 9040–9044. https://doi.org/10.1073/pnas.84.24.9040

Werner, T., Koshikawa, S., Williams, T. M., & Carroll, S. B. (2010). Generation of a novel wing colour pattern by the Wingless morphogen. *Nature*, *464*(7292), 1143–1148. https://doi.org/10.1038/nature08896

West, J. J., Zulueta-Coarasa, T., Maier, J. A., Lee, D. M., Bruce, A. E. E., Fernandez-Gonzalez, R., & Harris, T. J. C. (2017). An Actomyosin-Arf-GEF Negative Feedback Loop for Tissue Elongation under Stress. *Current Biology : CB*, *27*(15), 2260-2270.e5. https://doi.org/10.1016/j.cub.2017.06.038

Wilkin, M. B., Becker, M. N., Mulvey, D., Phan, I., Chao, A., Cooper, K., … MacIntyre, R. (2000). Drosophila Dumpy is a gigantic extracellular protein required to maintain tension at epidermal–cuticle attachment sites. *Current Biology*, *10*(10), 559–567. https://doi.org/10.1016/S0960-9822(00)00482-6

Williams, T. M., Selegue, J. E., Werner, T., Gompel, N., Kopp, A., & Carroll, S. B. (2008). The Regulation and Evolution of a Genetic Switch Controlling Sexually Dimorphic Traits in Drosophila. *Cell*, *134*(4), 610–623. https://doi.org/10.1016/j.cell.2008.06.052

Wilson, C., Bellen, H. J., & Gehring, W. J. (1990). Position Effects on Eukaryotic Gene Expression. *Annual Review of Cell Biology*, *6*(1), 679–714. https://doi.org/10.1146/annurev.cb.06.110190.003335

Wright, V. M., Vogt, K. L., Smythe, E., & Zeidler, M. P. (2011). Differential activities of the Drosophila JAK/STAT pathway ligands Upd, Upd2 and Upd3. *Cellular Signalling*, *23*(5), 920–927. https://doi.org/10.1016/j.cellsig.2011.01.020

Wunderlich, Z., Bragdon, M. D. J., Vincent, B. J., White, J. A., Estrada, J., & DePace, A. H. (2015). Krüppel Expression Levels Are Maintained through Compensatory Evolution of Shadow Enhancers. *Cell Reports*, *12*(11), 1740–1747. https://doi.org/10.1016/j.celrep.2015.08.021

Xu, Z., Schaedel, L., Portran, D., Aguilar, A., Gaillard, J., Marinkovich, M. P., … Nachury, M. V. (2017). Microtubules acquire resistance from mechanical breakage through intralumenal acetylation. *Science (New York, N.Y.)*, *356*(6335), 328–332. https://doi.org/10.1126/science.aai8764

Zeidler, M. P., Perrimon, N., & Strutt, D. I. (1999). Polarity determination in the Drosophila eye: a novel role for Unpaired and JAK/STAT signaling. *Genes & Development*, *13*(10), 1342–1353. https://doi.org/10.1101/gad.13.10.1342

Zhang, L., Mazo-Vargas, A., & Reed, R. D. (2017). Single master regulatory gene coordinates the evolution and development of butterfly color and iridescence. *Proceedings of the National Academy of Sciences of the United States of America*, *114*(40), 10707–10712. https://doi.org/10.1073/pnas.1709058114